Solid-State NMR Studies of Cobalamins

by

Christopher William Kirby

A thesis
presented to the University of Waterloo
in fulfilment of the
thesis requirement for the degree of
Doctor of Philosophy
in
Chemistry

Waterloo, Ontario, Canada, 2000

National Library of Canada
Acquisitions and Bibliographic Services
395 Wellington Street
Ottawa ON K1A 0N4
Canada

Bibliothèque nationale du Canada
Acquisitions et services bibliographiques
395, rue Wellington
Ottawa ON K1A 0N4
Canada

Your file Votre référence

Our file Notre référence

0-612-60546-9

Canada

The University of Waterloo requires the signatures of all persons using or photocopying this thesis. Please sign below, and give address and date.

Abstract

Solid state NMR studies have been performed on two members of the cobalamin family, namely vitamin B_{12} and methylcobalamin, using single-crystal NMR, static powder NMR, and magic angle spinning NMR techniques.

The chemical shift and quadrupolar coupling tensors of the cobalt centre of vitamin B_{12} have been determined *via* single-crystal ^{59}Co NMR at 11.75 T. The chemical shift tensor was found to span (Ω) 1173 $\pm$ 62 ppm, to have an isotropic shift (δ_{iso}) of 4549 $\pm$ 75 ppm, and possess a skew (κ) of 0.31 $\pm$ 0.02. The quadrupolar coupling tensor of vitamin B_{12} was found to be large with a quadrupolar coupling constant (χ) of 27.31 $\pm$ 0.08 MHz and an asymmetry (η) of 0.243 $\pm$ 0.005.

Selective labelling of the cyano group of vitamin B_{12} using ^{15}N and ^{15}N,^{13}C cyanide and preparation of methyl-^{13}C-cobalamin allowed for the study of these nuclei around the cobalt centre in these two cobalamins. The nitrogen was too far removed to see any effect due to the cobalt nucleus. However, the carbon spectra were greatly affected by both J-coupling and residual dipolar coupling due to the proximity of the directly bonded spin-$\frac{7}{2}$ (^{59}Co) nucleus. Simulation of the methyl-^{13}C-cobalamin was not possible, but that of cyano-^{15}N,^{13}C-cobalamin yielded a one bond Co-C J-coupling of 165 $\pm$ 10 Hz.

The two cobalamins in this study can be forced to adapt a base-off conformation *via* chemical means. Using ^{31}P NMR, we have been able to determine if a cobalamin is base-on or base-off from the isotropic chemical shifts (δ_{on}= -1.3 ± 1 ppm, δ_{off}= 4.6 ± 0.3 ppm), the spans of the chemical shift tensors (Ω_{on}= 184 ± 3 ppm, Ω_{off}= 112.5 ± 7.5 ppm), as well as the chemical shift tensor skews (κ_{on}= 0.355 ± 0.035, κ_{off}= -0.72 ± 0.01). We believe that this trend can be used to determine if an enzyme-bound cobalamin adapts a base-on or base-off conformation. We have also studied the ^{59}Co NMR spectra of the base-off cobalamins.

Deuterium NMR studies of methyl-d_3-cobalamin and its base-off analogue have revealed information about the dynamics of these two complexes. The activation energy for methyl group rotation of the base-off conformation is significantly less than that for the base-on conformation indicating that base-off cobalamins have a weaker cobalt-carbon bond.

Acknowledgements

There have been many people who have helped me to put this thesis together. First and foremost, I need to thank Professor Bill Power. Bill has been an excellent supervisor always having knowledge, giving encouragement, and willingness to work through a problem together when the situation needed. I also thank him for being patient and letting me start a position while trying to write-up. Thanks for the past few years, Bill.

Thanks to those who have given technical support to the NMR lab. Jan Venne is an excellent technician and it was a pleasure to work as her TA. Those in the science and electronic shops (Ivan, Reg, and Harmun) need to be thanked for their help with the NMR probes when problems occurred and for their help in designing the insert used to perform the single-crystal NMR experiments. I also thank Valerie Robinson at the University of Guelph for letting us use the ASX-200 to perform the low field ^{59}Co NMR experiments and Dr. Patricia Aroca-Ouellette at the University of Toronto for use of the ASX-200 to perform the low field ^{13}C NMR experiments.

During my graduate work, I am most proud of the single-crystal ^{59}Co NMR study of vitamin B_{12}. This study would not have been possible without the aid of an excellent X-ray crystallographer. I would like to thank Dr. Nick Taylor for all his help in making this study possible.

When I had decided to pursue NMR studies on the cobalamin family, Dr. John Honek was very helpful in giving me a few quick and dirty biochemical lessons on this class of compounds. These discussions confirmed to me that there would be many studies that could be performed on cobalamins. Thank you John for setting me on the right track.

Working in the Power group has been a good time. I had two excellent undergraduate students work with me on the cobalamin projects. Jennifer Garbutt and David Cescon aided in the synthesis as well as some of the NMR experiments described in this thesis. Having two fellow graduate students in Dr. Gillian Goward and Mike Ditty to discuss both NMR and life helped to keep my graduate work enjoyable. I would also like to thank Dr. Howard Hunter for his help in teaching me how to better process my NMR spectra.

Without the support of my family, I wouldn't have been able to finish this thesis. Thanks for always bugging me about being done Mom. Amanda you have always been there for me during my endless nights trying to get experiments done, and the long time in getting this document written. I hope that I can be as supportive as you start to write your thesis. I guess I'll have to take care of Beth.

But they that hope in the Lord will renew their strength. They will soar on wings like eagles; they will run and not grow weary, they will walk and not be faint. Isaiah 40:31

List of Abbreviations

α, β, γ	Euler angles relating a tensor in the principal axis system of a second tensor
B_o	magnetic field strength
B_{12}	vitamin B_{12}
$B_{12}BO$	vitamin B_{12} in a base-off conformation
CS	chemical shielding
χ	quadrupolar coupling constant
DD	direct dipolar
δ_{ii}	component of a chemical shift tensor
δ_{iso}	isotropic chemical shift
ΔJ	anisotropy of the spin-spin tensor
eq_{ii}	component of a quadrupolar tensor
$\hat{\mathcal{H}}$	Hamiltonian operator
η	asymmetry of the quadrupolar tensor
I, S	nuclear spin quantum numbers
J_{iso}	isotropic spin-spin coupling constant
κ	skew: a measure of the symmetry of the chemical shift/shielding tensor
m	z-component of a nuclear spin quantum number
MeB_{12}	methylcobalamin

$MeB_{12}BO$	methylcobalamin in a base-off conformation
ν_o	Larmor frequency
PAS	principal axis system
Q	quadrupolar
Q_{ii}	component of a quadrupolar tensor
θ, ϕ	angles which define the orientation of B_o in the PAS of the quadrupolar tensor
ϑ, φ	angles which define the orientation of B_o in the PAS of the chemical shift/shielding tensor
R_{DD}	dipolar coupling constant
RF	radiofrequency
SR	spin-rotation
σ	chemical shielding
σ_a	antisymmetric part of the chemical shielding tensor
σ_d	diamagnetic chemical shielding
σ_p	paramagnetic chemical shielding
σ_{ii}	principal component of a chemical shielding tensor
Ω	span of the chemical shift/shielding tensor
TST	transition state theory

Contents

List of Tables

List of Figures

Chapter 1

Introductory Comments

This thesis is concerned with the application of nuclear magnetic resonance (NMR) spectroscopy to the study of the vitamin B_{12} family. Vitamin B_{12} is famous as the "miraculous" treatment of pernicious anemia.[1] As early as 1824,[2] researchers described reports of megaloblastic anemia, noting that patients had both gastric and neurological problems, and suggested that the disease was a "disorder of the digestive and assimilative organs." Until the early 1900's, this disease was fatal due to the usual treatment with "Fowler's solution" (an arsenic-containing solution).[3] In 1926, Minot and Murphy[4], future Nobel Laureates, showed that a liver-rich diet (half a pound a day!) would greatly help patients with pernicious anemia. Castle[5] was the first to understand that pernicious anemia was characterized by either the lack of one or both of two essential components which he named the extrinsic and intrinsic factors. Vitamin B_{12} was the extrinsic factor and the intrinsic factor was a protein in the stomach that allows for absorption of the vitamin. Many companies were independently trying to discover the structure of vitamin B_{12} (B from the A/B

distinction given to the first organic (A) *vs.* water (B) soluble "vital amines" and 12 as it was the twelfth found in the water soluble vitamins), but it was not until Glaxo provided a crystalline sample to researchers at Oxford that the structure was determined. Hodgkin and co-workers published a series of papers concerning the structure of vitamin B_{12}[6, 7, 8, 9, 10, 11] of which the last of this series gives the crystal structure of vitamin B_{12} seen in Figure 1.1.[11] Things to note in this structure are the cobalt centre, the corrin ring which provides four nitrogens that are bonded to the cobalt, the dimethylbenzimidazole base (providing a fifth CoN bond) joined to the corrin ring with a nucleotide "tail," and the cyano group which completes the octahedral coordination about the cobalt.

Metals such as cobalt play a vital role in many biological systems, occurring at sites of catalytic or structural importance in various ring-based, protein, and nucleic acid assemblies.[1, 12] Numerous techniques have been used to study metal centres in such materials,[13] including X-ray diffraction (as was the case for vitamin B_{12} described above) and absorption, ultraviolet/visible spectroscopy, as well as magnetic resonance, both electron (ESR) and nuclear (NMR), techniques. Of these, NMR is the most versatile and widely used technique, with application to systems containing both paramagnetic and diamagnetic metal sites in both solution and the solid-state. NMR studies of biologically relevant materials containing metal centres have been predominantly ^{1}H solution NMR studies,[14] with extensions to ^{13}C and ^{15}N[15] to characterize the organic assembly surrounding the metal centre. Direct observation of the metal nuclei themselves has generally been avoided, although in many cases the metal is usually directly involved in the biological activity. In

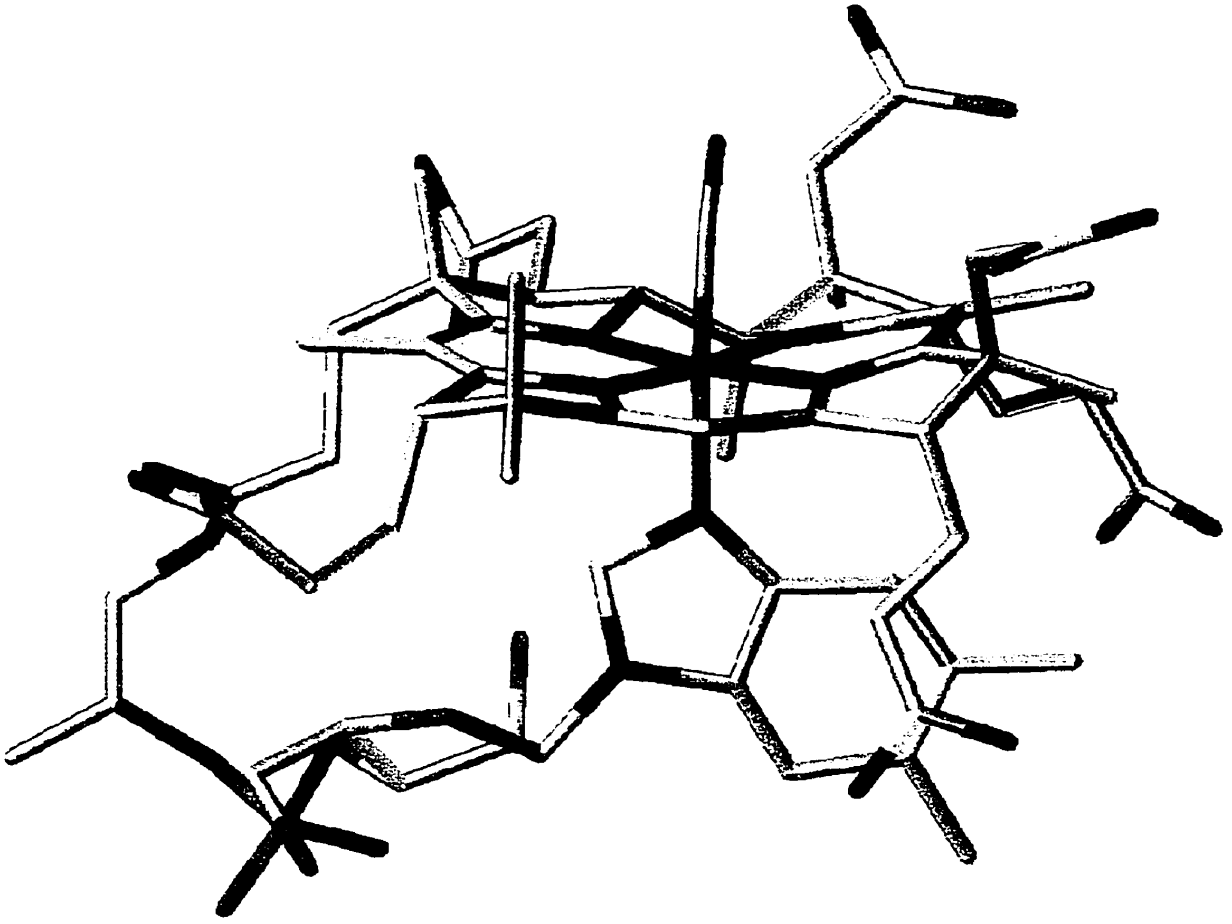

Figure 1.1: Crystal structure of vitamin B_{12} (from reference [11]).

cases where NMR of the metal nuclei has been used, the studies almost invariably are with spin-$\frac{1}{2}$ isotopes,[16] such as ^{111,113}Cd, ^{195}Pt, or ^{199}Hg. Quadrupolar nuclei (those nuclei with nuclear spin quantum number, I, $\geq$ 1), although naturally occurring, were deemed unsuitable because of their efficient quadrupolar relaxation and concomitant broad lines; hence they were often substituted by unnatural metals possessing spin-$\frac{1}{2}$ isotopes, *e.g.*, ^{67}Zn replaced by ^{113}Cd or ^{199}Hg. Such metal replacements often cause a severe decrease in, or complete loss of, biological activity.

Quadrupolar nuclei have become more accessible for study, especially for solid samples, over the past few years with the availability of high magnetic field strengths ($B_o \geq 11.75$ T), new advances in NMR probe design including dynamic angle spinning (DAS)[17] and double rotation (DOR)[18] probes, as well as new pulse techniques such as multiple quantum magic angle spinning (MQMAS).[19] These techniques have been developed to allow the acquisition of high resolution spectra of quadrupolar nuclei in solids. However, in high resolution experiments, the orientation dependence (or anisotropic nature) of the NMR interactions is lost. These anisotropic interactions, which are usually described by second-rank tensors, provide detailed descriptions of the local three-dimensional electronic environment. All of the NMR interactions will be described in some detail in chapter 2 which contains theory that will be used in the remainder of this thesis. The ability to interpret the NMR spectra presented in this document in terms of the local structure depends on an understanding of the values and the orientations that these tensors adopt in different environments.

The two compounds of interest in this thesis are vitamin B_{12} (cyanocobalamin

or B_{12}) and its related coenzyme methylcobalamin (MeB_{12}). These belong to a family of compounds for which a better understanding of the local environment of the metal centre (in this case cobalt) may lead to an increased comprehension of the biochemical structure (with regard to conformation around the metal). Cobalt is a good nucleus to pursue *via* NMR. The only naturally occurring isotope of cobalt is ^{59}Co, which has a high magnetogyric ratio (directly related to its resonance frequency) making it a highly receptive nucleus (approximately 27.7% of ^{1}H) and therefore a prime candidate for NMR studies. It is also a quadrupolar nucleus ($I = \frac{7}{2}$) with a nuclear quadrupole moment of 0.4×10^{-28} m^2. A further advantage (as well as difficulty) is its large chemical shift range (over 18 000 ppm) making ^{59}Co NMR very sensitive to the local environment, but this also makes it very difficult to observe the entire chemical shift range in a single experiment.

Vitamin B_{12} and its derivatives contain a metal-carbon bond which is rare in nature. Various features of the structures of this class of compounds have been suggested as factors in the cobalt-carbon bond scission that is at the root of their biochemical function. Deformation of the corrin ring has been proposed to facilitate the methyl transfer in MeB_{12}.[20] An X-ray crystal structure of MeB_{12} bound to a 27-kDa fragment of methionine synthase (*Escherichia coli*) has shown that the dimethylbenzimidazole tail is displaced by a histidine residue of the protein.[21] A second X-ray structure of a cobalamin bound to an enzyme (adenosylcobalamin with methylmalonyl-CoA mutase) was also found to be in a base-off conformation (the tail was displaced).[22] ESR investigations of adenosylcobalamin bound to dioldehydratase, however, show that the tail is not displaced in the holoenzyme.[23]

ESR results, however, are not of the natural complex (the cobalt must be reduced from Co(III) to Co(II) to do ESR studies). Changes in structure (both geometric and electronic) at the cobalt centre that accompany the actions of such mechanisms should be readily identifiable through characterization of a sensitive probe of the local metal environment. Since ^{59}Co is very sensitive to the local environment, a single-crystal ^{59}Co NMR study of vitamin B_{12} was performed (described in chapter 3). This is the first single-crystal NMR study of a metal nucleus in a biologically relevant molecule. The orientations of the chemical shift and quadrupolar coupling tensors at the cobalt centre were unambiguously determined by obtaining ^{59}Co NMR spectra as a function of the orientation of a single crystal of vitamin B_{12} in the magnetic field. These results provide the basis to understand changes in the chemical shielding and quadrupolar coupling interactions of ^{59}Co in cobalamins in terms of explicit variations in the metal environment.

Nuclei with $I = \frac{1}{2}$ near a metal site (*e.g.*, ^{13}C, ^{15}N, etc.) can sometimes be introduced using synthetic or biosynthetic methods and used to help probe the metal indirectly using magic angle spinning (MAS) as well as static NMR techniques. Chapter 4 contains static and MAS results of the cyano group or methyl group attached to the cobalt centre in B_{12} or MeB_{12} using both ^{13}C and ^{15}N NMR and selective labelling techniques. These results, as much as they reveal, show that it would be more efficient to study the metal itself in enzyme-bound B_{12} derivatives due to background signals that would be observed (especially with respect to ^{13}C NMR) even if selective labels are introduced.

Quadrupolar nuclei can be studied by static NMR techniques as well single-

crystal NMR techniques. Vitamin B_{12} and its active biological forms have been previously studied *via* static ^{59}Co NMR.[24] However, at least two of these active forms have been shown to adapt a base-off form when bound to an enzyme.[21, 22] There are synthetic methods available that permit one to obtain vitamin B_{12} and methylcobalamin in base-off forms. In chapter 5, a ^{59}Co NMR study of powder samples of the base-off forms of these two complexes is described. The only nucleus, other than the cobalt centre itself, that is unique in the structure of cobalamins is phosphorus. This lead us to examine the solid-state ^{31}P NMR spectra of the base-on and base-off forms of the two cobalamins. These ^{31}P NMR results show that the chemical shift tensors of the base-on forms are the same, the chemical shift tensors of the base-off forms are the same, but chemical shift tensors of the base-on and base-off forms are significantly different. This appears to give us a simple selective experiment using a naturally occurring and unique nucleus, to study cobalamin conformations.

Deuterium NMR is commonly used to study the dynamics of molecular systems. When ^{2}H is studied, a selective label is usually introduced into a molecule. Methylcobalamin is one of the two co-enzyme forms of vitamin B_{12}. Methyl-d_3-cobalamin is easily made and therefore we can use ^{2}H NMR to study the dynamics of this methyl group. From the results in chapter 5, it follows that it is possible to force MeB_{12} chemically into a base-off conformation. In chapter 6, a variable temperature ^{2}H spin-lattice relaxation study of the base-on and base-off forms of methyl-d_3-cobalamin is described.

The final chapter in this thesis briefly reviews the conclusions drawn in chapters

3 - 6 as well as future work that builds on the results of this project. Suggestions are made on how solid-state NMR techniques can be used in future work in biologically relevant systems, especially with respect to cobalamin dependent enzymatic reactions.

Chapter 2

NMR Theory

2.1 The Interactions

The full nuclear spin Hamiltonian of a diamagnetic compound is given as[25]

$$\hat{\mathcal{H}}_T = \hat{\mathcal{H}}_Z + \hat{\mathcal{H}}_{RF} + \hat{\mathcal{H}}_{CS} + \hat{\mathcal{H}}_{DD} + \hat{\mathcal{H}}_J + \hat{\mathcal{H}}_Q + \hat{\mathcal{H}}_{SR} \tag{2.1}$$

where the total Hamiltonian (T) is the sum of the Zeeman (Z), radiofrequency (RF), chemical shielding (CS), direct dipolar (DD), indirect spin-spin (J), quadrupolar (Q), and spin rotation (SR) Hamiltonians. The Zeeman interaction is the essential interaction for NMR spectroscopy; in general all of the other interactions are weaker than the Zeeman energy, thus are perturbations of this interaction in an NMR experiment. A brief discussion of each interaction will be provided here. For a more detailed picture, the following monographs and reviews are suggested.[25, 26, 27]

2.1.1 The Zeeman Interaction

If a nucleus possessing spin (*i.e.* I > 0) is placed in a magnetic field, $\vec{B}_o$, the 2I + 1 nuclear spin energy levels become non-degenerate. The energy between these levels is dependent on the magnetic moment of a nucleus, $\vec{\mu}$, and $\vec{B}_o$, as described by the Hamiltonian, $\hat{\mathcal{H}}_Z$, where

$$\hat{\mathcal{H}}_Z = -\hat{\vec{\mu}} \cdot \vec{B}_o = -\gamma_I \hbar \hat{\vec{I}} \cdot \vec{B}_o \tag{2.2}$$

with γ_I is the magnetogyric ratio for nuclear isotope I, $\hbar$ is Planck's constant divided by 2π, and $\hat{\vec{I}}$ is the nuclear spin angular momentum operator. By convention, $\vec{B}_o$ is chosen to be along the laboratory z-axis. The usual convention is to use frequency units rather than units of energy when discussing NMR spectra. The frequency at which a pure Zeeman transition occurs is given by the Larmor frequency, ν_o, of a given nuclear isotope,

$$\nu_o = \left| \frac{\gamma_I \vec{B}_o}{2\pi} \right| \tag{2.3}$$

where ν_o is in Hz. All of the remaining interactions are perturbations of the Zeeman interaction.

2.1.2 The Radiofrequency Interaction

NMR would not be possible without the radiofrequency (RF) interaction. In a pulse Fourier Transform (FT) NMR experiment, a time-dependent radio frequency field, $\vec{B}_{RF}$, is placed along an axis perpendicular to $\vec{B}_o$ (either x or y). This RF

pulse induces a transition between nuclear spin energy levels,

$$\hat{\mathcal{H}}_{RF} = -\gamma_I \hbar \hat{\vec{I}} \cdot \vec{B}_{RF} \tag{2.4}$$

where

$$\vec{B}_{RF}(t) = (B_1 \cos \omega t, 0, 0) \tag{2.5}$$

and B_1 is the amplitude of the RF field with a carrier frequency of $\omega/2\pi$. The time-dependent fields of the RF Hamiltonian can be used for all FTNMR experiments to allow observation (and suppression if desired) of the effects of the following Hamiltonians.

2.1.3 The Chemical Shielding Interaction

When an atom or a molecule is placed in a magnetic field, the electrons surrounding the nucleus (or nuclei) are induced to circulate. As the electrons circulate about the nucleus, a local magnetic field is created that will add to the applied field experienced by the nucleus. This phenomenon is known as chemical shielding. Chemical shielding is either positive or negative with respect to the magnetic field direction and, since this shielding is induced by the magnetic field, it is proportional to the magnetic field strength,

$$\hat{\mathcal{H}}_{CS} = -\gamma_I \hbar \hat{\vec{I}} \cdot \tilde{\sigma} \cdot \vec{B}_o \tag{2.6}$$

where $\tilde{\sigma}$ is the chemical shielding tensor. The chemical shielding tensor describes the effect of the circulating electrons as they modify the magnetic field experienced

by the nuclear spin, I.

The chemical shielding Hamiltonian can be written as

$$\hat{\mathcal{H}}_{CS} = \gamma_I \hbar \left\{ \begin{pmatrix} I_x & I_y & I_z \end{pmatrix} \begin{pmatrix} \sigma_{xx} & \sigma_{xy} & \sigma_{xz} \\ \sigma_{yx} & \sigma_{yy} & \sigma_{yz} \\ \sigma_{zx} & \sigma_{zy} & \sigma_{zz} \end{pmatrix} \begin{pmatrix} B_x \\ B_y \\ B_z \end{pmatrix} \right\}. \tag{2.7}$$

This form can be simplified since $\vec{B}_o$ is taken to be along the z-axis. I_x and I_y do not commute with $\hat{\mathcal{H}}_Z$ when $\vec{B}_o$ is along z, therefore only one term survives: $I_z \sigma_{zz}^{Lab} B_o$. This laboratory frame chemical shielding tensor can then be expressed as

$$\sigma_{zz}^{Lab} = \overline{\sigma} = \begin{pmatrix} \sigma_{11} & \sigma_{12} & \sigma_{13} \\ \sigma_{21} & \sigma_{22} & \sigma_{23} \\ \sigma_{31} & \sigma_{32} & \sigma_{33} \end{pmatrix} \tag{2.8}$$

where $\overline{\sigma}$ can be further broken down into symmetric ($\overline{\sigma}^s$) and antisymmetric ($\overline{\sigma}^a$) terms using the transpose ($\overline{\sigma}^T$) of the tensor in equation 2.8. These two terms are

$$\overline{\sigma}^s = \frac{1}{2}(\overline{\sigma} + \overline{\sigma}^T) \tag{2.9}$$

and

$$\overline{\sigma}^a = \frac{1}{2}(\overline{\sigma} - \overline{\sigma}^T). \tag{2.10}$$

In NMR experiments, only the symmetric part of a chemical shielding tensor can

be observed directly and is usually described in its principal axis system (PAS) as

$$\sigma^s = R_{PAS}^{-1}\overline{\sigma}^s R_{PAS} = \begin{pmatrix} \sigma_{11} & 0 & 0 \\ 0 & \sigma_{22} & 0 \\ 0 & 0 & \sigma_{33} \end{pmatrix} \tag{2.11}$$

where R_{PAS} and R_{PAS}^{-1} are rotational transformations[28] from the lab frame to the PAS. The three diagonal elements above are known as the three principal components of the chemical shielding tensor where σ_{11} is the least shielded, σ_{33} is the most shielded, and σ_{22} is between, or equal to one of, the two extremes.

Two common quantities used to describe the CS tensor are span (Ω - the breadth of the chemical shift tensor) and skew (κ - a measure of the symmetry of the chemical shift tensor).[29] Span is the difference between the least shielded and most shielded component of the tensor

$$\Omega = \sigma_{11} - \sigma_{33} \tag{2.12}$$

and skew is given as

$$\kappa = \frac{3(\sigma_{iso} - \sigma_{22})}{\Omega}. \tag{2.13}$$

Skew can have values ranging from +1 to -1. Figure 2.1 gives examples of positive and negative κ. Both Ω and κ are measures of the orientation dependence of the chemical shielding tensor.[29]

The anisotropic chemical shielding interaction can be represented in its PAS which is seen in Figure 2.2, where ϑ and φ are the polar and azimuthal angles

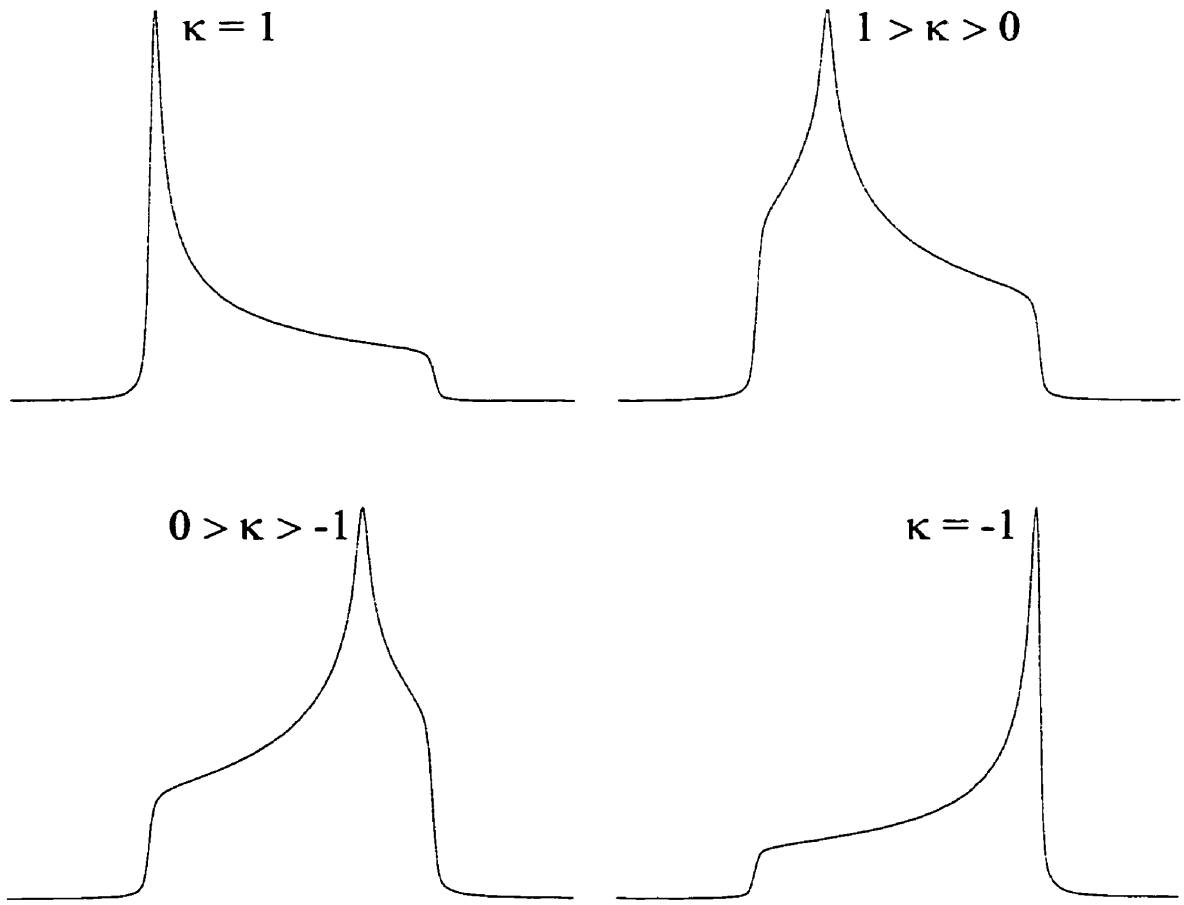

Figure 2.1: Examples of skews: A) $\kappa = 1$, B) $1 > \kappa > 0$, C) $0 > \kappa >$ -1, and D) κ = -1.

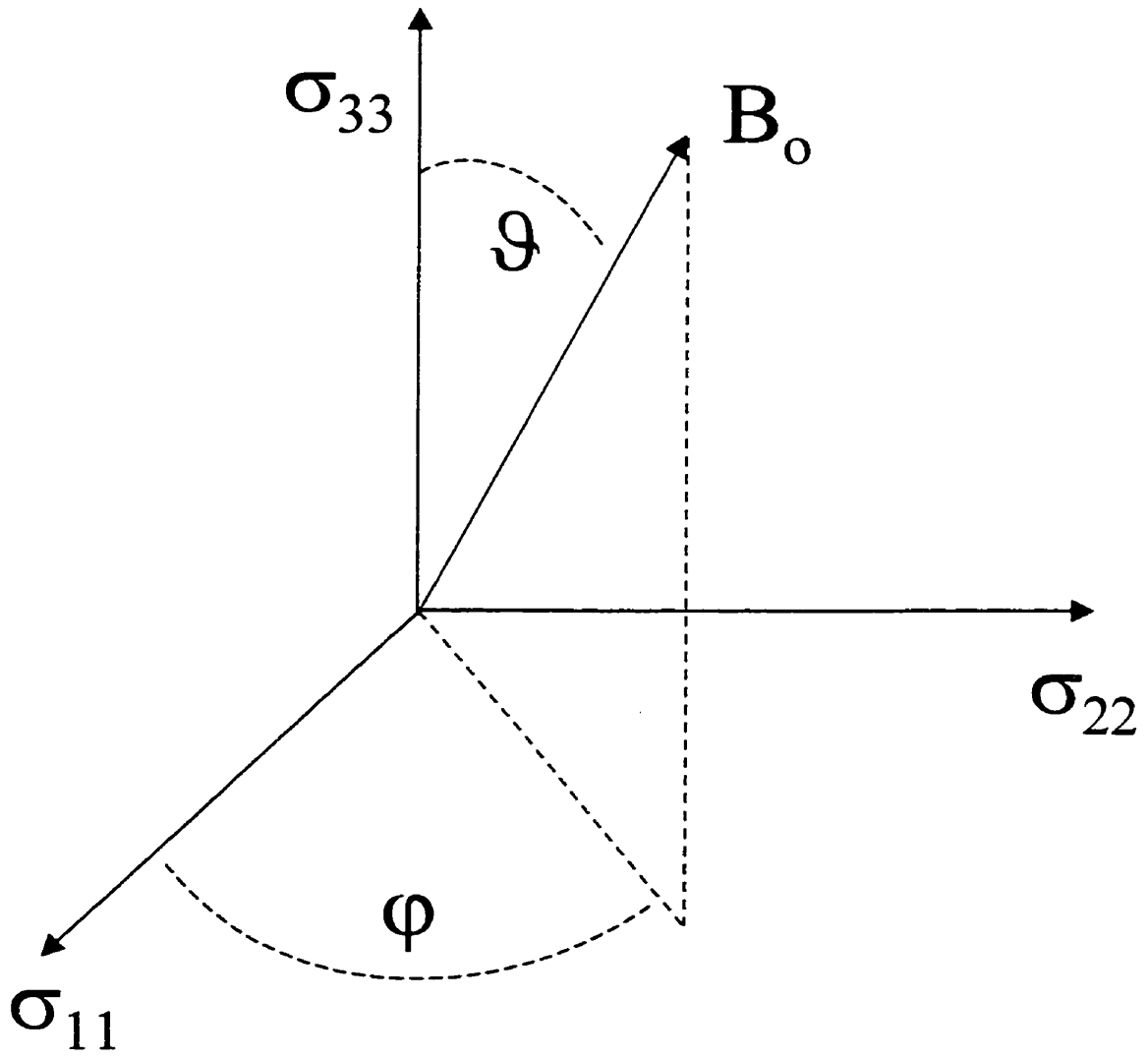

Figure 2.2: The orientation of B_o in the PAS of the chemical shielding tensor.

describing the orientation of B_o in the PAS. These two angles and the three principal components of the chemical shielding tensor give rise to the anisotropic lineshapes observed in many solid-state NMR experiments. The lineshape (ν_σ) of a nucleus in a powder sample dominated by chemical shielding can be described as

$$\nu_\sigma = \nu_o[1 - (\sigma_{11}\sin^2\vartheta\cos^2\varphi + \sigma_{22}\sin^2\vartheta\sin^2\varphi + \sigma_{33}\cos^2\vartheta)]. \tag{2.14}$$

Figure 2.3 gives examples of powder lineshapes for nuclei in sites of cubic, axial, and less than axial symmetry. Cubic symmetry is observed for nuclei in sites with tetrahedral or higher point symmetry. In these cases all components are equal ($\Omega = 0$). Axial symmetry is observed in sites with 3-fold or higher point symmetry. In such cases, $\kappa = +1$ or -1 and $\Omega \neq 0$. In sites with less than 3-fold point symmetry, $\Omega \neq 0$, $1 > \kappa > -1$, and a non-axially symmetric powder pattern is observed.

The above breakdown of a tensor was purely mathematical. It it useful, however, to interpret chemical shielding tensors through a theoretical model of molecular structure or bonding. Ramsey[30] proposed that chemical shielding could be broken down into two terms; diamagnetic and paramagnetic. These two terms are given as follows:[31]

$$\sigma = \sigma_d + \sigma_p \tag{2.15}$$

$$\sigma_d = \frac{e^2}{2m}\frac{\mu_o}{4\pi}\left\langle 0\left|\sum_k r_{kN}^{-3}(\vec{r}_k\cdot\vec{r}_{kN}\hat{1} - \vec{r}_k\vec{r}_{kN})\right|0\right\rangle \tag{2.16}$$

$$\sigma_p = -\frac{e^2}{2m}\frac{\mu_o}{4\pi}\sum_{n\neq 0}\frac{\left\langle 0\left|\sum_k r_{kN}^{-3}\hat{l}_{kN}\right|n\right\rangle\left\langle n\left|\sum_k \hat{l}_k\right|0\right\rangle + \left\langle 0\left|\sum_k \hat{l}_k\right|n\right\rangle\left\langle n\left|\sum_k r_{kN}^{-3}\hat{l}_{kN}\right|0\right\rangle}{{}^1E_n - E_o} \tag{2.17}$$

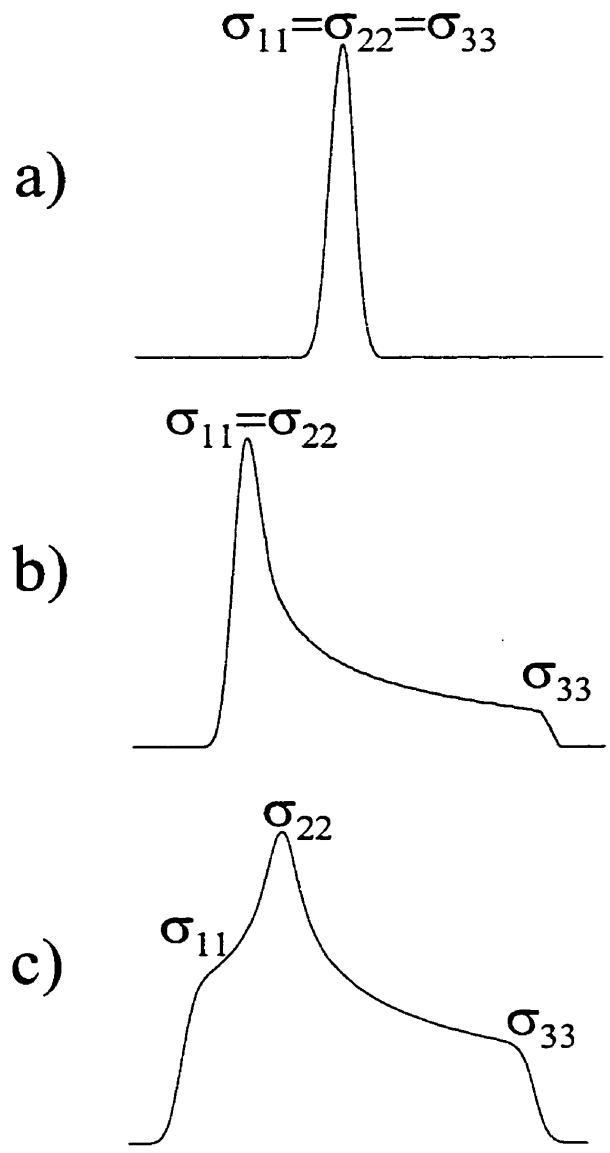

Figure 2.3: NMR spectra for nuclei in sites of a) cubic, b) axial, and c) less than axial symmetry.

where $\vec{r}$ is the position vector for an electron and $\hat{l}$ is the angular momentum operator, both are with respect to either a chosen origin (k) or to the observed nucleus (kN). The diamagnetic term in equation 2.16 is only dependent on the ground state wave functions and is almost invariant for a given nucleus. The paramagnetic term, which is dependent on both ground and excited state wave functions, causes the variation in chemical shielding from compound to compound for most nuclear isotopes; exceptions are hydrogen and lithium since these nuclei only have high energy excited states and small ranges in chemical shifts. Both terms also include a radial density (r^{-3}) term. Cobalt-59, the focus of two of the experimental chapters of this thesis, has one of the largest r^{-3} terms for its d-orbitals resulting in large sensitivity in its shielding, thus its large chemical shift range. Diamagnetic shielding is more readily calculated than paramagnetic shielding (since diamagnetic is only dependent on the ground state wave functions) and the diamagnetic shielding constant for many atoms have been calculated.[32, 33] Calculated NMR chemical shieldings are defined on a scale with respect to the bare nucleus (a nucleus with no electrons around it, or at least no net circulation of electrons) at 0 ppm (parts per million). This scale is known as the absolute chemical shielding scale.

NMR spectra, however, are recorded with respect to a reference compound in terms of the chemical shift (*e.g.*, TMS for ^{1}H and ^{13}C) in field-independent units of ppm. The reference for chemical shielding is the bare nucleus and also uses a field-independent scale of ppm. To convert between these two scales, the value of the chemical shift of the bare nucleus is necessary. From this, the absolute shielding of the reference compound (σ_{ref}) can be determined. The following equation then

provides absolute chemical shieldings:

$$\sigma_{ii} = \sigma_{ref} - \delta_{ii}(1 - \sigma_{ref}) \tag{2.18}$$

Therefore, NMR spectra can be obtained, analyzed to give the chemical shift tensor, and these results can be converted to the chemical shielding scale using equation 2.18 to allow for comparison with *ab initio* calculations.

2.1.4 The Direct Dipolar Interaction

Nuclear spins, like bar magnets, can interact through space. This interaction is known as the direct dipolar (to be referred to as only dipolar henceforth) interaction and can be expressed as

$$\hat{\mathcal{H}}_{DD} = \hbar \hat{\vec{I}} \cdot \tilde{D} \cdot \hat{\vec{S}} \tag{2.19}$$

where $\hat{\vec{I}}$ and $\hat{\vec{S}}$ can be like or unlike spins, and $\tilde{D}$ is the dipolar tensor. The dipolar Hamiltonian can also be written in the following form, commonly called the dipolar alphabet.

$$\hat{\mathcal{H}}_{DD} = r^{-3}\gamma_I\gamma_S\hbar^2[A + B + C + D + E + F]\mu_o/4\pi \tag{2.20}$$

where

$$A = -\hat{I}_z\hat{S}_z(3cos^2\theta - 1) \tag{2.21}$$

$$B = \frac{1}{4}[\hat{I}_+\hat{S}_- + \hat{I}_-\hat{S}_+](3cos^2\theta - 1) \tag{2.22}$$

$$C = -\frac{3}{2}[\hat{I}_z\hat{S}_+ + \hat{I}_+\hat{S}_z](sin\theta cos\theta e^{-i\phi}) \tag{2.23}$$

$$D = -\frac{3}{2}[\hat{I}_z\hat{S}_- + \hat{I}_-\hat{S}_z](sin\theta cos\theta e^{i\phi}) \tag{2.24}$$

$$E = -\frac{3}{4}\hat{I}_+\hat{S}_+ sin^2\theta e^{-2i\phi} \tag{2.25}$$

$$F = -\frac{3}{4}\hat{I}_-\hat{S}_- sin^2\theta e^{2i\phi} \tag{2.26}$$

and θ and ϕ are the polar and azimuthal angles giving the orientation of the two spins with respect to the magnetic field. At the large magnetic fields at which NMR experiments are performed, the dipolar interaction is much smaller than the Zeeman interaction (typically four orders of magnitude). Therefore only the terms that commute with $\hat{\mathcal{H}}_Z$ survive; the A and B terms (B only if the spins are the same) remain while the other terms (C, D, E, and F) are truncated.

One of the first reported dipolar coupling constants was that between the two protons of water in gypsum ($CaSO_4 \cdot 2H_2O$).[34] Figure 2.4 gives the ^{1}H NMR spectrum of gypsum. This characteristic pattern has come to be known as the Pake pattern. The information in the Pake pattern of gypsum agreed with the single-crystal ^{1}H NMR on this complex (also given in this seminal paper) and together, these gave the best early structure determination of the water molecule.

An observed dipolar tensor of two unlike spins (the A term) is always axially symmetric and traceless. The dipolar tensor can then be given as

$$\tilde{D} = R_{DD}\begin{pmatrix} 1 & 0 & 0 \\ 0 & 1 & 0 \\ 0 & 0 & -2 \end{pmatrix} = R_{DD}(3cos^2\theta - 1) \tag{2.27}$$

Therefore, one need only know the dipolar coupling constant, R_{DD}, to completely

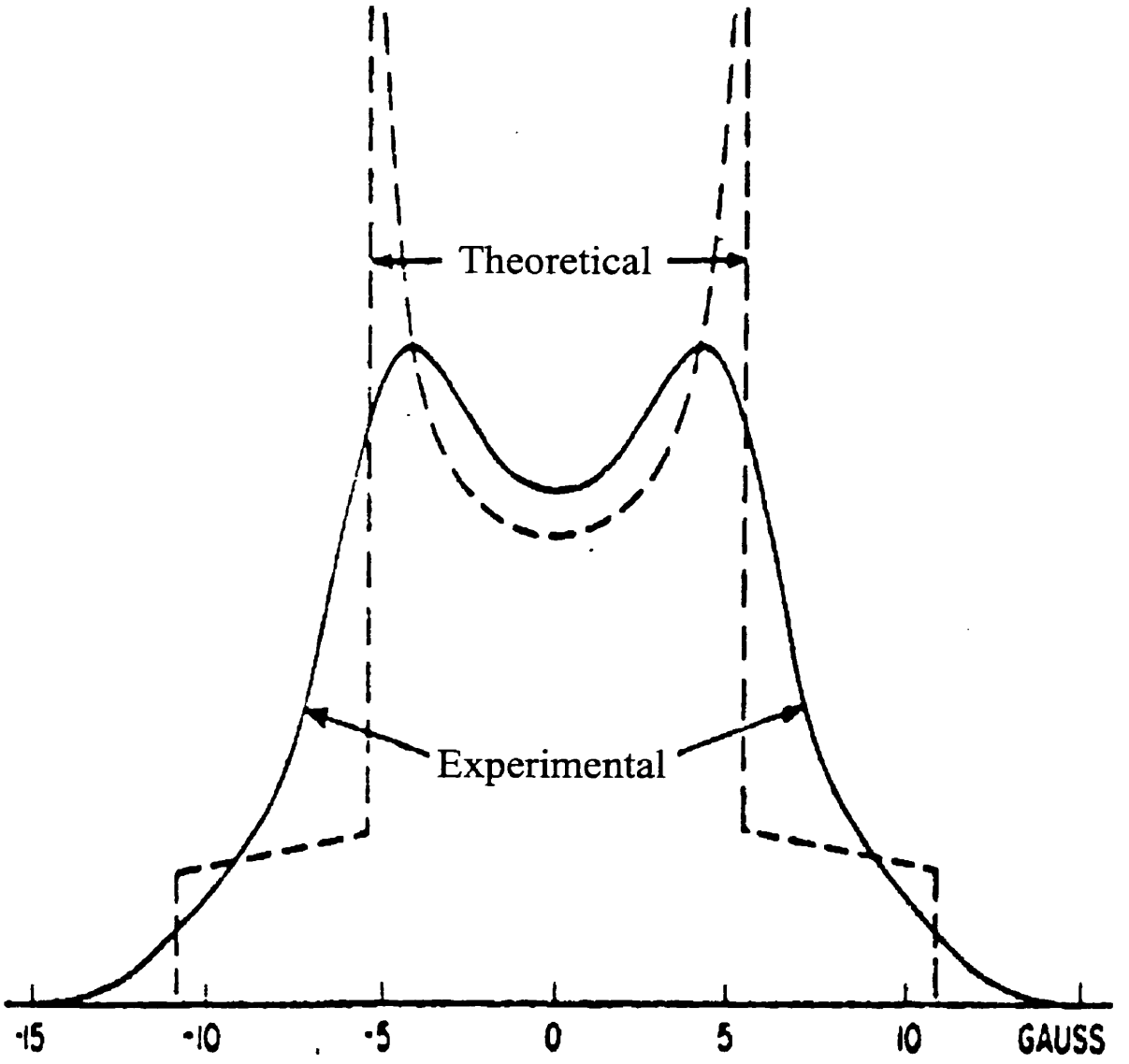

Figure 2.4: The first Pake pattern. Reproduced from reference [34].

characterize the dipolar interaction of two unlike spins,

$$R_{DD} = \frac{\mu_o}{4\pi}\frac{\gamma_I\gamma_S}{r_{IS}^3}\frac{\hbar}{2\pi} \tag{2.28}$$

where r_{IS} is the internuclear distance and R_{DD} is given in Hz.

As seen in the above equation, dipolar coupling is stronger for shorter internuclear distances and for larger magnetogyric ratios. Dipolar coupling can broaden lines as observed from ^{1}H coupling to other nuclei. The dipolar interaction can, however, be used to increase the sensitivity of other nuclei using cross polarization to transfer magnetization from protons.[35, 36] Bond distances (r_{IS}) can also be obtained directly from NMR spectra *via* R_{DD}.

2.1.5 The Indirect Spin-Spin Interaction

Nuclei can communicate with each other through the electrons between them. This communication gives rise to the indirect spin-spin interaction and is given as

$$\hat{\mathcal{H}}_J = \hat{\vec{I}} \cdot \tilde{J} \cdot \hat{\vec{S}} \tag{2.29}$$

where $\tilde{J}$ is the indirect spin-spin coupling tensor. Equation 2.29 can be expanded similarly to $\tilde{\sigma}$ to obtain a general tensor with both symmetric and antisymmetric terms.[37] The indirect spin-spin interaction is usually assumed to be axially symmetric, but, unlike the dipolar interaction, it is not traceless. Recent results have shown this assumption to not be exclusively true,[37] but for this discussion, the axially symmetric assumption will be used. The isotropic average that can be

measured in both solution and the solid state is J_{iso}. Assuming axial symmetry, $\tilde{J}$ can be written as

$$\tilde{J} = \begin{pmatrix} J_\perp & 0 & 0 \\ 0 & J_\perp & 0 \\ 0 & 0 & J_{||} \end{pmatrix} = J_{iso}\mathbf{1} + \begin{pmatrix} -\Delta J/3 & 0 & 0 \\ 0 & -\Delta J/3 & 0 \\ 0 & 0 & 2\Delta J/3 \end{pmatrix} \tag{2.30}$$

where

$$\Delta J = J_{||} - J_\perp. \tag{2.31}$$

$J_\perp$ and $J_{||}$ are the perpendicular and parallel components of $\tilde{J}$ with respect to the internuclear vector and $\mathbf{1}$ is the unit tensor. As shown in equation 2.30, $\tilde{J}$ can be broken down into isotropic and anisotropic terms. Due to rapid molecular tumbling the anisotropic term can not be determined from solution NMR. It must be observed using solid-state NMR. Due to the identical spin operators for the dipolar and spin-spin interactions (see eqns. 2.19 and 2.29), ΔJ can only be observed in combination with the dipolar interaction. Therefore, if ΔJ is non-zero, one observes an effective dipolar coupling constant,

$$R_{eff} = R_{DD} - \frac{\Delta J}{3}. \tag{2.32}$$

If a bond length is available from a different technique (*e.g.*, X-ray or neutron diffraction), R_{DD} can be calculated using equation 2.28. Using solid-state NMR it is now possible to measure R_{eff} and therefore obtain a value of ΔJ.[38, 39]

2.1.6 The Quadrupolar Interaction

In this research, the quadrupolar interaction is very important as cobalt is at the centre of all the cobalamins and ^{59}Co, its sole natural isotope, is a quadrupolar nucleus (I = 7/2). The quadrupolar interaction, in general, is large in comparison to the effects of the other NMR interactions. In fact, nuclei with a large quadrupolar constant relative to the Larmor frequency, such as ^{59}Co, need to be dealt with using second order perturbation theory to describe the effect of the quadrupole interaction on the resulting NMR spectra (all of the other NMR interactions have been described using first order perturbation theory).

The nuclear quadrupole moment is due to the asymmetric charge distribution within a nucleus. The other important quantity to consider, when dealing with quadrupolar nuclei, is the electric field gradient (efg) which is the Laplacian of the potential of the electrons surrounding a nucleus. These two couple to give the quadrupolar interaction,

$$\hat{\mathcal{H}}_Q = \frac{eQ}{2I(2I-1)} \hat{\vec{I}} \cdot \tilde{V} \cdot \hat{\vec{I}} \tag{2.33}$$

where $\tilde{V}$ is the efg (or quadrupolar) tensor. $\hat{\mathcal{H}}_Q$ can also be broken down to the first order ($H_Q^{[1]}$) and second order ($H_Q^{[2]}$) perturbation terms as follows:

$$\hat{\mathcal{H}}_Q = H_Q^{[1]} + H_Q^{[2]} \tag{2.34}$$

$$H_Q^{[1]} = \frac{eQ}{4I(2I-1)\hbar} [3\hat{I}_z^2 - I(I+1)] V_{zz} \tag{2.35}$$

$$H_Q^{[2]} = -\frac{1}{\gamma B_o}\left[\frac{eQ}{4I(2I-1)\hbar}\right] \times \left\{(-2(V_{xz}^2 + V_{yz}^2)\hat{I}_z[4I(I+1) - 8\hat{I}_z^2 - 1]) + \left(\frac{1}{2}(V_{xx} - V_{yy})^2 + 2V_{xy}^2)\hat{I}_z[2I(I+1) - 2\hat{I}_z^2 - 1]\right)\right\} \quad (2.36)$$

where V_{ii} are the components of efg tensor. Note that there is an inverse dependence on magnetic field strength in the second order term but no field dependence in the first order term. Thus when studying nuclei with large quadrupolar moments, it is beneficial to perform experiments at multiple magnetic field strengths to study the field effects from the second order perturbation term.

The quadrupolar tensor can be represented in the same fashion as the chemical shielding tensors except ϑ and φ are replaced by θ and ϕ and the σ_{ii} are replaced by eq_{ii} (where eq_{11}, eq_{22}, and eq_{33} are the three principal components of the quadrupolar tensor). The quadrupolar tensor, like the dipolar tensor, is traceless, but it may be non-axially symmetric. In the solid state, the quadrupolar coupling constant, χ (this is a measure of the strength of the quadrupolar interaction) and the asymmetry parameter, η, completely describe the efg tensor.

$$\chi = \frac{eQeq_{33}}{h} \quad (2.37)$$

$$\eta = \frac{eq_{22} - eq_{11}}{eq_{33}} \quad (2.38)$$

The quadrupolar interaction will be important throughout this thesis when studying quadrupolar nuclei directly using single-crystal and/or powder NMR techniques; or indirectly when studying a spin-$\frac{1}{2}$ nucleus in close proximity to a quadrupolar nucleus. In this case residual dipolar effects from the quadrupolar nucleus may be

present in the CPMAS spectrum of the spin-$\frac{1}{2}$ nucleus.

When studying a quadrupolar nucleus with a large quadrupolar tensor, such as ^{59}Co, the only other perturbation of the Zeeman interaction that is important is chemical shielding. This simplifies the nuclear spin Hamiltonian (equation 2.1) to three terms (Z, CS, and Q). Also, when studying a quadrupolar nucleus with a large quadrupolar coupling tensor, usually only the central transition is observable (the satellite transitions are well spread out to high and low frequency of the acquired spectral width). In frequency units, the lineshape equation for the central transition for a nucleus with a large quadrupolar interaction is given as,

$$\nu_{\frac{1}{2}\leftrightarrow-\frac{1}{2}} = \nu_o(\delta_{11}\sin^2\vartheta\cos^2\varphi + \delta_{22}\sin^2\vartheta\sin^2\varphi + \delta_{33}\cos^2\vartheta) - \frac{9\chi^2[I(I+1)-\frac{3}{4}]}{6\nu_o[2I(2I-1)]^2}[A(\phi)\cos^4\theta + B(\phi)\cos^2\theta + C(\phi)] \tag{2.39}$$

where

$$A(\phi) = -\frac{27}{8} - \frac{9}{4}\eta\cos 2\phi - \frac{3}{8}\eta^2\cos^2 2\phi \tag{2.40}$$

$$B(\phi) = -\frac{30}{8} - \frac{1}{2}\eta^2 + 2\eta\cos 2\phi + \frac{3}{4}\eta^2\cos^2 2\phi \tag{2.41}$$

$$C(\phi) = -\frac{3}{8} + \frac{1}{3}\eta^2 + \frac{1}{4}\eta\cos 2\phi - \frac{3}{8}\eta^2\cos^2 2\phi \tag{2.42}$$

It is, however, more convenient to compare the relative orientation of the quadrupolar tensor with respect to the chemical shift tensor. This is done *via* the Euler angles. Figure 2.5 shows the conversion from the polar and azimuthal angles to the Euler angles. To be able to perform such a conversion, the following equations, which were determined using a rotational transformation matrix, $R(\alpha\beta\gamma) =$

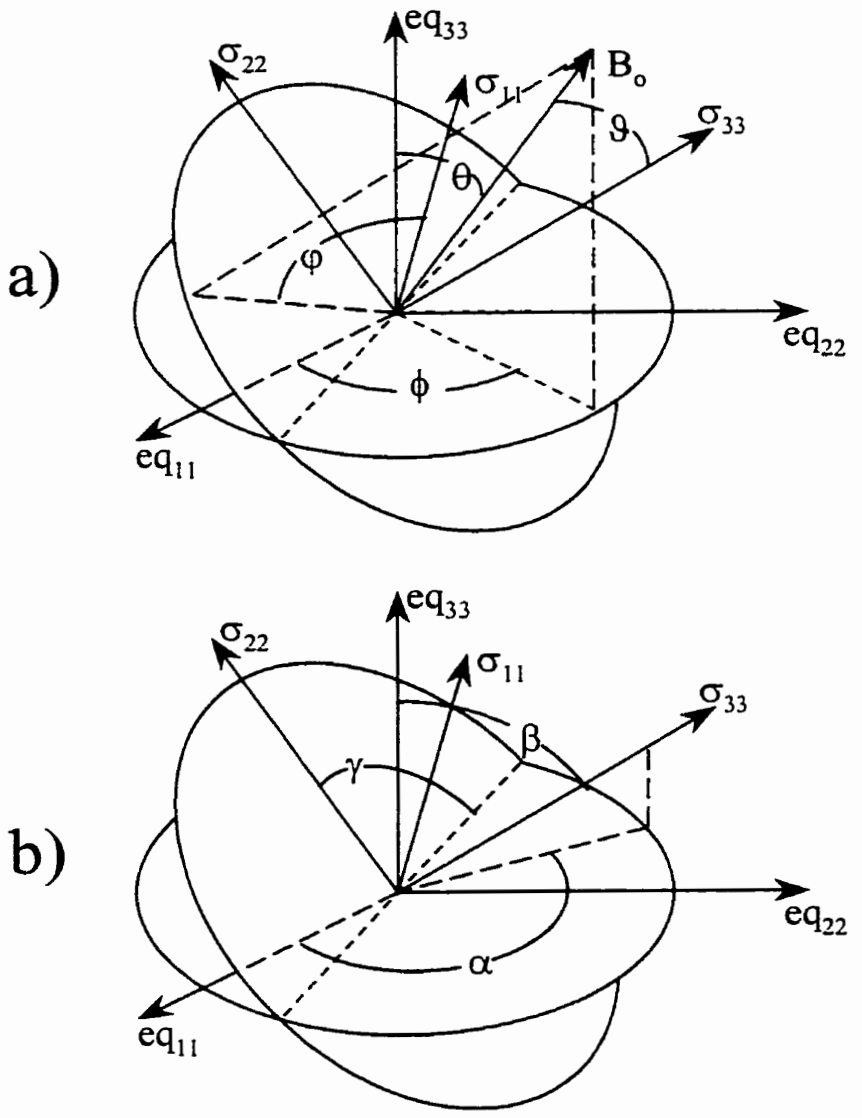

Figure 2.5: a) The magnetic field vector, B_o, is oriented in the PAS of the chemical shift tensor by (ϑ, φ) and in the PAS of the quadrupolar tensor by (θ, ϕ). b) The Euler angles α, β, and γ give the relative orientation of the chemical shift tensor in the PAS of the quadrupolar tensor.

$R_{z'}(\gamma)R_{y'}(\beta)R_z(\alpha)$, are needed.[28]

$$\begin{aligned}
\sin\vartheta\cos\varphi &= \cos\gamma\cos\beta\cos(\phi-\alpha)+\sin\gamma\sin\theta\sin(\phi-\alpha)-\cos\gamma\sin\beta\cos\theta \\
\sin\vartheta\sin\varphi &= -\sin\gamma\cos\beta\sin\theta\cos(\phi-\alpha)+\cos\gamma\sin\theta\sin(\phi-\alpha)+\sin\gamma\sin\beta\cos\theta \\
\cos\vartheta &= \sin\beta\sin\theta\cos(\phi-\alpha)+\cos\beta\cos\theta
\end{aligned} \tag{2.43}$$

Now, if the orientation of one tensor is known in the molecular frame, the orientation of the second tensor is also known through the Euler angles. However, the orientation of either tensor in the molecular frame is not yet determined. Extra information is needed to place either tensor in the molecular frame. Such information can be obtained from a dipolar interaction with an adjacent nucleus, on the basis of the symmetry of the crystal lattice, or from a single-crystal NMR experiment.

2.1.7 The Spin-Rotation Interaction

The spin-rotation interaction arises from the coupling of a molecule's rotational angular momentum, $\mathcal{J}$, to the nuclear spin of nuclei within the molecule,

$$\hat{\mathcal{H}}_{SR} = \tilde{\vec{I}}\cdot\tilde{c}\cdot\mathcal{J} \tag{2.44}$$

where $\tilde{c}$ is the spin-rotation tensor relating $\tilde{\vec{I}}$ and $\mathcal{J}$. If a molecule can rotate, magnetic fields are produced by the circulating electrons which couple with the nuclear spins. As the rate of molecular rotation changes, the rotation field fluctuates and this causes relaxation of the nuclear spins. This interaction is generally important in the gas phase only and therefore will not be discussed any further.

2.2 Single-Crystal NMR

In a single-crystal NMR experiment, NMR spectra are acquired at different orientations of the crystal in the magnetic field. Figure 2.6 gives an example showing how spectra change as a crystal of vitamin B_{12} is rotated. At each orientation, the chemical shifts, quadrupolar shifts, and splittings due to the other NMR interactions are recorded. The shifts and/or splittings are then plotted with respect to the angle from which the experiment was started and this data is fitted using equations described below. The equations used for the fitting can be described by a first order perturbation theory approach for all of the NMR interactions except when the quadrupolar interaction is large. In this case, second order perturbation theory must be used. To obtain a sense of how single-crystal NMR works, a complete derivation of the equations used in single-crystal NMR will be given using first order perturbation theory (which is all that is needed when studying spin-$\frac{1}{2}$ nuclei). This will be followed by a conversion of Volkoff's equations[40] used for second order perturbation theory (needed when studying quadrupolar nuclei with large quadrupolar coupling constants) into modern terms.

2.2.1 First Order Perturbation Theory

For a small quadrupolar interaction, as well as all of the other NMR interactions, NMR can be described using first order perturbation theory. All of the interactions,

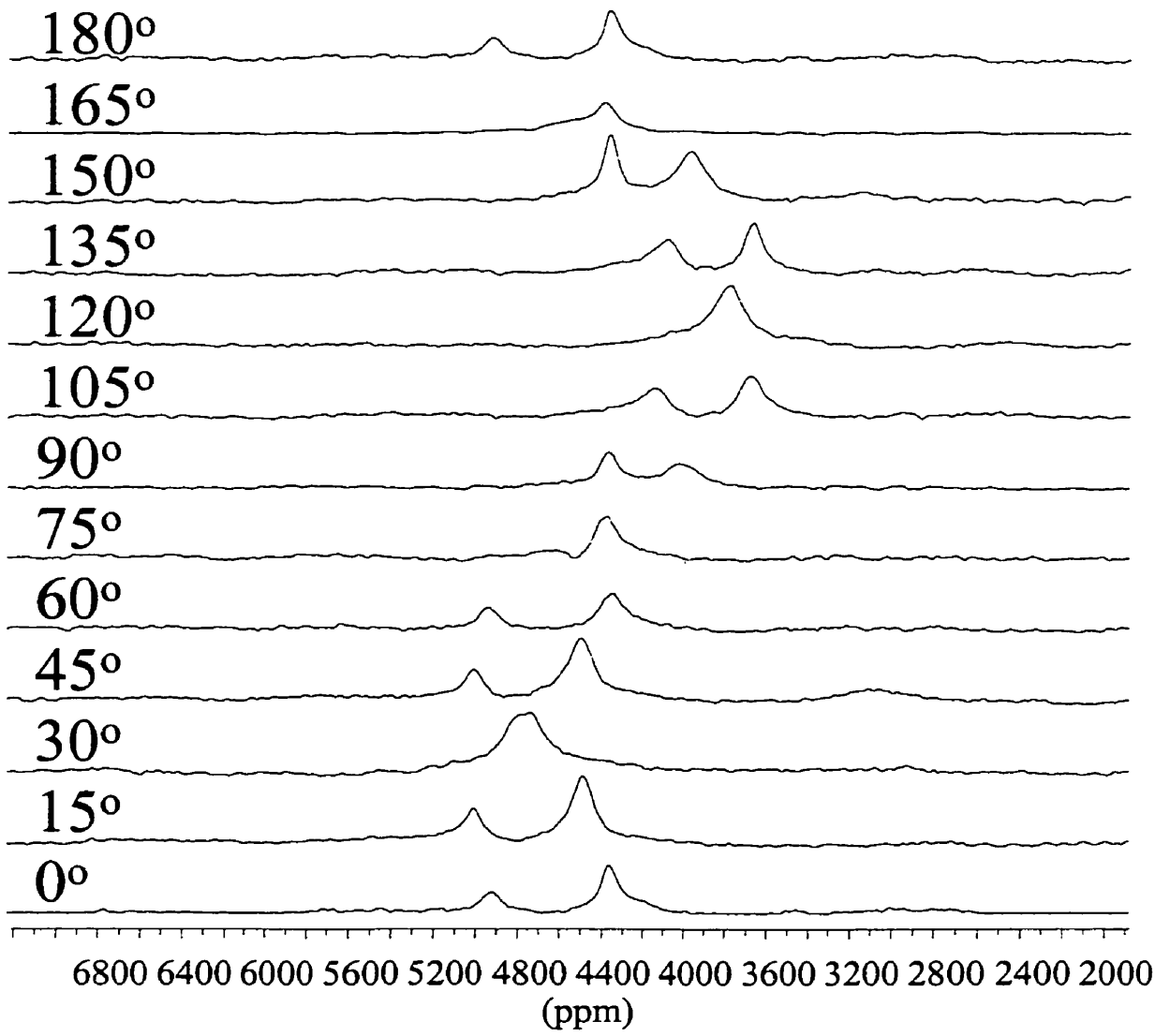

Figure 2.6: Example of single-crystal ^{59}Co NMR spectra of vitamin B_{12} as a function of crystal orientation. The two peaks are due to magnetically non-equivalent sites.

can be represented, generally, by a tensor T.

$$T = \begin{pmatrix} T_{ii} & T_{ij} & T_{ki} \\ T_{ij} & T_{jj} & T_{jk} \\ T_{ki} & T_{jk} & T_{kk} \end{pmatrix} \tag{2.45}$$

Note the unusual labelling of its elements due to the symmetric nature of NMR. If NMR experiments are performed on a single-crystal, the observed frequency (for chemical and second-order quadrupolar shifts) or frequency splitting (for the remaining interactions) can be given as F which is a product of the direction cosines with T.

$$\begin{aligned} F &= \left\{ \begin{pmatrix} \cos\gamma_i & \cos\gamma_j & \cos\gamma_k \end{pmatrix} \begin{pmatrix} T_{ii} & T_{ij} & T_{ki} \\ T_{ij} & T_{jj} & T_{jk} \\ T_{ki} & T_{jk} & T_{kk} \end{pmatrix} \begin{pmatrix} \cos\gamma_i \\ \cos\gamma_j \\ \cos\gamma_k \end{pmatrix} \right\} \\ &= T_{ii}\cos^2\gamma_i + T_{jj}\cos^2\gamma_j + T_{kk}\cos^2\gamma_k + 2T_{ij}\cos\gamma_i\cos\gamma_j + \\ &\quad 2T_{jk}\cos\gamma_j\cos\gamma_k + 2T_{ki}\cos\gamma_k\cos\gamma_i \end{aligned} \tag{2.46}$$

Assuming that the crystal is rotated at an angle of β with respect to B_o through increments of ρ degrees, starting with an i rotation and B_o lies in the ij plane, then the direction cosines of the field with respect to the sample frame are given as follows.

$$cos\gamma_i = cos\beta \tag{2.47}$$

$$cos\gamma_j = sin\beta cos\rho \tag{2.48}$$

$$cos\gamma_j = sin\beta sin\rho \tag{2.49}$$

Substitution of equations 2.47 - 2.49 into 2.46 yeilds F_i as

$$\begin{aligned} F_i &= T_{ii}\cos^2\beta + T_{jj}\sin^2\beta\cos^2\rho + T_{kk}\sin^2\beta\sin^2\rho + 2T_{ij}\cos\beta\sin\beta\cos\rho + \\ & 2T_{jk}\sin^2\beta\sin\rho\cos\rho + 2T_{ki}\cos\beta\sin\beta\sin\rho \end{aligned} \tag{2.50}$$

F_i can be rearranged and written in terms of cosρ and cos2ρ.

$$F_i = A_i + B_i\cos\rho + C_i\sin\rho + D_i\cos 2\rho + E_i\sin 2\rho \tag{2.51}$$

where

$$A_i = \frac{1}{2}\sin^2\beta(T_{jj} + T_{kk}) + \cos^2\beta T_{ii} \tag{2.52}$$

$$B_i = 2\sin\beta\cos\beta T_{ij} \tag{2.53}$$

$$C_i = 2\sin\beta\cos\beta T_{ik} \tag{2.54}$$

$$D_i = \frac{1}{2}\sin^2\beta(T_{jj} - T_{kk}) \tag{2.55}$$

$$E_i = \sin^2\beta T_{jk} \tag{2.56}$$

If β is set to 90° (*i.e.*, the crystal is rotated perpendicular to B_o), F_i is further simplified to

$$F_i = \frac{1}{2}(T_{jj} + T_{kk}) + \frac{1}{2}(T_{jj} - T_{kk})\cos 2\rho + T_{jk}\sin 2\rho \tag{2.57}$$

Therefore, to completely determine the orientation dependence of NMR interactions, three perpendicular rotations (x, y, $z = i$, j, k) must be performed to obtain all nine components of T. The tensor can then be diagonalized to obtain the principal components as well as the direction cosines (orientation dependence) of the tensor in the crystal frame.

2.2.2 Second Order Perturbation Theory

When studying a nucleus with a large quadrupolar interaction (such as ^{59}Co), second order perturbation theory must be considered when doing single-crystal NMR experiments. Volkoff[40] was the first to describe the importance of second order effects when studying quadrupolar nuclei. In the following equations, only the quadrupolar interaction was considered because the chemical shift interaction was insignificant with respect to it in Volkoff's study of ^{27}Al.[41] The frequency of the central transition, ν_x, of an x-rotation is given as

$$\nu_x = n_x + p_x \cos 2\theta_x + r_x \sin 2\theta_x + u_x \cos 4\theta_x + v_x \sin 4\theta_x \tag{2.58}$$

where

$$n_x = \frac{1}{576\nu_o}(18c_2a_x^2 + (c_2 - 4c_1)(b_x^2 + c_x^2) + 4(c_2 - c_1)(c_y^2 + c_z^2)) \tag{2.59}$$

$$p_x = \frac{1}{576\nu_o}(-12c_2a_xb_x + 4(c_2 + c_1)(c_y^2 - c_z^2)) \tag{2.60}$$

$$r_x = \frac{1}{576\nu_o}(-12c_2a_xc_x + 8(c_2 + c_1)c_yc_z) \tag{2.61}$$

$$u_x = \frac{1}{576\nu_o}(c_2 + 4c_1)(b_x^2 - c_x^2) \tag{2.62}$$

$$v_x = \frac{1}{576\nu_o}(c_2 + 4c_1)2b_x c_x \tag{2.63}$$

The coefficients a_x, b_x, c_x, c_y, and c_z are dependent on the principal components of the quadrupolar tensor given as

$$a_x = \frac{\nu_o\lambda(\phi_{yy} + \phi_{zz})}{eq} \tag{2.64}$$

$$b_x = \frac{\nu_o\lambda(\phi_{yy} - \phi_{zz})}{eq} \tag{2.65}$$

$$c_x = \frac{-2\nu_o\lambda\phi_{yz}}{eq} \tag{2.66}$$

$$c_y = \frac{-2\nu_o\lambda\phi_{zx}}{eq} \tag{2.67}$$

$$c_z = \frac{-2\nu_o\lambda\phi_{xy}}{eq} \tag{2.68}$$

c_1 and c_2 are functions of I and m_I given as

$$c_1 = 4((I + \frac{3}{2})(I - \frac{1}{2}) - 6(m_I - \frac{1}{2})^2) \tag{2.69}$$

$$c_2 = 2((I + \frac{3}{2})(I - \frac{1}{2}) - 3(m_I - \frac{1}{2})^2) \tag{2.70}$$

and

$$\lambda = \frac{3C_z}{2I(2I-1)\nu_o} \tag{2.71}$$

$$C_z = \frac{eQ\phi_{zz}}{h} \tag{2.72}$$

Substitution of equations 2.71 and 2.72 into equation 2.64 gives

$$a_x = \frac{3eQ}{2I(2I-1)h}(\phi_{yy} + \phi_{zz}) \tag{2.73}$$

This equation can be re-written in modern terms as

$$a_x = 3(Q_{yy} + Q_{zz}) \tag{2.74}$$

where

$$Q_{\alpha\beta} = \frac{eQ\phi_{\alpha\beta}}{2I(2I-1)h}. \tag{2.75}$$

Likewise, equations 2.65 - 2.68 can be written as

$$b_x = 3(Q_{yy} - Q_{zz}) \tag{2.76}$$

$$c_x = -6Q_{yz} \tag{2.77}$$

$$c_y = -6Q_{zx} \tag{2.78}$$

$$c_z = -6Q_{xy} \tag{2.79}$$

Since only the central transition is observed for large quadrupolar nuclei, $m_I = \frac{1}{2}$ and c_1 and c_2 can be simplified to

$$c_1 = -(3 - 4I(I+1)) \tag{2.80}$$

$$c_2 = -\frac{1}{2}(3 - 4I(I+1)) = \frac{c_1}{2} \tag{2.81}$$

Substitution of equations 2.74 - 2.81 into Volkoff's equation (2.58), the following five coefficients (A - E) are given as

$$A_x = \frac{q}{8}(-11(Q_{yy}^2 + Q_{zz}^2) - 50Q_{yy}Q_{zz} + 28Q_{yz}^2 + 16(Q_{zx}^2 + Q_{xy}^2)) \tag{2.82}$$

$$B_x = \frac{3q}{2}(Q_{yy}^2 - Q_{zz}^2 + 4Q_{zy}^2 - 4_{zx}^2) \tag{2.83}$$

$$C_x = -3q((Q_{yy} + Q_{zz})Q_{zy} + 4Q_{zx}Q_{zy}) \tag{2.84}$$

$$D_x = \frac{-9q}{8}((Q_{yy} - Q_{zz})^2 - 4Q_{yz}^2) \tag{2.85}$$

$$E_x = \frac{9q}{2}(Q_{yy} - Q_{zz})Q_{zy} \tag{2.86}$$

where

$$q = \frac{3 - 4I(I+1)}{16\nu_o} \tag{2.87}$$

To modify these equations to include the chemical shielding interaction, the chemical shift terms (under first order perturbation theory as in 2.2.1) simply can be added to these equations. Below are the equations used to study a quadrupolar nucleus which also has a non-zero chemical shift tensor (using the same sense of x, y, z = i, j, k as above).

$$F_i = A_i + B_i \cos 2\rho + C_i \sin 2\rho + D_i \cos 4\rho + E_i \sin 4\rho \tag{2.88}$$

where

$$A_i = \frac{q}{8}(-11(Q_{jj}^2 + Q_{kk}^2) - 50Q_{jj}Q_{kk} + 28Q_{jk}^2 + 16(Q_{ki}^2 + Q_{ij}^2)) + \frac{1}{2}(\delta_{jj} + \delta_{kk})\nu_o \tag{2.89}$$

$$B_i = \frac{3q}{2}(Q_{jj}^2 - Q_{kk}^2 + 4Q_{ij}^2 - 4_{ki}^2) + \frac{1}{2}(\delta_{jj} - \delta_{kk})\nu_o \tag{2.90}$$

$$C_i = -3q((Q_{jj} + Q_{kk})Q_{jk} + 4Q_{ki}Q_{ij}) + \delta_{jk}\nu_o \tag{2.91}$$

$$D_i = \frac{-9q}{8}((Q_{jj} - Q_{kk})^2 - 4Q_{jk}^2) \tag{2.92}$$

$$E_i = \frac{9q}{2}(Q_{jj} - Q_{kk})Q_{jk} \tag{2.93}$$

$$q = \frac{3 - 4I(I+1)}{16\nu_o} \tag{2.94}$$

$Q_{\alpha\beta}$ and $\delta_{\alpha\beta}$ are components of the quadrupolar and chemical shift tensors, and ν_o is the Larmor frequency. Similar to first order perturbation theory, rotations about three perpendicular axes need to be performed to obtain the nine components of the quadrupolar and chemical shift tensors.

The results that come out from the analysis described above will result in a quadrupolar tensor that does not include the spin of the quadrupolar nucleus being studied. To obtain a value for χ in the usual convention, a nuclear spin factor of 2I(2I-1) must be taken into account. Since ^{59}Co has an I value of $\frac{7}{2}$, the spin factor of 42 must be included in the analysis of the single-crystal NMR data.

2.3 Experiments at the Magic Angle

2.3.1 Single-Crystal NMR at the Magic Angle

In single-crystal NMR, we are not limited to crystal rotations at 90° with respect to B_o. One convenient method would be to do single-crystal NMR in a standard CPMAS (cross polarization with magic angle spinning) probe which is available

in all standard solid-state NMR laboratories. Thus, instead of the result shown in equation 2.57 where $\beta = 90^o$ was substituted into equation 2.51, we substitute the value of β equal to the magic angle (54.74^o or $\cos^{-1}(\frac{1}{\sqrt{3}})$) into equation 2.51 to obtain the following result for a first-order NMR interaction.

$$F_i = \frac{1}{3}(T_{ii} + T_{jj} + T_{kk}) + \frac{2}{3}(\sqrt{2}T_{ij}cos\rho + \sqrt{2}T_{ik}sin\rho + \frac{1}{2}(T_{jj} - T_{kk})cos2\rho + T_{jk}sin2\rho) \tag{2.95}$$

From this one rotation it is immediately obvious that all 6 components of a general tensor are contained in the 5 parameters. Thus only two rotations would be needed to fully determine the magnitude and orientation of the tensor. It would also be possible to just do one rotation and use that information in combination with a static powder or magic angle spinning NMR experiment to completely determine the orientation of the tensor. The main advantage of performing single-crystal NMR at the magic angle *vs.* perpendicular to the magnetic field is that a specialized single-crystal probe or special inserts for a solenoid probe are not needed where a MAS probe is already available.

2.3.2 NMR While Spinning Samples at the Magic Angle

In the single-crystal experiments described above, spectra were acquired at specific orientations of a crystal. However, it is not always possible to obtain large enough single-crystals to perform such NMR experiments. In such cases, powder and/or magic angle spinning (MAS) experiments are useful techniques to study solids. In powders all possible orientations of molecules are present and broad lines are ob-

served. To narrow these lines, MAS can be used to average many NMR interactions. In MAS, as in static NMR, all possible orientations of a crystal are present. However, we can look at the effects of magic angle spinning on a single-crystal and by analogy get an understanding of a non-crystalline (or multi-crystalline) sample as a whole.

In MAS experiments, samples are spun rapidly about the magic angle described above. When spinning occurs, ρ in equation 2.95 becomes time dependent and thus we must replace ρ with ω_rt (where ω_r is the rotation rate and t is time).

$$F_i = T_{iso} + \frac{2}{3}(\sqrt{2}T_{ij}cos\omega_r t + \sqrt{2}T_{ik}sin\omega_r t + \frac{1}{2}(T_{jj} - T_{kk})cos2\omega_r t + T_{jk}sin2\omega_r t) \quad (2.96)$$

Here T_{iso} is the isotropic (non-angular dependent) term ($\frac{1}{3}(T_{ii} + T_{jj} + T_{kk}) = T_{iso}$), known as the isotropic or average value of the tensor. As a sample is spun at the magic angle, T_{iso} is always observed. The angular dependent terms give rise to lines that are at frequencies spaced at intervals of $\omega_r/2\pi$ from T_{iso}. As the spinning rate increases, the centerband (T_{iso}) becomes more intense and the sidebands become less dominant. When the spinning speed is as large as the strength of the NMR interaction, only T_{iso} is observed. Herzfeld and Berger[42] developed a method to use the intensity distribution at different spinning speeds to elucidate the chemical shift tensor, thus, sidebands can be useful to study NMR interactions. For a more detailed description, the following readings are suggested.[42, 43, 44]

Chapter 3

Single-Crystal Cobalt-59 NMR of Vitamin B_{12}

3.1 Introduction

This chapter describes the first single-crystal NMR study of a biological metal. We have completed a single-crystal ^{59}Co NMR on cyanocobalamin (vitamin B_{12}). Before discussing this data, a brief description of single-crystal NMR in general and previous single-crystal NMR ^{59}Co NMR studies on inorganic complexes will be presented.

The best technique available to the NMR spectroscopist to obtain the orientation dependence of NMR interactions unambiguously at a nuclear site is single-crystal NMR. In this experiment, spectra are recorded as a function of the orientation of a crystal in the magnetic field. From the data obtained in this experiment, information concerning the local structure around the nuclear site can be elucidated.

The first report of single-crystal NMR dates back to one of the most significant early structure determinations of water in a seminal NMR paper. In 1948, Pake reported the single-crystal ^{1}H NMR of gypsum ($CaSO_4 \cdot 2H_2O$).[34] In this paper, he was able to characterize the distance between the two protons of a given water molecule (*via* the dipolar interaction) to be 1.58 Å and therefore an O-H distance of 0.98 Å using a bond angle of 108° from the crystal structure.[45] This early low field experiment (0.682 T or 50.5 MHz for ^{1}H) illustrated the power of NMR to the scientific community.

The first single-crystal ^{59}Co NMR study was reported in 1969 by Spiess, Hass, and Hartman and contained the chemical shift and quadrupolar coupling tensors of five cobalt(III) complexes.[46] These complexes were all simple inorganic salts. The next three papers on single-crystal ^{59}Co NMR were reported by Sheline and co-workers.[47, 48, 49] The cobalt complexes in these studies were all cobalt-carbonyl complexes with large quadrupolar coupling constants (ranging from 89.3 MHz to 159.88 MHz). In 1974, Reynhardt published two papers on single-crystal ^{59}Co NMR on $[Co(NH_3)_6]Cl_3$ and $Co(acac)_3$.[50, 51] All of the single-crystal ^{59}Co NMR studies mentioned above were performed at low magnetic field strengths (maximum of 1.6 T), therefore the precision of the experiments was low with respect to the chemical shift tensors.

The next single-crystal ^{59}Co NMR study did not come out until 1997 where $Co(acac)_3$ was reinvestigated at 9.4 T by Wasylishen and co-workers.[52] In this study, two magnetically distinct cobalt sites of this crystal were observed. All of the transitions (central and satellites) could be followed during rotations of the

crystal. Since the satellite splittings were due solely to the quadrupolar interaction, the quadrupolar coupling tensor was determined independently. This interaction was taken into account in terms of its effects on the central transition and the chemical shift tensor was determined. These new results did not agree well with those of Reynhardt,[51] but those in Wasylishen's report give a more reasonable determination of both the quadrupolar coupling and chemical shift tensors.

When studying quadrupolar nuclei that are in sites of low crystallographic symmetry, hence large quadrupolar coupling, generally only the central transition can be observed in the NMR spectra. As described in section 2.2.2 of this thesis, both the chemical shift and quadrupolar coupling interactions can be determined completely by following the central transition alone.[40] Jakobsen's group[53] have described how a solenoid NMR probe with an additional homemade insert could be used to acquire single-crystal NMR data.

In this chapter the results of a single crystal ^{59}Co NMR experiment are described. A solenoid probehead using a homemade goniometer designed after that of Jakobsen was used. Due to the large quadrupolar coupling constant in vitamin B_{12}, only the central transition was observed. This is the first single-crystal NMR study of a quadrupolar metal in a biologically relevant molecule (vitamin B_{12}) reported in the literature.

3.2 Theory

As described in Chapter 2, when studying a nucleus with a large quadrupolar interaction, second order perturbation theory must be used to interpret the spectra.

Therefore, to understand the single-crystal ^{59}Co NMR spectra of the cobalt centre of vitamin B_{12}, equations 2.88 - 2.94 must be used for the analysis of the results of the rotations about the three orthogonal rotation axes (i, j, k = x, y, z). To compare the results of these single crystal NMR experiments with other literature values, all of the chemical shift values can be related directly, but to compare the quadrupolar results to quadrupolar coupling constants reported in the literature, the nuclear spin factor of equation 2.75 (2I(2I-1)) must be taken into account. For ^{59}Co (I = 7/2) this factor is 42.

3.3 Experimental

3.3.1 The Crystal

A single-crystal of vitamin B_{12} (Sigma) was grown from an aqueous solution over approximately six months. The crystal (2.6 mm × 1.9 mm × 1.1 mm) was coated with epoxy to prevent dehydration. The crystal was then indexed by single-crystal X-ray diffraction and the cell dimensions agreed with those originally reported by Hodgkin[11] (space group of $P2_12_12_1$, z = 4, with cell parameters of a = 15.92 Å, b = 22.32 Å, and c = 25.33 Å; a and c are permuted from the original report due to the modern convention of crystal indexing). Figure 3.1 reveals the crystal indices as well as the dimensions. This crystal was then mounted on a brass slide for the NMR experiments.

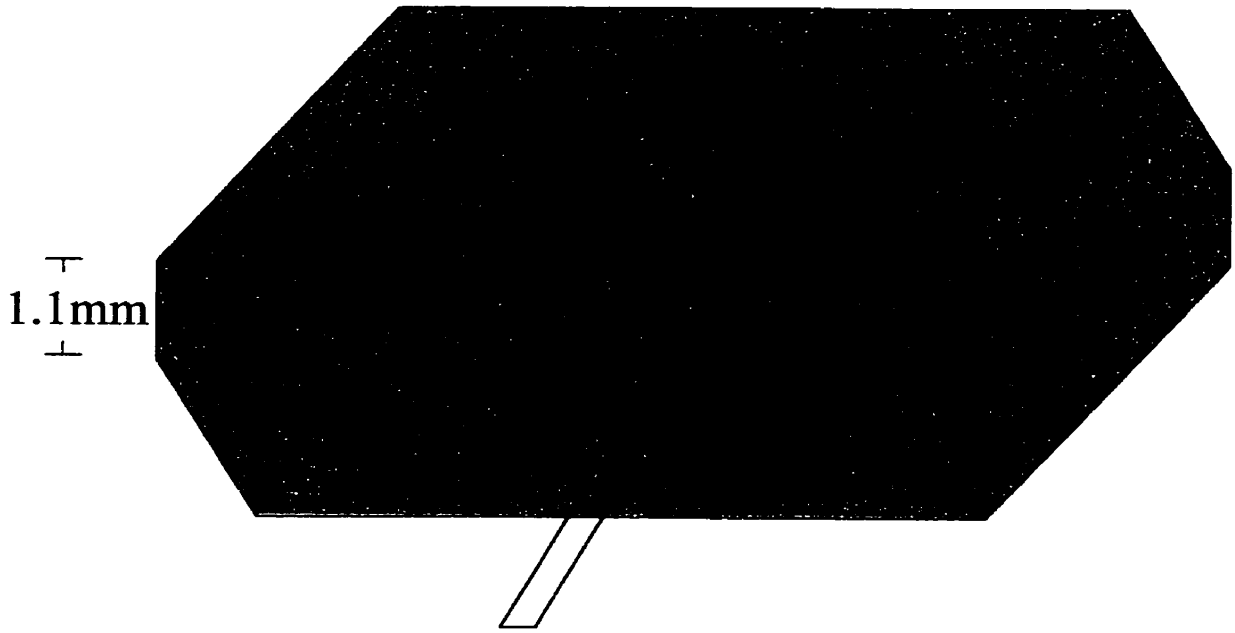

Figure 3.1: Crystal of vitamin B_{12} used in the single-crystal ^{59}Co NMR experiments.

3.3.2 NMR Experiments

All ^{59}Co NMR spectra were acquired on a Bruker AMX-500 NMR spectrometer (B_o = 11.75 T) which corresponds to a ^{59}Co Larmor frequency of 118.67 MHz. The ^{59}Co chemical shifts were referenced to the cobalt standard (1.0 M $K_3[Co(CN)_6]$ (aq)) at 0 ppm. The typical sweep width was 1 MHz (dwell time = 0.5 μs) therefore pulses were kept short (0.8 - 1.0 μs where the 90° pulse was 3.3 μs) to ensure excitation over the entire spectrum. A recycle time of 50 ms was used between the collection of 1024 data points for each scan and 153 600 - 921 600 (150 k - 900 k) scans were collected for each orientation of the crystal depending on sensitivity (2 - 12 hours per experiment).

3.3.3 Single-Crystal NMR

The spectra were acquired using a single-channel Bruker wide-line solenoid probe with a home-built goniometer insert containing the vitamin B_{12} crystal. The goniometer, shown in Figure 3.2, was modeled after that of Vosegaard.[53] The upper goniometer in Figure 3.2 was used for rotations x and z, while the lower was used for rotation y. In all cases, the crystal was kept attached to the Teflon goniometer using two-sided tape. Single-crystal ^{59}Co NMR spectra were acquired as a function of goniometer rotation in increments of 15°. The chemical shifts (in frequency units) were then plotted as a function of crystal orientation and fitted using equation 2.88 with Microsoft Excel97 to obtain the coefficients A - E for each of the rotations (for a total of 15 coefficients).

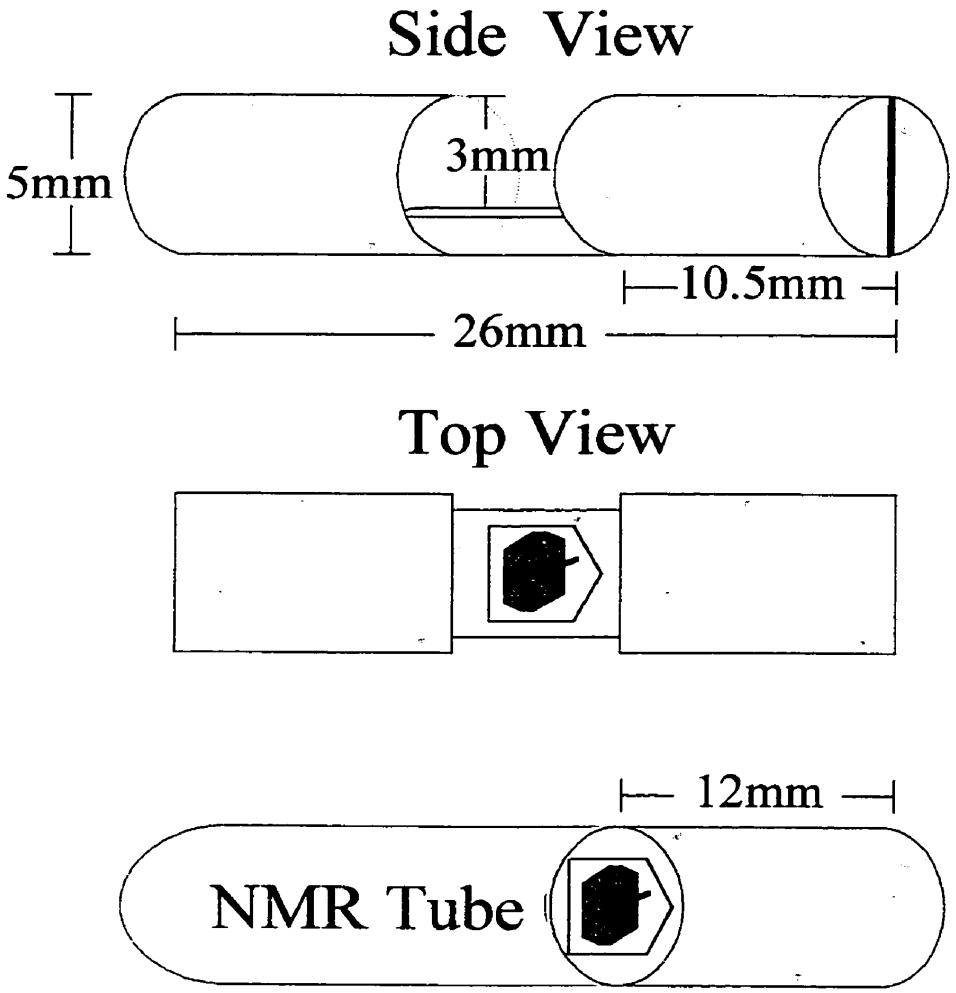

Figure 3.2: Goniometers designed to be used for single-crystal NMR experiments at 11.75 T. The upper goniometer shows the orientation of the crystal for rotation x, rotation y is shown on the lower goniometer, and rotation z was obtained using the upper goniometer but the crystal was at 90° from that shown.

3.4 Results

Vitamin B_{12} crystallizes from aqueous solution in the orthorhombic space group $P2_12_12_1$ (D_4^2, no. 19). All of the cobalt sites in this space group are crystallographically equivalent related *via* 2-fold screw axes. This condition makes all of the cobalt sites magnetically distinct (magnetic equivalence only occurs when nuclei are related by a centre of inversion) and will give four NMR signals.[26] However, if an NMR experiment is performed when the rotation axis is one of the crystallographic axes (a, b, or c), the three dimensional space group reduces to two dimensions. This two dimensional space group, p2gg, does have an inversion relation such that there are two pairs of nuclei and thus, two NMR signals are observed when performing experiments in such a rotation. This is the case for the results seen previously in Figure 2.6. The x rotation in this study was performed about the a-axis (100) and, therefore, only two distinct cobalt sites are observed. In this rotation, at angles of 30° and 120°, only one peak is observed. This is due to a special projection when the crystallographic c- (for 30°) and b-axes (for 120°) are directed along the magnetic field. In such cases, complete coincidence of the signals arises. These special projections permitted spectral assignment of the crystal axes to within 1°, substantially reducing any indeterminate error resulting from the mounting of the crystal.

The crystal was oriented in the goniometer such that the x, y, z, rotation axes correspond to the 100, 021, and $0\bar{2}5$ directions, respectively. As already described, only two signals are observed for rotation x due to symmetry constraints. For the other two rotations, four signals always should have been observed. The results,

shown in the form of rotation plots in Figure 3.3, include the special projections described above. In this figure, as stated, only two signals were observed in rotation x, four signals are observed in rotation y, but only three signals were observed in rotation z. This observation of three signals in rotation z is fortuitous. Two of the sites are very similar in rotation z and their spectra overlap extensively, but not due to any crystal symmetry constraint. This point will be discussed further below. The lines in this figure indicate the "best-fit" results obtained using a least-squares regression analysis of equation 2.88.

The ^{59}Co NMR signals from the single crystal gave relatively narrow lines (4 - 10 kHz) compared to the overall range of frequencies observed in the experiments (approximately 240 kHz or 2000 ppm). The frequencies of the peaks, F (in Hz), as a function of the rotation angle, ρ (in degrees), about each of the rotation axes (i, j, $k = x, y, z$) are given in Appendix A. These frequencies were subjected to a linear least-squares fit to equation 2.88, the results of which are given in Figure 3.3. In single crystal NMR, the $\rho = 90°$ frequencies of a given rotation must equal those of the $\rho = 0°$ frequencies of the next rotation (*i.e.*, 90° for x rotation = 0° for the y rotation, $y(90°) = z(0°)$, and $z(90°) = x(0°)$). To get these end points to match, a phase angle of -6.8° is required for the x rotation and -4.7° for the z rotation. The phase angles are added to correct for small errors in the alignment of the crystal in the goniometer at the beginning of each set of rotations. The best fit parameters of the fits seen in Figure 3.3 are given in Table 3.1.

Using the 15 variables obtained from the fits of each site, the chemical shift and quadrupolar tensors can be obtained for the cobalt nuclei in the x, y, z axis

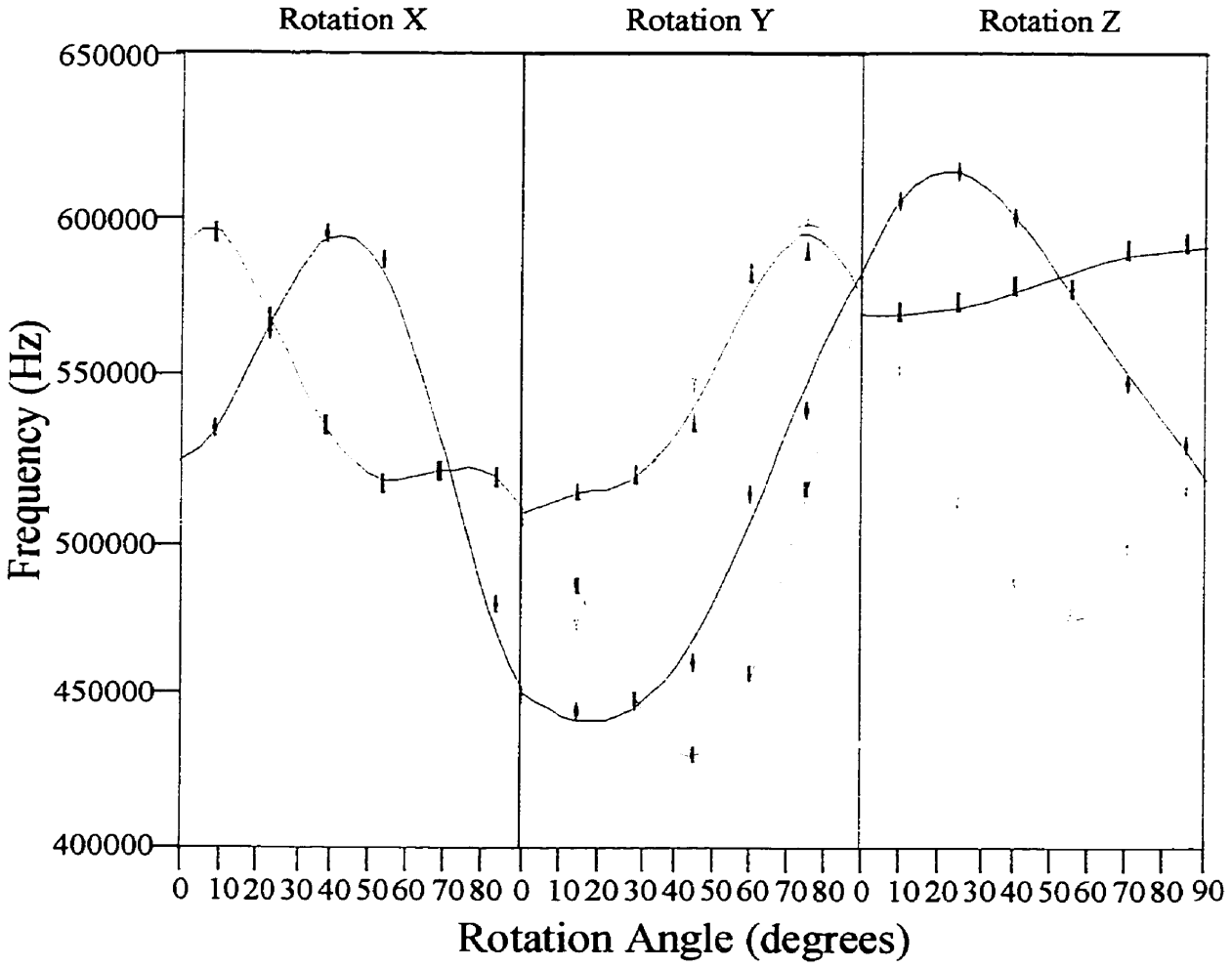

Figure 3.3: Plots of ^{59}Co NMR frequency *vs.* rotation angle for each of the three rotations in the single crystal experiments of vitamin B_{12}. The dotted lines result from a linear least squares fit to equation 2.88. Rotation x show the crystal orientation at which the crystallographic b- and c-axes (special projections where all of the sites give the same shift) are directed along B_o.

Table 3.1: Best-fit parameters for the ^{59}Co single-crystal NMR experiments (values in Hz with errors given in parentheses).

	Rotation x	Rotation y	Rotation z
site 1			
A	515 889 (1 581)	511 134 (1 481)	539 082 (576)
B	36 164 (2 076)	-66 318 (2 028)	32 005 (790)
C	45 426 (2 195)	-40 980 (2 159)	63 036 (839)
D	-31 046 (2 097)	4 763 (2 028)	10 324 (794)
E	-10 528 (2 175)	5 075 (2 158)	6 908 (834)
site 2			
A	516 184 (1 025)	510 546 (953)	579 572 (912)
B	42 884 (1 409)	-32 671 (1 305)	-10 433 (1 252)
C	39 390 (1 490)	-54 233 (1 390)	-2 923 (1 328)
D	34 171 (1 424)	27 593 (1 305)	-718 (1 258)
E	-5 350 (1 476)	16 492 (1 390)	-798 (1 322)
site 3			
A	516 184 (1 025)	511 169 (908)	579 572 (912)
B	42 884 (1 409)	-32 009 (1 243)	-10 433 (1 252)
C	39 390 (1 490)	53 281 (1 323)	2 923 (1 328)
D	34 171 (1 424)	27 619 (1 243)	-718 (1 258)
E	-5 350 (1 476)	-15 647 (1 323)	798 (1 322)
site 4			
A	515 889 (1 511)	512 105 (1 790)	541 395 (1 345)
B	36 164 (2 076)	-65 170 (2 451)	29 890 (1 844)
C	45 426 (2 195)	41 538 (2 609)	-55 548 (1 957)
D	-31 046 (2 097)	3 693 (2 451)	9 993 (1 854)
E	-10 528 (2 175)	-6 061 (2 689)	-7 981 (1 948)

system for the goniometer. A complete description of the analysis of site 3 is included in Appendix B. This appendix also includes a complete error analysis for this site using methods described by Prof. R. LeRoy.[54] Diagonalization of the chemical shift tensor provides the principal components of the chemical shift tensor (as Eigenvalues) as well as the orientation of the tensor in the goniometer reference frame (as Eigenvectors). The principal components of the chemical shift tensor were found to be $\delta_{11} = 5075 \pm 45$ ppm, $\delta_{22} = 4670 \pm 43$ ppm, and $\delta_{33} = 3902 \pm 42$ ppm. Likewise, the quadrupolar tensor can be diagonalized to obtain the principal components and the orientation of the tensor. The usual convention is to deal with χ and η when discussing a quadrupolar tensor. The values of these quantities from this study are $\chi = 27.31 \pm 0.08$ MHz and $\eta = 0.243 \pm 0.005$. Knowledge of the orientation of the unit cell with respect to the goniometer reference frame by indexing the crystal prior to the NMR experiments permitted the assignment of the principal axis systems of the chemical shift and quadrupolar tensor to discrete directions with respect to the molecular structure of vitamin B_{12}. However, each NMR site must be assigned to the appropriate crystallographic site. The differences in the three rotation patterns provided the information needed for this problem. In rotation z, only one of the pairs of sites that were related in rotation x were magnetically similar; the other pair of sites was readily resolved as two independent peaks. Inspection of the crystal structure for this orientation of the crystal revealed that one pair of sites conserved a pseudo-twofold rotation about B_o for all crystal orientations within rotation z; these crystallographic sites could be assigned to specific sets of spectral lines by symmetry. The assignments of the four sites are

given in Figure 3.4.

Assignment of crystallographic sites to spectroscopic sites permits determination of the orientation of the quadrupolar and chemical shift tensors with respect to the molecular framework of vitamin B_{12}. The results from this process on the vitamin B_{12} crystal sites are given in Table 3.2. Two views of a vitamin B_{12} molecule are given in Figures 3.5 and 3.6 which show the results from Table 3.2 pictorially. These views allow for a three dimensional sense of the orientation of the two tensors of interest in this study. The top view looks down the CoCN axis of the molecule; the side view looks approximately perpendicular to the CoCN bond (approximately 80° with respect to the top view). The two tensor interactions shown are centrosymmetric so each tensor could be represented by a full inversion of each axis through the cobalt site. For the chemical shift tensor, the analysis only yields a centrosymmetric tensor, because, as described in section 2.1.3, only the symmetric part of this nonsymmetric tensor is directly observable.

The quadrupolar coupling constant, χ, for ^{59}Co was found to be significantly large (27.31 MHz). The largest component of the electric field gradient at the cobalt sites lies very close (9.6°) to the the C-N(benzimidazole) bond. This direction is also approximately along the the Co-CN bond (since the tensor is centrosymmetric). In either case, this is approximately perpendicular to the corrin ring plane which places the two minor components of the quadrupolar coupling tensor in the corrin ring plane. These components are not identical (as apparent from Table 3.2) and the quadrupolar coupling is slightly nonaxially symmetric with an η of 0.243. This is a reflection of the nonsymmetrical nature of the corrin ring surrounding the cobalt

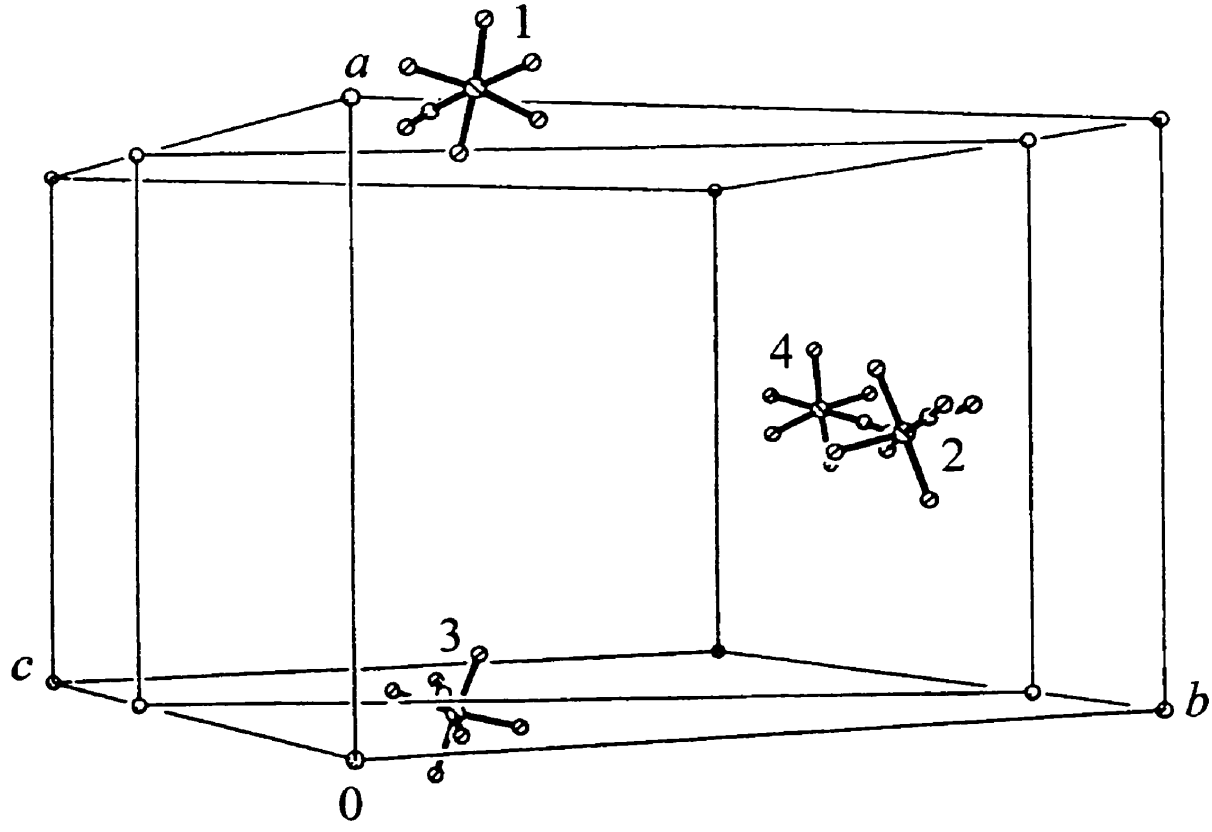

Figure 3.4: View of the four sites of vitamin B_{12} relevant to the z rotation $(0\bar{2}5)$. The structure has been simplified and only the core nuclei (Co, five N bonded to Co, and the CN group) are given for clarity of the B_{12} sites. Assignments of each of the NMR-characterized sites to their respective crystallographic sites are indicated. The plane perpendicular to the z-direction is superimposed on the unit cell, showing that two molecules are positioned such that the nitrogens of the corrin ring lie approximately in this plane.

Table 3.2: Quadrupolar coupling (Q_{ii}, i = 1, 2, 3) and chemical shift (δ_{ii}, i = 1, 2, 3) tensors in the crystal axis system (a, b, c) for vitamin B_{12} (crystal axes in modern convention showing the principal components and the direction cosines of each tensor).

Quadrupolar Coupling (kHz)			Chemical Shift (ppm)		
-404.0 (2.5)	-246.3 (2.3)	650.3 (1.8)	5075 (45)	4670 (43)	3902 (42)
0.302 (0.007)	0.355 (0.005)	-0.885 (0.002)	-0.796 (0.038)	-0.117 (0.036)	-0.594 (0.060)
0.766 (0.005)	0.462 (0.007)	0.447 (0.003)	-0.384 (0.030)	-0.661 (0.055)	0.645 (0.055)
0.576 (0.003)	-0.813 (0.002)	-0.132 (0.001)	-0.476 (0.018)	0.742 (0.065)	0.481 (0.028)

For complete error analysis, see Appendix B.

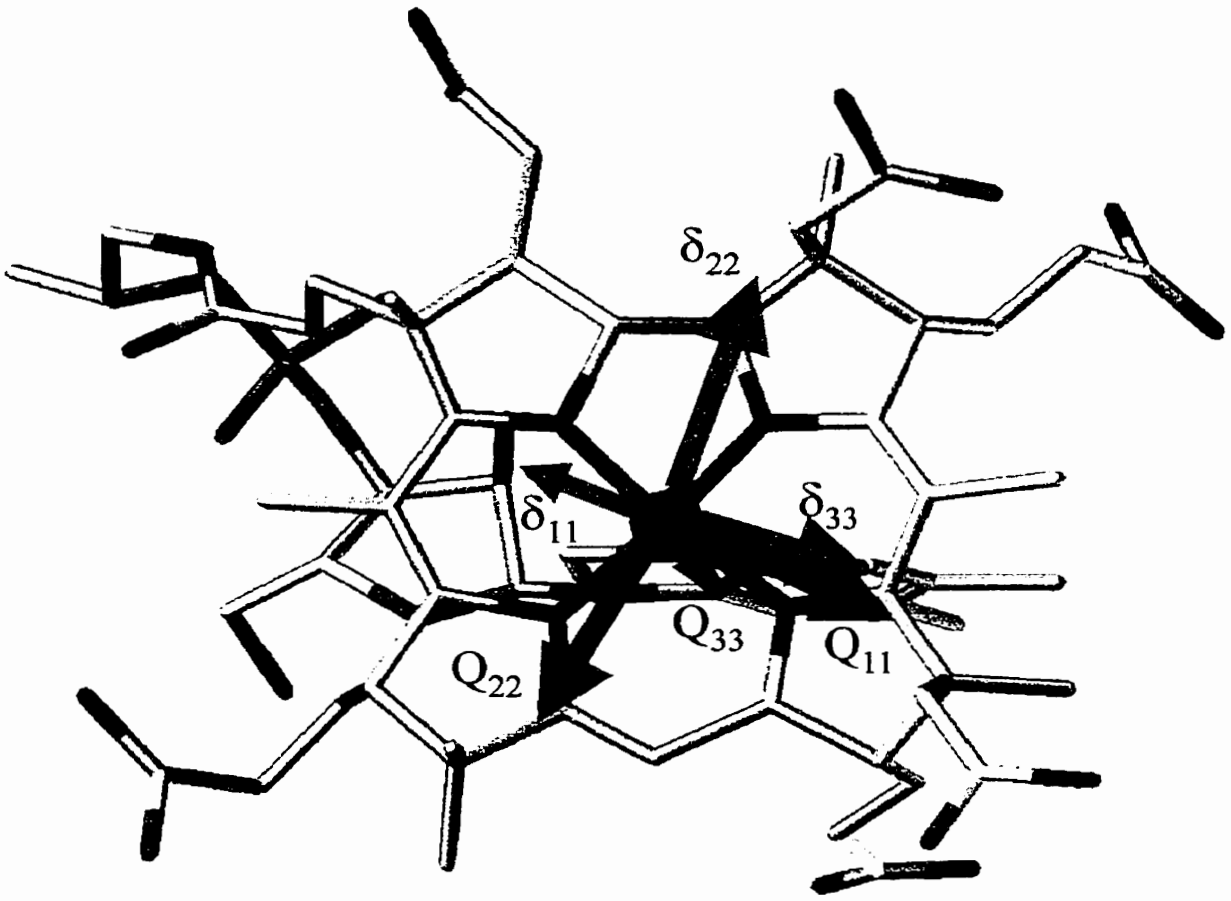

Figure 3.5: Molecular structure of vitamin B_{12} (from reference [11]) with the orientation of the principal components of the quadrupolar coupling (blue) and chemical shift (green) tensors superimposed on a view looking down the NCCo axis.

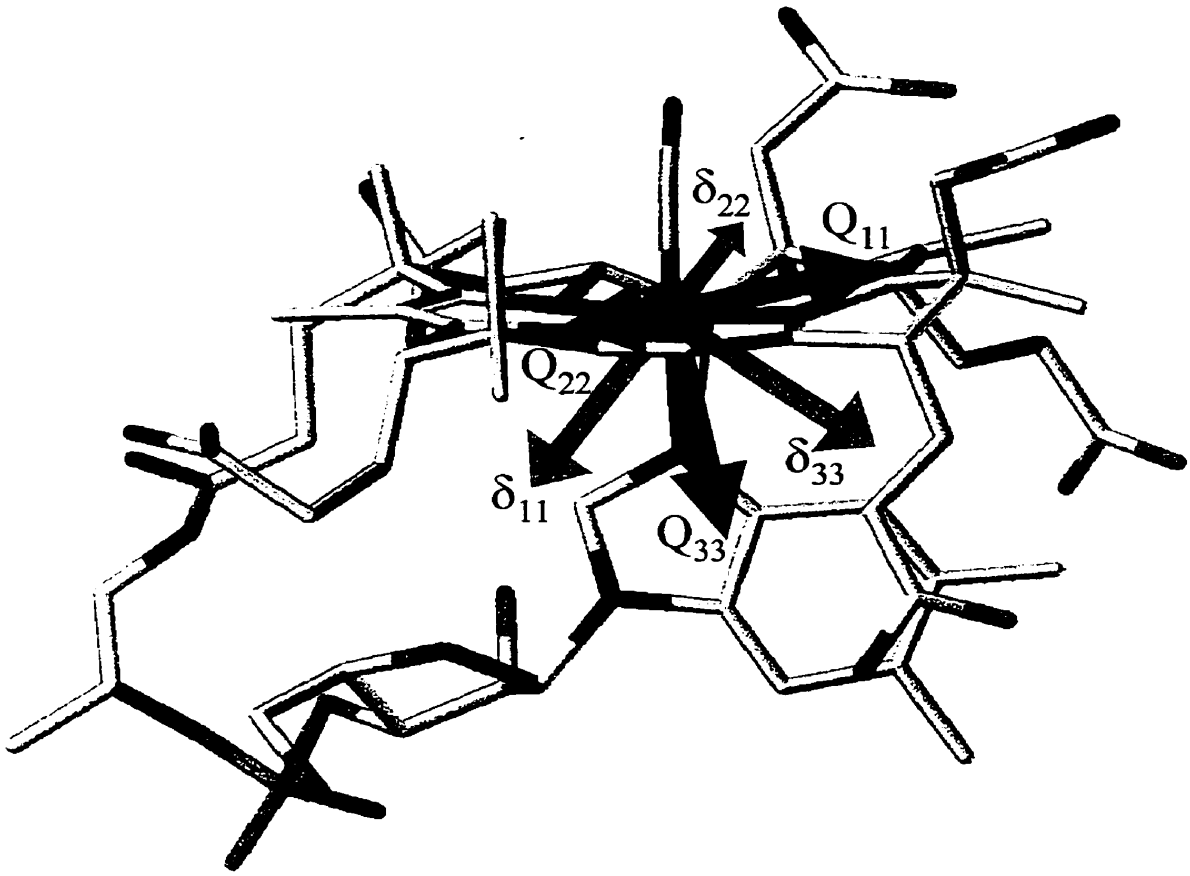

Figure 3.6: Molecular structure of vitamin B_{12} (from reference [11]) with the orientation of the principal components of the quadrupolar coupling (blue) and chemical shift (green) tensors superimposed on a view approximately perpendicular to the CoCN axis (approximately 80° rotated with respect to the top view in Figure 3.5).

site: two of the pyrrolidine rings are directly attached, whereas the other three inter-ring linkages have an intervening carbon. These directly bonded rings have a significant effect on the orientation of the minor components of the quadrupolar coupling tensor. The intermediate component (Q_{22}) lies almost directly along the Co-C(1) vector, where C(1) is the corrin ring carbon of the short linkage of the right-hand side of both views in Figure 3.5. This carbon is also the point of the greatest "pucker" in the corrin ring, lying below the approximate plane formed by the other atoms in the corrin ring.

The isotropic chemical shift (δ_{iso}), obtained by an average of the three principal components of the chemical shift tensor, is 4749 ppm. The span (Ω) of the cobalt chemical shift tensor is approximately 1200 ppm about the isotropic shift from 5075 ppm at high frequency to 3902 ppm at low frequency. The skew (κ) is 0.31 revealing a nonaxially symmetric shift tensor with δ_{22} to high frequency of the isotropic chemical shift. With respect to orientation of the chemical shift tensor, none of the principal components lie directly along a bond of the cobalt coordination sphere. The most shielded component, δ_{33}, is directed through one of the triangular faces of the cobalt octahedron, away from the phosphate tail and along the plane of the benzimidazole group. This orients δ_{11} directly along the internuclear vector between the cobalt centre and the phosphorus atom of the nucleotide tail. The intermediate component, δ_{22}, lies approximately in the corrin ring plane and, as found for Q_{22}, is close to the Co-C(1) vector (off by approximately 15°).

In solid-state powder NMR experiments, the orientation of the tensors in the molecular frame is not directly obtained. Only the relative orientations of the two

tensors is accessible. Such orientations are usually given in the form of Euler angles. The Euler angles, in single crystal NMR experiments, are the angles that relate the two sets of direction cosines. The Euler angles for the relative orientation of the chemical shift tensor with respect to the quadrupolar coupling tensor in this study are $\alpha = 334.0 \pm 13.0°$, $\beta = 41.4 \pm 1.7°$, and $\gamma = 207.3 \pm 2.5°$ (see Appendix B for information regarding how the Euler angles are determined).

3.5 Discussion

The results presented above compare well with previous investigations of vitamin B_{12} *via* ^{59}Co solution NMR. The first reported isotropic ^{59}Co chemical shift for vitamin B_{12} was 4750 ppm (0.01 M in D_2O) with a linewidth at half height of 11.1 kHz.[55] A more recent report[24] gives a similar shift at 4650 ppm (concentration and solvent not reported) with a linewidth of 28 kHz. Both of these values are in close agreement with that of the 4549 ppm obtained in this single-crystal NMR study. The broad solution linewidths are in accordance with the large quadrupolar coupling constant of 27.31 MHz obtained here in that the solution NMR linewidths are indicative of efficient quadrupolar relaxation. The variation in linewidths is probably due to concentration effects as it has been previously reported that ^{59}Co solution linewidths/relaxation are significantly affected by concentration.[56]

Comparison of these results to a solid-state powder NMR study of vitamin B_{12} yields good agreement.[24] In this report, ^{59}Co NMR spectra of B_{12} recrystallized from water were acquired at three magnetic field strengths (4.7 T, 7.1 T, and 11.8 T). From fitting of the spectra at these multiple fields, a quadrupolar coupling

constant of 26.1 $\pm$ 0.4 MHz and an η of 0.1 $\pm$ 0.2 were obtained. This report uses an older convention (based on solution relaxation parameters) to present the chemical shift tensor, but these numbers can be translated to compare to those presented here. The three principal components of their shift tensor were 5040, 4910, and 4000 ppm. These values are also in fairly close agreement with the results from this single-crystal NMR study. From powder NMR simulations, only the relative orientation of the two tensors, *via* the Euler angles, is available. Single-crystal NMR, however, gives the orientation of the tensors directly at a given nucleus and also more reliable values of the Euler angles. Their estimate of the Euler angle β (40 $\pm$ 20°) is in close agreement with the single-crystal NMR results. Their other two Euler angles ($\alpha = 45°$ and $\gamma = 20°$), however, do not match very well with the results presented here. It is not surprising that the β from the powder study is in closer agreement than the other two angles because β is the Euler angle that has the greatest effect on solid-state NMR spectra of quadrupolar nuclei where both the quadrupolar and chemical shift interactions contribute.

Understanding chemical shift and quadrupolar coupling tensors for metal centres in general, and the cobalt in B_{12} in particular, *via* solid-state NMR studies appears to be particularly convenient and insightful in probing the local structure in metal-centred biological systems. In the static ^{59}Co NMR studies[24] powder samples showed significant differences in their ^{59}Co lineshapes when recrystallized samples were compared with samples that came "out of the bottle." The most significant differences were seen in the quadrupolar coupling tensors (17.7 MHz from bottle and 26.1 MHz recrystallized). As reported, this is due to the effect of solvation

within the crystal lattice probably causing some deformation of the ligands on the corrin ring or axial cobalt ligands that are then transmitted electronically to the cobalt site. In a follow-up to this study,[57] Frydman and co-workers were able to distinguish the two vitamin B_{12} polymorphs that were first described in Hodgkin's X-ray studies[9, 11] by doing a series of solvation studies (*i.e.*, crystallizing vitamin B_{12} from different solvents and at various temperatures). These studies described "wet" and "dry" forms of vitamin B_{12}. In our study, our crystal is the "wet" form since we coated the crystal with epoxy immediately after removing it from the mother liquor so that dehydration would not occur. In comparison to Frydman's solvation study, a "wet" sample would be obtained by evaporation from pure water *vs.* an organic solvent or mixed organic/water solution. It was difficult to tell the differences between purely "wet" and purely "dry" vitamin B_{12} *via* ^{59}Co static spectra (due to a mixture of polymorphs unless fresh "wet" or new "dry" samples were used), therefore NMR studies of spin-$\frac{1}{2}$ nuclei were undertaken to investigate this more fully. It is interesting that the largest effects are seen on the quadrupolar coupling tensor and only small effects are observed in the chemical shift tensor in the "dry" *vs.* "wet" study. Using the assignment of the tensors given in our study, with Q_{33} approximately along the axial ligand direction and the other two components approximately in the corrin ring plane, the quadrupolar coupling tensor would be much more sensitive to deformations perpendicular to the corrin ring. This supports their hypothesis of axial ligand deformation as the difference between the two crystal forms.[24]

We believe that solid-state ^{59}Co NMR may aid in the study of enzyme-bound B_{12}

derivatives such as the structure of methylcobalamin in methionine synthase.[21]. Changes in the axial ligands, apparent from this X-ray diffraction study, should be observed also in the ^{59}Co NMR lineshape of free and bound forms of the coenzymes. Characterization of the cobalt centre *via* solid-state NMR also looks to be the best spectroscopic avenue to pursue. A recent study of ^{13}C and ^{15}N chemical shift tensors of several metal-tetraphenylporphyrin complexes showed little change in the magnitudes of the principal components, although some sensitivity of the ^{15}N data to metal-nitrogen separation was reported.[58] However, if the metal is studied directly, problems of sensitivity (low natural abundances) and spectral overlap due to multiple nuclear sites are avoided. Natural abundance studies of cobalamins bound to an enzyme would be next to impossible when considering the lower sensitivity obtained in ^{15}N NMR of vitamin B_{12}[57] as well as our labelling studies of a specific carbon (described in Chapter 4) where there is significant background signal even in this "small" molecule compared to the large complexes like methionine synthase.[21]

The absolute orientations of the chemical shift and quadrupolar coupling tensors at the cobalt site in vitamin B_{12} constitute the most significant results of this study. Absolute orientations of both of these interactions are rare in the literature, even for simpler cobalt complexes. The anisotropic NMR spectral properties of ^{59}Co have attracted much attention recently, through experimental characterization of chemical shift and quadrupolar coupling tensors in simple complexes from solid-state NMR spectra of static powder samples[59, 60] and single crystals,[52] as well as powder samples of cobalt clusters[61] and larger cobalt-centred ring-

based systems.[24, 62] These studies have shown that the chemical shift tensors of cobalt are highly anisotropic, with Ω values of up to 2500 ppm for cobalt(III)-tetraphenylporphyrin-di-isoquinoline.[62] The orientations of the chemical shift and quadrupolar tensors for cobalt have been found to be independent of each other *via* simulation of powder ^{59}Co NMR[24, 59, 60] as well as single-crystal ^{59}Co NMR studies,[52] unless forced by crystallographic symmetry.[63] This is evidence of the fundamental differences between these two NMR interactions, the ground-state dependence of the quadrupolar coupling interaction through the local electric field gradient *vs.* the singlet-excited-electronic-state dependence of the chemical shift interaction. The significance of the characterization of these tensors, in vitamin B_{12} as well as other metal systems, lies in the complementary information they provide concerning the local metal environment, rather than on any common origin or fundamental connection. As more compounds are studied with regards to the behavior of these interactions and their relative orientations in a wide range of chemical environments, the understanding of their distinct sensitivities in terms of local structure will become available.

Recent theoretical reports, using density functional theory methods, allow for optimism in predicting chemical shift data for cobalt nuclei.[64, 65, 66] Unfortunately, most of these reports only give isotropic information and no data concerning the orientation of the predicted chemical shift tensor. This is probably due to the use of idealized symmetries for the simple complexes in these computational studies. The capability of these methods to correctly predict the quadrupolar coupling parameters still remains an open (and important) question, considering the orientation

of the quadrupolar coupling tensors determined here for vitamin B_{12} and its apparent sensitivity to the crystallization as reported by Frydman and co-workers.[24]

NMR studies of quadrupolar nuclei have, in general, been avoided in biological systems in the past; however, it is important to note the useful features of such nuclei. As demonstrated here, the characterization of two separate NMR spectroscopic interactions, as well as their orientation dependence, provides a fuller description of the local electronic environment of the metal centre. Single-crystal NMR studies, such as the one described here, can be time consuming, but this is partially alleviated by efficient quadrupolar relaxation, which permits rapid signal averaging. The information obtained from such a study as this provides complete and unambiguous determination of both the quadrupolar coupling and chemical shift tensors. Avenues are continuing to open that allow the study of metal nuclei in bioinorganic complexes, including high-resolution solid-state NMR of quadrupolar metal nuclei,[18, 19] and the development of cross-polarization[67, 68, 69] and other magnetization transfer techniques involving quadrupolar nuclei.[70, 71, 72] These techniques may aid in determining the explicit role of the metal in biochemical pathways. However, these new techniques are not useful when large χ's are involved, thus single-crystal and powder NMR techniques will always be the avenue of choice when studying ^{59}Co in cobalamins until better methods can be discovered.

3.6 Conclusions

The cobalt chemical shift and quadrupolar coupling tensors of the cobalt site in vitamin B_{12} have been unambiguously determined *via* single crystal ^{59}Co NMR at

11.75 T. This is the first example of single crystal NMR of a quadrupolar or metal nucleus in a biologically relevant compound. The results reveal that the cobalt chemical shift tensor is highly anisotropic with $\delta_{iso} = 4549 \pm 75$ ppm, $\Omega = 1173 \pm 62$ ppm, and $\kappa = 0.31 \pm 0.02$. The ^{59}Co quadrupolar coupling tensor is large with $\chi = 27.31 \pm 0.08$ MHz and deviates only slightly from axial symmetry with $\eta = 0.243 \pm 0.005$. The largest component of the quadrupolar coupling tensor was found to lie about 10° from the Co-N(benzimidazole) bond, with the minor components of the tensor lying approximately in the corrin ring plane. The most shielded component of the chemical shift tensor, δ_{33}, points approximately through the centre of one triangular face of the octahedral cobalt coordination and away from the nucleotide "tail," whereas the least shielded component, δ_{11}, is directly along the Co-P internuclear vector, and δ_{22} in approximately in the place of the corrin ring. These results demonstrate that NMR of quadrupolar metal isotopes in biological materials is feasible, contrary to popular belief, and particularly so for solid materials, where higher magnetic fields and modern pulse techniques now permit acquisition of wide-line and high-resolution spectra for smaller samples.

Chapter 4

^{13}C and ^{15}N NMR Studies of Cobalamins

4.1 Introduction

Unlike the single ^{59}Co nucleus in vitamin B_{12}, there are multiple carbon and nitrogen nuclei in all cobalamins. Studying these nuclei, which are directly bonded or in close proximity to the cobalt centre, could aid in the understanding of the metal centre indirectly. When a spin-$\frac{1}{2}$ nucleus is next to and/or in close proximity to a quadrupolar nucleus that has a large quadrupolar coupling constant with respect to its Larmor frequency, residual dipolar effects can be observed in the MAS spectra of the spin-$\frac{1}{2}$ nucleus.[73] We know of no such examples of cobalt-carbon residual coupling constants reported, but there are examples of ^{59}Co-^{31}P residual dipolar coupling being observed in vitamin B_{12} model compounds.[74, 75] To study carbon and nitrogen nuclei in cobalamins requires selective labelling experiments.

This chapter describes the results of NMR experiments where ^{15}N and ^{13}C,^{15}N labelling of the cyano group in vitamin B_{12}, and ^{13}C labelling of the methyl group in methylcobalamin have been performed. To understand the NMR spectra of these complexes, it is beneficial to know what has been observed in solution ^{13}C and ^{15}N NMR of cobalamins as well as in solid-state NMR studies of similar compounds.

Solution NMR experiments of spin-$\frac{1}{2}$ nuclei in cobalamins have been studied extensively and are described in a recent review.[76] The solution ^{15}N δ_{iso} of the cyano nitrogen of vitamin B_{12} has been determined to be -91.1 ppm with respect to CH_3NO_2 at 0 ppm.[77] This paper also includes the J-coupling between the nitrogen and carbon of the cyanide group which was shown to be 8.9 Hz.

The first solid-state ^{15}N NMR study of a cyano group reported was that of acetonitrile.[78] In this study the span of the chemical shift tensor was found to be 488 ppm and axially symmetric. Since that time, there have only been three other studies of cyano nitrogens.[79, 80, 81] In the benzonitrile study,[79] ten *para* substituted benzonitriles were studied using both solid-state NMR and computational methods. The spans of the chemical shift tensors were all found to be about 400 ppm and skews were positive (but not 1.0 and therefore not axially symmetric). Cyano groups of other organic cyanides have not been recently investigated because they are assumed to be fairly well understood. The only two cyano nitrogen studies of a cyanide bound to metal centres are that of potassium mercury(II)cyanide[80] and potassium copper(I)cyanide.[81] The ^{15}N chemical shift tensors were found to be axially symmetric and have similar spans (477 ppm for the mercury complex and 495 ppm for the copper complex) as well as similar isotropic chemical shifts

(δ_{iso} was -89.1 ppm in the Hg complex and the two shifts in the Cu complex were -97.2 ppm and -91.5 ppm). A two bond J-coupling between the ^{15}N and ^{63}Cu was found to be 19 Hz and 20 Hz for the two sites in the copper complex. However, no residual dipolar coupling between the copper and nitrogen was observed in the ^{15}N MAS spectra of this complex.

The ^{13}C isotropic chemical shifts of both the cyanide of cyanocobalamin and the methyl group of methylcobalamin have been studied *via* solution NMR. In cyano-^{13}C-cobalamin, δ_{iso} was found to be 121.4 ppm in aqueous solution.[82] Reported chemical shifts for methyl-^{13}C-cobalamin depend on the solvent.[83] In 0.1 M $NaClO_4$ δ_{iso} was found to be 9.54 ppm and in 0.32 M HCl, a "base-off" form (*vide infra*), δ_{iso} was found to be 1.76 ppm.

Solid-state ^{13}C NMR spectra of many cyanides and methyl groups have been previously investigated.[84] The isotropic chemical shifts of organic cyanides are found to range between 111 ppm and 125 ppm.[84] Solid-state carbon chemical shifts of carbon nuclei bound to metals are limited to group 10, 11, and 12 tetracyanometallates.[81, 85, 86, 87] In square planar group 10 compounds, the isotropic chemical shifts range from 128 ppm to 139 ppm.[85] The group 12 compounds form tetrahedral complexes and the δ_{iso}'s are found to be between 148 ppm and 153 ppm.[86] Group 11 tetrahedral complexes are found to be be slightly more deshielded with δ_{iso}'s from 157 ppm to 162.4 ppm.[81, 87] Organic methyl groups range in isotropic chemical shifts from 10 ppm to 25 ppm.[84] When a carbon is bound to a metal, as in $Hg(CH_3)_2$,[88] its δ_{iso} is found to be more shielded at 0 ppm.

In this study, we have obtained the ^{15}N solid-state CPMAS and CP static spectra of cyano-^{15}N-cobalamin as well as the ^{15}N CP static spectrum of cyano-$^{15}N^{13}C$-cobalamin. The ^{15}N CS tensor as well as the dipolar coupling constant between ^{15}N and ^{13}C has been determined. *Ab initio* chemical shielding calculations of the ^{15}N tensor of acetonitrile (as a model) have also been performed and compared to our results. With regard to ^{13}C NMR data, ^{13}C CPMAS NMR spectra of cyano-$^{15}N^{13}C$-cobalamin and methyl-^{13}C-cobalamin have been obtained. From the ^{13}C CPMAS spectra of cyano-$^{15}N^{13}C$-cobalamin, the indirect spin-spin coupling constant between carbon and cobalt has been determined. Unfortunately $^{1}J_{iso}$(Co,C) was not accurately determined for methyl-^{13}C-cobalamin, but an estimate has been made.

4.2 Theory

The basic concepts of MAS were described in section 2.3.2. However, when a quadrupolar nucleus is dipolar coupled to a spin-$\frac{1}{2}$ nucleus, the situation becomes more complicated. The complication is that the dipolar interaction, which is normally averaged by MAS, is reintroduced *via* the C and D terms of the dipolar alphabet.[73] The quadrupolar interaction also affects the chemical shielding and indirect spin-spin interactions as well. Since we will be studying nuclei dipolar coupled to ^{59}Co, the following will describe a a spin-$\frac{1}{2}$ nucleus directly bound to a spin-$\frac{7}{2}$ nucleus.

A spin-$\frac{7}{2}$ nucleus (S) will J-couple to a spin-$\frac{1}{2}$ nucleus (I) yielding an eight line pattern in the spin-$\frac{1}{2}$ nucleus spectrum. The splitting between the adjacent lines,

however, will not all have the same spacing. The frequency of a given line is given by the following equation:[73]

$$\nu_m = -mJ_{iso} + \frac{3\chi R_{eff}}{20\nu_s}\frac{S(S+1)-3m^2}{S(2S-1)}(3cos^2\beta - 1 + \eta sin^2\beta cos2\alpha) \qquad (4.1)$$

where ν_m is the frequency of a line, m is the z-component of the nuclear spin quantum number S (ranging from S, S-1, ... -S), J_{iso} is the isotropic spin-spin coupling, χ is the quadrupolar coupling constant of the quadrupolar nucleus, R_{eff} is the effective dipolar coupling between the quadrupolar nucleus and the observed nucleus, ν_s is the frequency of the quadrupolar nucleus at the field strength of the experiment, S is the spin of the quadrupolar nucleus, η is the asymmetry of the quadrupolar tensor, and α and β give the orientation of the largest component of the quadrupolar tensor with respect to the dipolar vector (in most cases the chemical bond). The lines are unevenly spaced due to the quadruoplar distortion which changes with the value of m. From the uneven splittings observed between adjacent lines it is possible to determine information about the quadrupolar tensor indirectly from the spin-$\frac{1}{2}$ spectrum.

4.3 Experimental

4.3.1 Synthesis

99% labeled ^{15}N and $^{13}C^{15}N$ cyanocobalamin were prepared using the following general method with slight modifications:[89] 118.7 mg (1.795 mmol) of ^{15}N-labelled potassium cyanide was dissolved in water (8 mL) and added to 198.8 mg (0.148

mmol) of vitamin B_{12a} also dissolved in water (47 mL). Hydrochloric acid (0.1 M) was added dropwise until the pH was slightly acidic (between 5 and 6). The mixture was desalted *via* a Sephadex G-10 (Sigma) column. The B_{12} solution collected from the G-10 column was evaporated to approximately 1 mL under reduced pressure. Acetone (45 mL) was added to the evaporated solution and refrigerated overnight. The fine, needle-like crystals of ^{15}N-labeled vitamin B_{12} were recovered by filtering under reduced pressure and washing with cold acetone. The final mass of product recovered was 187.5 mg (94% yield). Using the same procedure, 124.2 mg (1.85 mmol) of $^{13}C^{15}N$-labeled potassium cyanide was added to 200.5 mg (0.145 mmol) of vitamin B_{12a} to produce 184 mg of $^{13}C^{15}N$-labeled cyanocobalamin (91% yield).

Methyl-^{13}C-cobalamin was prepared by modification of a known synthesis.[90] The synthesis of methylcobalamins must be done exclusively under red light or the cobalt-carbon bond will cleave. Vitamin B_{12} (250 mg) was dissolved with stirring in degassed water (20 mL) in a stoppered 125 mL flask while bubbling argon through it. A solution of sodium borohydride (120 mg in 1.5 mL degassed water) was added *via* syringe. This solution was stirred for 15 minutes during which time it changed colour from red (cobalt(III)) to brown (cobalt(II)) and finally to a blue/green colour (cobalt(I)). A degassed solution (2 mL water) of $FeSO_4(NH_4)_2SO_4{\cdot}6H_2O$ (35 mg) and $FeCl_3$ (175 mg) was added dropwise *via* syringe over 15 minutes to react and complex with the boron-containing materials. This solution was then left to stir for an additional 15 minutes to allow for the reaction to complete. Methyl-^{13}C-iodide (1g vial) was dissolved in degassed methanol (1 mL) and then added to the solution causing the solution to turn red again. To remove the iron salts, the solution was

centrifuged, decanted, centrifuged again, then decanted again and finally filtered through a fine frit. This solution was evaporated under reduced pressure to approximately a 1 mL volume. Acetone was added to this solution until it started to show slight turbidity after which it was stored at 4°C to crystallize. The crystals were collected yielding 220 mg (87%) of methyl-^{13}C-cobalamin. The product was characterized by electrospray ionization mass spectrometry (Mircomass Quatro II), showing a molecular ion at m/z = 1345 Da as compared to the unlabelled methylcobalamin at 1344 Da.

4.3.2 Solid-State NMR Experiments

Solid-state ^{15}N NMR spectra were acquired at 50.68 MHz on a Bruker AMX-500 NMR spectrometer (B_o = 11.75 T). The samples were packed in 4 mm zirconium oxide o.d. rotors. Cross polarization (CP) under the Hartmann-Hahn matching condition was used to increase the sensitivity of the spectra with a CP contact time of 5 ms. A proton 90° pulse of 4 μs was used. High-power proton decoupling was used during the acquisition of the spectra. A recycle delay time of 10 s was used. The chemical shifts were referenced to $^{15}NH_4NO_3$ at -358.45 ppm.[91]

Solid-state ^{13}C NMR spectra were acquired at 125.7 MHz on a Bruker AMX-500 NMR spectrometer (B_o = 11.75 T) and at 50.3 MHz on a Bruker-200 ASX NMR spectrometer (B_o = 4.7 T) . The samples were packed in 4 mm zirconium oxide o.d. rotors (at both field strengths). Cross polarization (CP) under the Hartmann-Hahn matching condition was used to increase the sensitivity of the spectra with a CP contact time of 7 ms. A proton 90° pulse of 4 μs was used at 11.75 T and 6 μs at 4.7

T. High-power proton decoupling was used during the acquisition of the spectra. A recycle delay time of 10 s was used. The carbon chemical shifts were referenced to TMS using by setting the lower chemical shift peak of adamantane to 29.5 ppm.

4.3.3 Simulations and Calculations

Simulation of the MAS powder lineshapes with performed on a personal computer using the program WSOLIDS from Dr. Rod Wasylishen's lab.[92] This software uses the POWDER routine[93] for simulation of static spectra and the Herzfeld-Berger method[42] for MAS spectra.

Calculations of the ^{15}N chemical shift tensor of acetonitrile were carried out on a Silicon Graphics Indigo^2 workstation using the GIAO method available in Gaussian94[94] using RHF/6-311+G(2d,p). The geometries were fully optimized with the same program using B3LYP/6-31G(d) except for the CCN angle which was incremented between 180^o and 160^o in 2^o increments.

4.4 Results

4.4.1 Nitrogen-15 NMR

The ^{15}N CPMAS and CP static NMR spectra of cyano-^{15}N-cobalamin as well as the simulations of these spectra are seen in Figure 4.1 (lower spectra experimental, upper spectra simulations). The tensor was found to be axially symmetric with an isotropic shift of -85.8 ppm and a span (Ω) of 524.5 ppm. A summary of the ^{15}N NMR results is seen in Table 4.1.

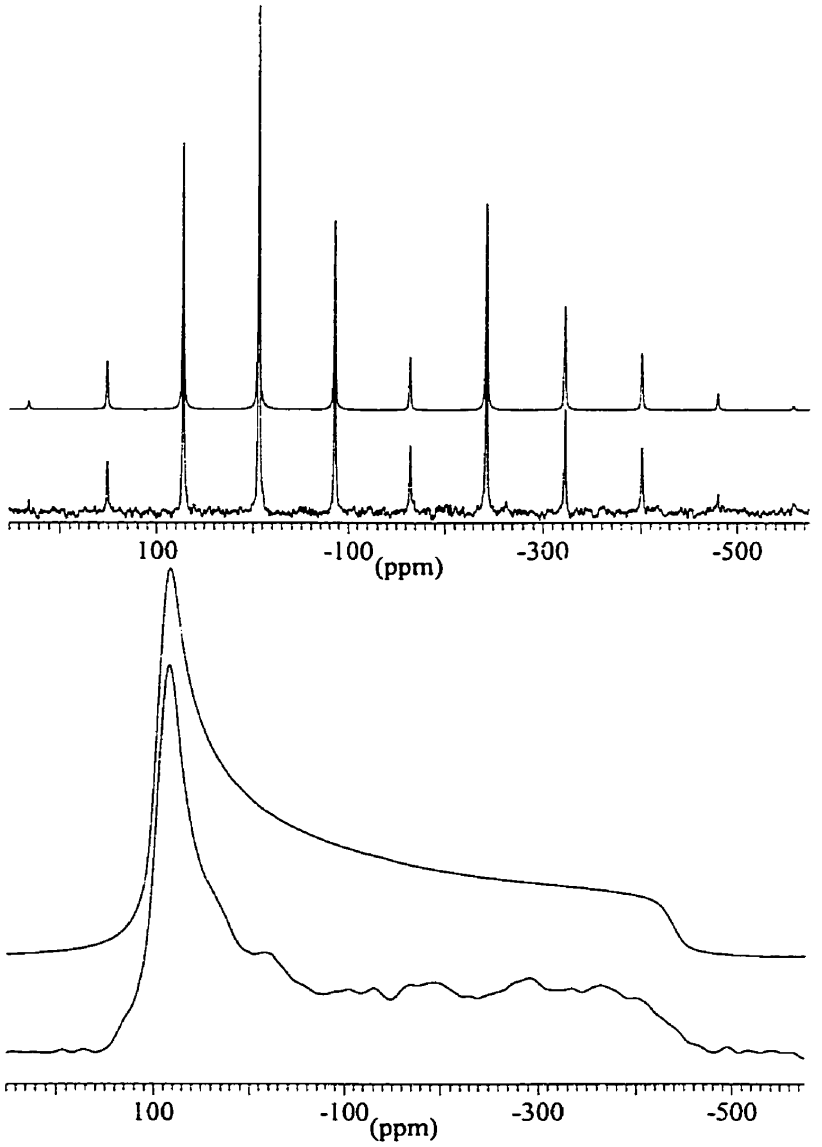

Figure 4.1: Solid-state ^{15} NMR data for cyano-^{15}N-cobalamin. Lower spectra are experimental, upper are simulations using a $\delta_{\perp}$ of 89 ppm and $\delta_{||}$ of -435.5 ppm. The MAS spectrum has a spinning rate of 4 kHz.

Table 4.1: Solid-state ^{15}N NMR results of vitamin B_{12} experiments.

Cobalamin	δ_{iso} (ppm)	$\delta_{\perp}$ (ppm)	$\delta_{\parallel}$ (ppm)	Ω (ppm)	R_{CN}
^{15}N	-85.8	89 $\pm$ 2.5	-435.5 $\pm$ 10	524.5	N/A
$^{15}N^{13}C$	-85.8	89 $\pm$ 2.5	-435.5 $\pm$ 10	524.5	1800 $\pm$ 75

The ^{15}N CP static spectrum of cyano-$^{15}N^{13}C$-cobalamin is given in Figure 4.2 (lower experimental, upper simulation). The spectrum is very similar to that of the ^{15}N labelled analogue except for splitting on both ends of the spectrum. The splittings are due to the dipolar interaction between ^{15}N and ^{13}C. The splitting on the high field end of the spectrum is R_{CN} (where R_{CN} is the dipolar coupling constant between ^{13}C and ^{15}N defined in equation 2.28) and at the low field end is $2R_{CN}$. From the splittings, R_{CN} was found to be 1800 $\pm$ 75 Hz. The dipolar coupling constant directly reveals the distance between the two nuclei by using equation 2.28. Solving for r_{CN}, a bond distance of 1.19 $\pm$ 0.02 Å is obtained which is in close agreement to the 1.15 Å distance found in the crystal structure at 88 K.[95]

We have used acetonitrile as a model to study the cyano nitrogen of vitamin B_{12} because the solid-state NMR results reveal spans that are similar to acetonitrile. Table 4.2 shows the results of an *ab initio* study of acetonitrile. Theoretically, the ^{15}N CS tensor of cyano-^{15}N-cobalamin does not have to be axially symmetric unless the CoCN bond angle is 180°. The reported CoCN angle in the crystal structure is 179°. As seen in Table 4.2, it would not be possible to tell if the experimental spectrum was non-axially symmetric until a CoCN bond angle of at least 176° and experimentally not really until 172° due to the resolution in the experiment.

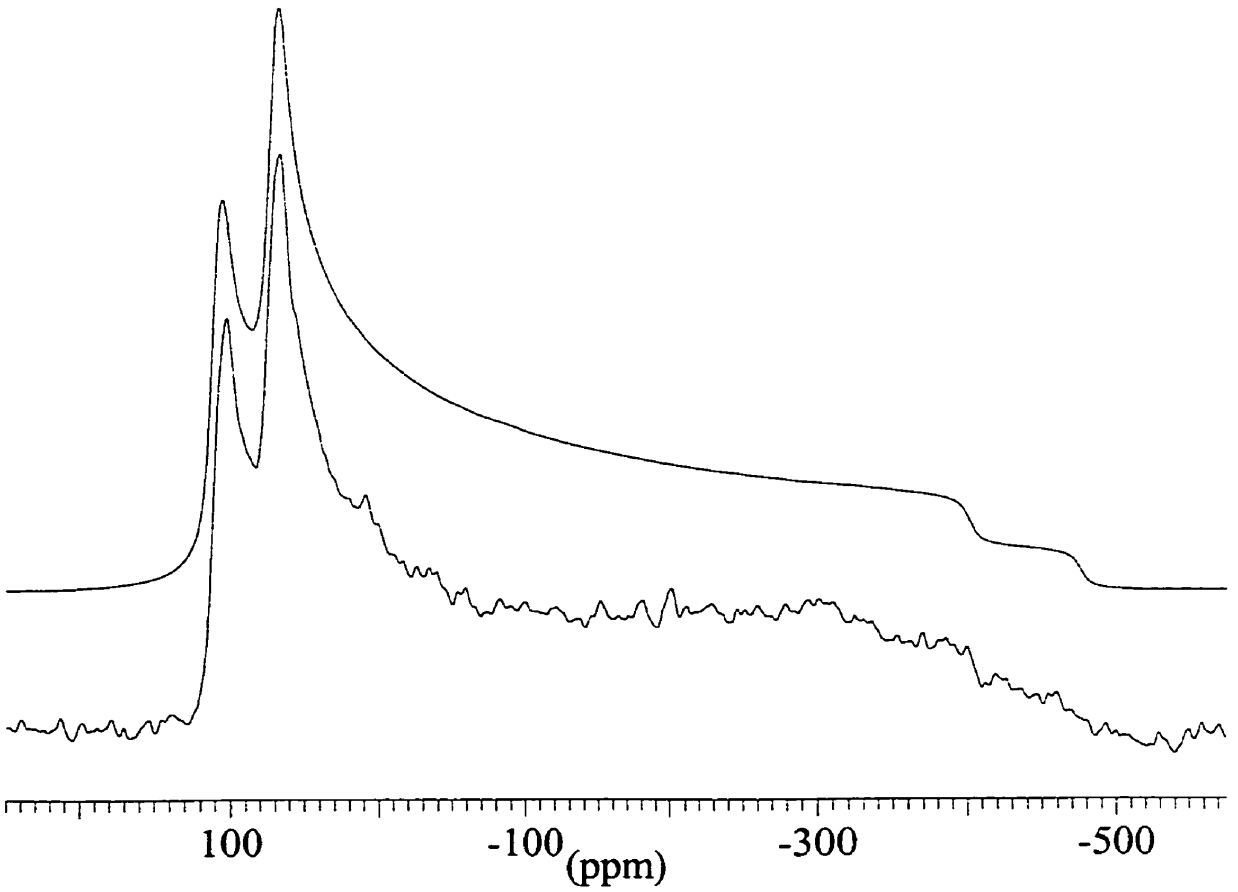

Figure 4.2: Solid-state ^{15}N NMR spectrum (lower) and simulation (upper) of cyano-$^{13}C^{15}N$-cobalamin. R_{CN} was found to be 1800 $\pm$ 75 Hz.

Table 4.2: Summary of ^{15}N NMR calculations on acetonitrile.

NCC angle (°)	σ_{iso} (ppm)	σ_{11} (ppm)	σ_{22} ppm	σ_{33} (ppm)
180	-37.9	-210.2	-210.2	306.7
178	-38.1	-210.5	-210.4	306.7
176	-38.7	-211.7	-210.8	306.6
174	-39.7	-213.9	-211.5	306.4
172	-41.4	-217.1	-212.4	306.2
170	-42.9	-221.2	-213.5	305.9
168	-45.2	-226.3	-214.8	305.5
166	-47.9	-232.3	-216.4	305.0
164	-51.2	-239.4	-218.2	304.4
162	-54.7	-247.4	-220.2	303.6
160	-58.7	-256.5	-222.5	302.8

4.4.2 Carbon-13 NMR

Figure 4.3 contains the ^{13}C CPMAS NMR spectra of cyano-$^{13}C^{15}N$-cobalamin at 4.7 T and 11.75 T. The spectra shown are those of the cyanide carbon region alone and are a summation of the spinning side bands as to get the best intensity distribution of the centre band since the span of the chemical shift tensor was extremely large, approximately 350 ppm, thus it was not possible to spin fast enough to get all of the intensity into the centre band. The spectrum at 11.75 T is a difference spectrum between labelled and unlabelled vitamin B_{12}. Thus, only a spectrum of the cyano carbon is observed. The spectrum at 4.7 T, however, has signals that overlap with the centre band. Therefore, a difference spectrum left large distortions and was not performed. The best fit simulations of the experimental spectra are given slightly offset above the experimental spectra. The simulations were made simpler since α, β, χ, and η were known from the single-crystal ^{59}Co NMR results presented in

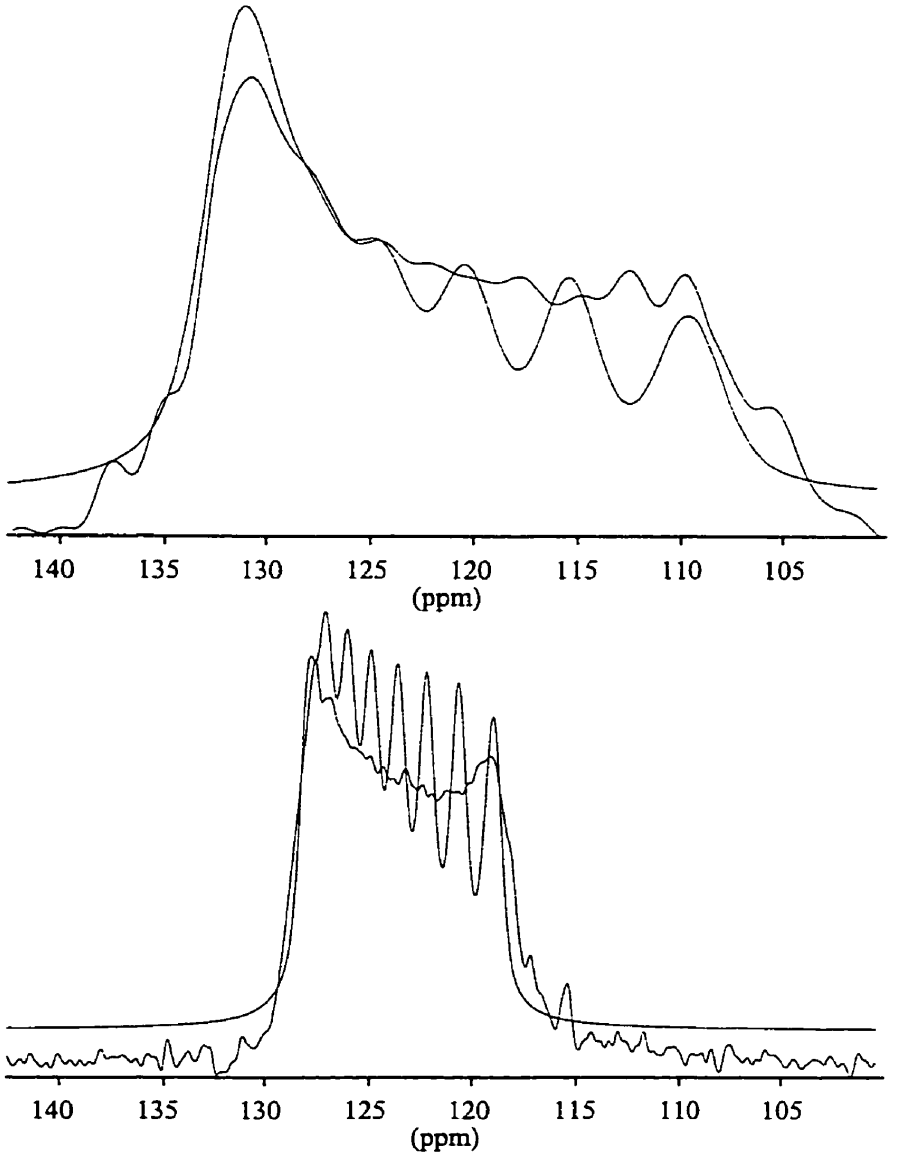

Figure 4.3: Solid-state ^{13}C NMR spectra of cyano-$^{13}C^{15}N$-cobalamin at 4.7 T (upper) and 11.75 T (lower). Simulations using a δ_{iso} = 123.5 ppm, R_{eff} = 600 Hz, J_{CoC} = 165 Hz, $\alpha = 18°$, $\beta = 165°$, χ = 27.31 MHz, and η = 0.243 are offset slightly above experimental spectra.

chapter 3. Thus only 3 parameters needed to be optimized: δ_{iso}, R_{eff}, and J_{CoC}. From the fits the one bond Co-C J_{iso} was determined to be 165 $\pm$ 10 Hz, the effective dipolar coupling is 600 $\pm$ 100 Hz, and δ_{iso} is 123.5 ppm.

The ^{13}C NMR spectrum of methyl-^{13}C-cobalamin was more complicated than that of the cyanocobalamin. Figure 4.4 shows the full ^{13}C spectrum (labelled a) as well as the labelled methyl group (labelled b) of methyl-^{13}C-cobalamin. Only experimental spectra are shown for this complex since it was not possible to obtain good fits of the data. From the width of the centre band, an estimate of the Co-C J_{iso} of 100 $\pm$ 15 Hz can be given.

4.5 Discussion

With regards to the nitrogen chemical shift tensors, the span of the ^{15}N CS tensor of cyano-^{15}N-cobalamin is approximately 125 ppm larger than other nitriles on aromatic rings.[79] In fact, $\delta_\perp$ is deshielded about 65 - 75 ppm more than aromatic nitriles and $\delta_\parallel$ is shielded by approximately 45 - 55 ppm. This larger span could possibly be due to lack of conjugation of the cyano group in vitamin B_{12} as compared to aromatic nitriles.

Acetonitrile, however, has a span which is only about 35 ppm less than that of cyano-^{15}N-cobalamin. Like vitamin B_{12}, the cyano group is "isolated" in acetonitrile and therefore a similar span of the CS tensors of the two compounds is not surprising. However, the whole acetonitrile CS tensor is shielded compared to that of cyano-^{15}N-cobalamin ($\delta_\perp$ is shielded by 83 ppm and $\delta_\parallel$ is shielded by 46 ppm). This would be due to lower excitation energies in a cyano group bonded to a metal

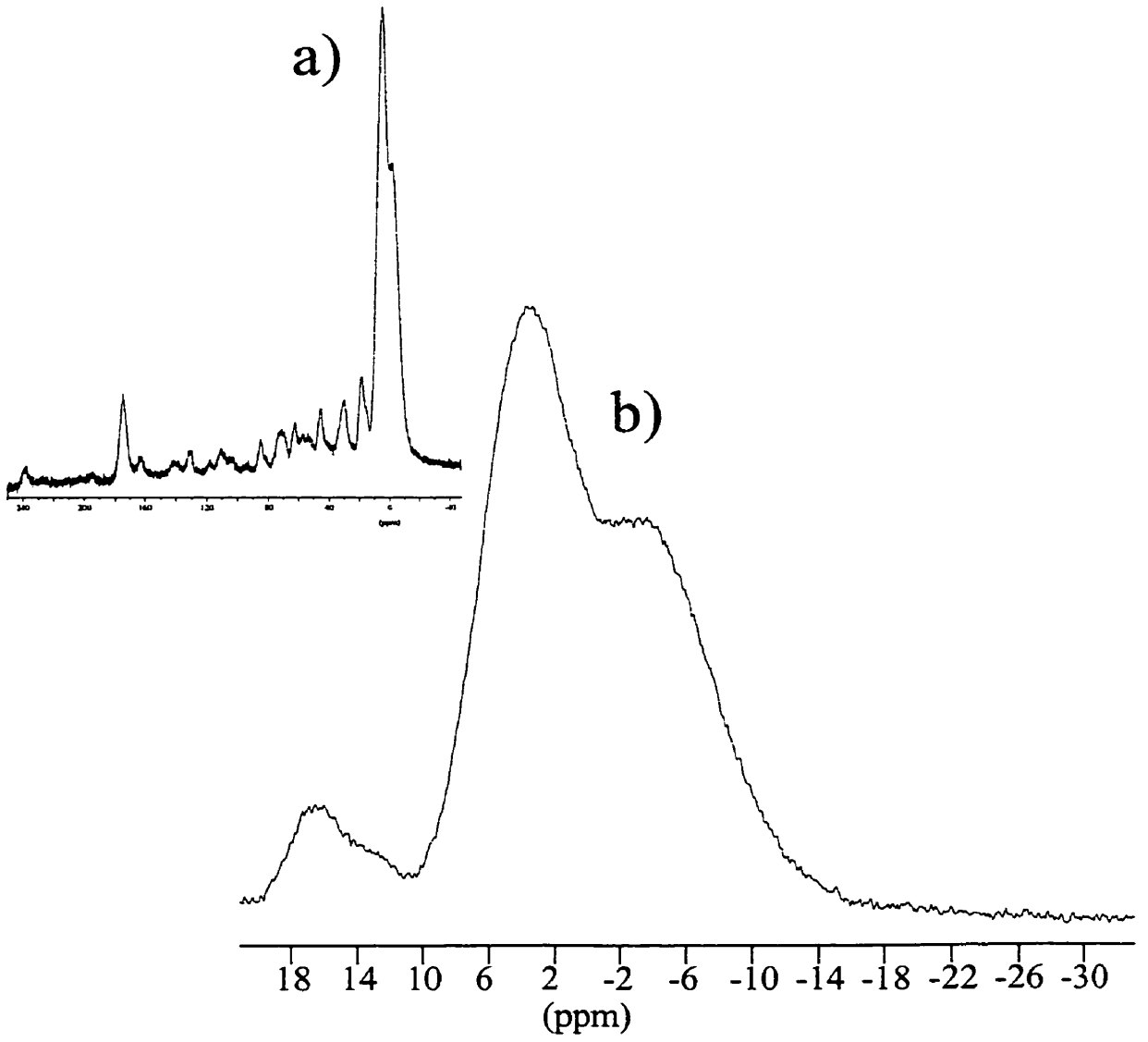

Figure 4.4: Solid-state ^{13}C NMR spectra of methyl-^{13}C-cobalamin at 11.75 T. a) Full spectrum of methyl-^{13}C-cobalamin and b) expansion of the labelled carbon region.

vs. bonded to an organic moiety. To compare the calculated shielding tensor of acetonitrile with the experimental ^{15}N shift tensor of cyanocobalamin, equation 2.18 can be used to convert ^{15}N shifts to shielding. The σ_{ref} for ^{15}N is -135.4 ppm.[96] Using the results of the calculations for 178°, $\delta_{\perp}$ is found to be 85 ppm and $\delta_{||}$ is -441.1 ppm. These values are only slightly more shielded (4 - 6 ppm) than the experimental tensors of the cyano group cyano-^{15}N-cobalamin as compared to them being greatly deshielded compared to the experimental acetonitrile tensor.

The ^{15}N chemical shift tensor of cyano-^{15}N-cobalamin is found to be similar to those of other cyanometallates. The δ_{iso}'s of $K_3Cu(CN)_4$ (-97.2 ppm and -91.5 ppm for the two sites) and $K_2Hg(CN)_4$ (-89.1 ppm) are only slightly deshielded to that of -85.8 ppm in vitamin B_{12}. The span of the ^{15}N chemical shift tensor of vitamin B_{12} was found to only be slightly larger (524.5 ppm) than those of the copper (495 ppm) and mercury (477 ppm) complexes. Thus the ^{15}N chemical shift tensors of cyanides bound to metal are all very similar and have spans that are approximately 100 ppm larger that those of organic nitriles.

The carbon shielding in cyano-^{13}C-cobalamin can be compared to other cyanide-containing compounds. The solution δ_{iso} of 121.4 ppm[82] is very similar to that of 123.5 ppm found in the solid-state. This solid-state shift is more shielded than those found in cyanometallates.[81, 85, 86, 87] In fact, the ^{13}C chemical shift of the cyano group of vitamin B_{12} is more similar to that of nitriles[84] than of cyanometallates. The cobalt-carbon one-bond J-coupling of 165 $\pm$ 10 Hz is found to be significantly larger than the $^1J(Co,C)$ of 126 Hz in $K_3Co(CN)_6$[97] found in solution. An effective dipolar coupling constant of 600 Hz was determine for the Co-C bond which would

correspond to a bond length of 2.28 Å. This is significantly larger than that found in the X-ray structure (1.86 Å). This leads us to believe that the J-coupling is anisotropic in this complex. Using the bond length of 1.86 Å, a ΔJ of 1500 $\pm$ 300 Hz is determined. This is a very large ΔJ and thus further investigation into this complex is warranted.

Unlike the ^{13}C δ_{iso} of cyano-^{13}C-cobalamin, which is very similar to organic cyanide shifts, the carbon chemical shift of methyl-^{13}C-cobalamin is shielded compared to organic methyl groups.[84] The ^{13}C δ_{iso} of methyl-^{13}C-cobalamin, however, is very similar to that of other methyl-metal carbons such as $Hg(CH_3)_2$ at 0 ppm. A solution Co-C J-coupling of methyl-^{13}C-cobalamin has been previously estimated from relaxation measurements to be 105 Hz[98] which is similar to our estimate of 100 $\pm$ 15 Hz.

As seen in Figure 4.4a, even with selective labelling in cobalamins, there is significant background from the naturally occurring carbons (1.1 %). Therefore techniques other than selective labelling must be used to study carbon nuclei in cobalamins. In cases where there is a spin-pair (such as a ^{15}N next to a ^{13}C or two ^{13}C's) multipulse techniques could be used for selective editing, (*e.g.*, double CP[99], TEDOR[100], rotational resonance[101], RFDR[102], etc.), thus resolution that is not available in conventional CPMAS spectra might be obtained.

4.6 Conclusions

The ^{15}N chemical shift tensor of cyano nitrogen of vitamin B_{12} has been determined to be axially symmetric with a δ_{iso} of -85.8 ppm and a Ω of 524.5 ppm. The R_{CN}

of cyano-$^{15}N^{13}C$-cobalamin was found to give a $^{13}C^{15}N$ distance in close agreement to that of the crystal structure. Acetonitrile has been found to be a good model to aid in the understanding of the cyano moiety of vitamin B_{12}. The δ_{iso} of the cyano carbon of vitamin B_{12} is 123.5 ppm and the carbon-cobalt J_{iso} was found to be 165 $\pm$ 10 Hz. Using the orientation data from the single crystal ^{59}Co NMR (chapter 3) and the cobalt-carbon bond length from the crystal structure, an effective dipolar coupling constant of 600 $\pm$ 100 Hz was determined for this complex. Using this dipolar coupling constant, ΔJ is determined to be 1500 $\pm$ 300 Hz. This is an extremely large ΔJ and thus further investigations of this complex are needed. The carbon spectrum of methyl-^{13}C-cobalamin was not able to be simulated but the Co-C J_{iso} was estimated to be 100 $\pm$ 15 Hz.

Chapter 5

Base Conformation Study *via* Solid-State NMR

5.1 Introduction

When a co-enzyme form of vitamin B_{12} binds to an apoenzyme, the holoenzyme is formed. When the first crystal structure of a cobalamin bound to an apoenzyme was published,[21] a debate concerning the conformation around the cobalt centre in the holoenzyme began; is the B_{12} cofactor in a base-on or base-off conformation? Base-on or base-off refers to the dimethylbenzimidazole "tail" of the cobalamin being attached to the cobalt or free from the cobalt. Figure 5.1 gives a schematic of base-on *vs.* base-off using chemical means. It may be possible to study this phenomenon using NMR by directly observing the powder lineshape at the cobalt centre or by studying a nucleus that is unique and present in the tail (in this case the phosphorus nucleus). There is a wealth of literature detailing solution studies of

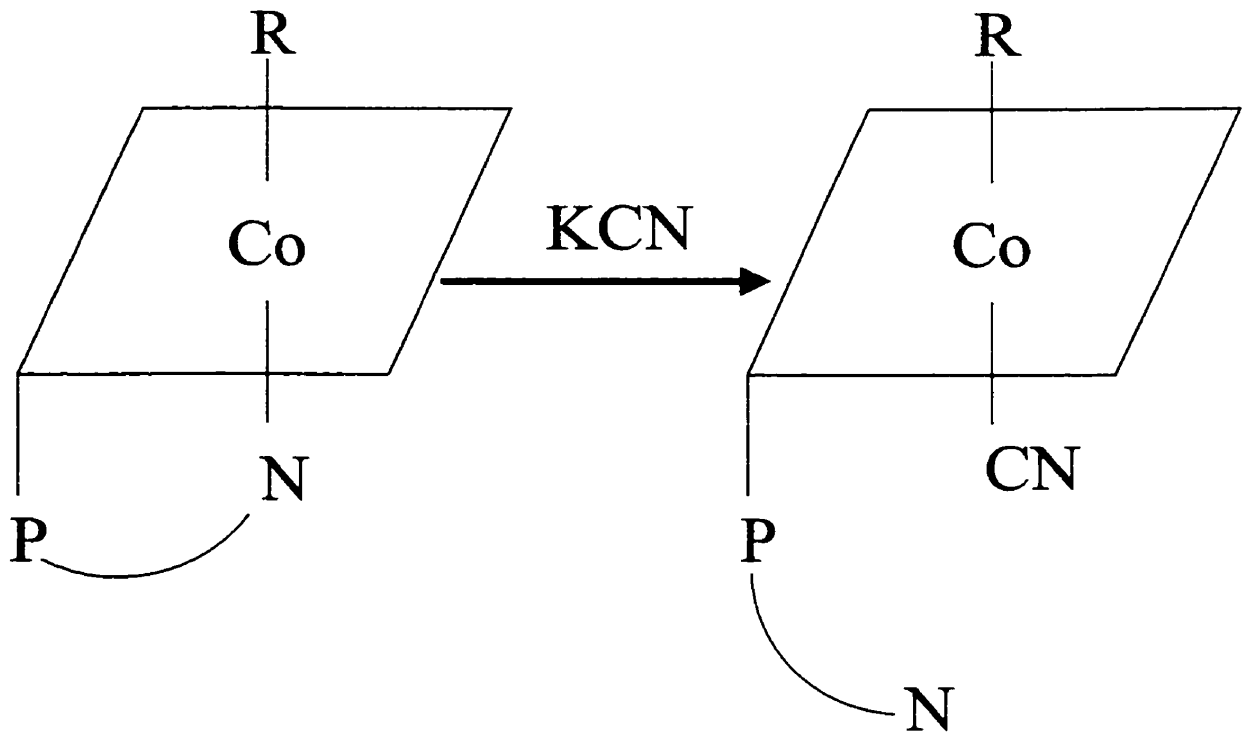

Figure 5.1: A base-on cobalamin converting to a base-off cobalamin *via* reaction with KCN.

nuclei around the cobalt centre, yet few reports concerning the cobalt centre itself.

In chapter 3, the power of single-crystal ^{59}Co NMR was demonstrated with a study of vitamin B_{12}. Single-crystal NMR studies, however, are time consuming and only possible when crystals of sufficient size are available. The chemical shift and quadrupolar interactions can be determined also using powder NMR techniques. Similar to the low number of single-crystal ^{59}Co NMR studies, powder ^{59}Co NMR studies are quite rare in the literature. This is due particularly to the lack of knowledge concerning the simulation of powder lineshapes of half-integer quadrupolar nuclei (I= n/2 where n = 3, 5, 7, or 9) when the chemical shift and quadrupolar tensors are both non-axially symmetric and non-coincident. In 1990, two groups separately published the analytical procedure for powder lineshapes under these conditions[63, 103] allowing for quadrupolar nuclei to be studied and analyzed successfully in the solid state without restrictions based on site symmetries.

The first reported powder NMR study of ^{59}Co complexes appeared in 1987,[104] a full three years before the lineshapes could be properly simulated. In this study, spectra of six simple cobalt complexes at 11.75 T were given. The eight parameters that were needed to describe the powder lineshapes were not reported but the chemical shift anisotropies of three complexes with high symmetry were estimated (no chemical shift or quadrupolar tensor tensor information was given on the other three complexes).

The first reported ^{59}Co powder NMR spectra with all eight parameters used to fit the spectra was published in 1993.[105] In this paper, spectra of two simple cobalt complexes ($Na_3[Co(NO_2)_6]$ and *trans*-$[Co(NO_2)_2en_2]NO_3$) were simulated at 9.5 T

and 7.1 T. The fits of the symmetric cobalt complex were straightforward due to symmetry constraints. The fits of the *trans* complex, however, were more difficult to obtain because the quadrupolar and chemical shift tensors are not dictated by symmetry to be coincident (and in fact they are not). This complex had been studied previously *via* single-crystal ^{59}Co NMR[46] and, in the powder NMR study, the tensors were assumed to be coincident due to high symmetry. This assumption was close (the Euler angle β was only 3.5°), but poor fits of the powder spectra were obtained if the tensors were assumed to be coincident indicating that, unless crystal symmetry dictates that the tensors are coincident, this assumption should not be made.

Recently we have acquired a series of ^{59}Co NMR static spectra at 11.75 T and 4.7 T[59] for ten simple cobalt complexes with four different arrangements of ligands (CoX_6, CoX_5Y, *cis*-CoX_4Y_2, and *trans*-CoX_4Y_2). From our results, we were able to assign specific ligand planes (N and O ligands) that give rise to specific chemical ranges of chemical shifts. These results show the need to perform more *ab initio* calculations on cobalt chemical shielding so the origin of cobalt chemical shifts can be determined and accurately predicted.

The most recent ^{59}Co static NMR spectra of simple cobalt complexes was obtained for a series of polyammonium salts of cobalt cyanide.[106] The results of multi-field ^{59}Co NMR experiments of six polyammonium salts as well as the potassium salt of $Co(CN)_6^{3-}$ were presented. The eight parameters needed to fully describe the lineshape of each of the seven complexes was given. This study also included DFT results showing how modern calculations are now possible on met-

als with d-electrons and will hopefully lead the way to better predictions of ^{59}Co chemical shifts.

In the area of organometallic chemistry, solid-state ^{59}Co NMR spectra of four cobalt clusters have been described completely *via* experiments at two magnetic field strengths (7.1 T and 4.7 T).[107] A second paper by this same group has been published on another cobalt cluster complex, but the chemical shift and quadrupolar interactions were not determined due to multiple sites in the unit cell making simulation impossible.[108]

Cobalt-59 NMR has also been utilized in the area of materials chemistry.[109] In $LiCoO_3$, a material in lithium ion batteries, the cobalt sites are assumed to be CoO_6 octahedral and therefore should exhibit narrow lines in a ^{59}Co NMR spectrum. Three "distinct" lines were described which were assigned to two types of diamagnetic cobalt and one type of paramagnetic cobalt. However, the ^{59}Co MAS spectrum of the complex only exhibits one isotropic peak and there does not appear to be any shape in the spinning side bands indicative of multiple sites.

In the area of biologically significant ^{59}Co NMR studies, the group headed by Frydman has published four excellent papers.[24, 57, 62, 110] The first was a study of cobalt(III) porphyrins.[62] These types of complexes are to be used as a model for the isoelectronic iron(II) complexes (as well as being structurally similar) that are known as hemes. Static and MAS studies were performed on eight cobaltporphryin complexes at multiple fields to obtain spectra which could be simulated with high levels of precision. This group was also the first to report static ^{59}Co NMR results on cobalamins.[24] The parameters needed to simulate the lineshape of vitamin

B_{12}, methylcobalamin, co-enzyme B_{12}, dicyanocobyrinic acid heptamethylester (a precursor in the synthesis of B_{12}), as well as six cobaloximes (vitamin B_{12} model compounds) were described. As discussed in chapter 3, the static values from this study on vitamin B_{12} agree well with those of our single-crystal ^{59}Co NMR study showing the power of static NMR experiments. Last year Frydman and co-workers published a study on cobaltophthalocyanines.[110] The cobalt is surrounded by six nitrogen ligands (four in the macrocycle plane, and two other ligands at the top and bottom to complete the octahedron. The quadrupolar coupling constants in these complexes are fairly large (up to 45 MHz). When spectra have large spectral widths, it has been found that acquiring multiple spectra at different offsets and adding the spectra together yields a better intensity distribution of the powder pattern with respect to the simulated spectra.[110] A ^{59}Co NMR study on vitamin B_{12} with different solvation states was described[57] as a follow-up paper to the vitamin B_{12} static ^{59}Co paper.[24] In the first paper, it was noted that the quadrupolar tensors of the "as purchased" complexes were quite different from the complexes recrystallized from water. In the most recent study, spectra (^{59}Co, ^{13}C, ^{15}N and ^{31}P) from seven different crystallizations were studied showing two different polymorphs originally described in Hodgkin's crystallographic studies.[6, 7, 8, 9, 10, 11]

Phosphorus-31 solution NMR has been used to study biological systems since the early 1970s[111, 112] because ^{31}P NMR is very sensitive (100% natural abundance, high γ, etc.). In the early studies, the interest was usually the O-P-O bond angles and how they affected the ^{31}P chemical shifts. Starting in the early 1980s, Brown and co-workers reported a series of solution ^{31}P NMR studies of base-on and base-

off cobalamins.[82, 113, 114, 115]. The group's work reported shifts, J-coupling to nearby protons, and pH effects on a variety of cobalamins. These investigators have also reported the ^{31}P NMR spectra of aquocobalamin bound to haptocorrin (a protein).[116] More recently, ^{31}P chemical shifts have been correlated to the distance between the cobalt centre and the base in base-on forms of cobalamin.[117]

Similarly, solid-state ^{31}P NMR studies of biological systems have been performed since the mid 1970s in the study of lipids[118, 119] and nucleic acids[120] using both powder and single-crystal NMR techniques. More recently, Brown *et al.* have published the powder ^{31}P NMR spectrum of aquocobalamin.[121] The aim of this study was to estimate the ^{31}P chemical shift anisotropy to aid in the understanding of the relaxation behavior of the aquocobalamin-haptocorrin complex. In doing so, the ^{31}P chemical shift tensor of aquocobalamin was determined to have the following principal components: δ_{11} = 79.4 ppm, δ_{22} = 26.4 ppm, and δ_{33} = -106.1 ppm (these correspond to a span of 185.5 ppm and a skew of 0.42). With this first cobalamin ^{31}P chemical shift tensor now determined, it would be interesting to see if other cobalamins have similar ^{31}P chemical shift tensors and if they are the same in base-on and base-off conformations.

In this chapter, the ^{59}Co NMR spectra of the base-off forms of B_{12} and MeB_{12} will be presented and compared to the base-on forms. Phosphorus-31 NMR spectra of both base-on and base-off forms of B_{12} and MeB_{12} will also be presented. All of these results will then be discussed with respect to their relevance in cobalamin biochemistry.

5.2 Theory

The theory required to simulate quadrupolar lineshapes is given in section 2.1.6. Particularly relevant is equation 2.39, the lineshape equation used to simulate the ^{59}Co NMR spectra. From these simulations, eight parameters(δ_{11}, δ_{22}, δ_{33}, χ, η, α, β, and γ) were determined for the base-off cobalamins. These parameters fully describe the chemical shift and quadrupolar tensors as well as the relative orientation of the tensors with respect to each other.

With regard to the lineshape theory for ^{31}P NMR, section 2.1.3 includes a description of chemical shielding and equation 2.14 is the lineshape equation for a static spectrum that only contains anisotropy in the chemical shift. The chemical shift tensors can be described using the three principal components of the tensor, but, in general, discussions pertaining to ^{31}P NMR results will be in terms of the isotropic chemical shift (δ_{iso}), the span (Ω), and the skew (κ) of the chemical shift tensor. Since CPMAS spectra of ^{31}P were acquired, δ_{iso} was obtained directly from these spectra and only two parameters (Ω and κ) were simulated for the ^{31}P spectra.

5.3 Experimental

5.3.1 Synthesis of Base-Off Cobalamins

Base-off forms of cobalamins were synthesized by adding a dry cobalamin and KCN to a small vessel, adding a minimal amount of water, and letting the solution sit in the dark for 7 days, or, in the case of the base-off form of vitamin B_{12} left to reflux for 24 hours. To determine the conversion of the base-on form of a cobalamin to a

base-off form, UV-visible spectroscopy was used.

To synthesize the base-off form of vitamin B_{12} (to be referred to as $B_{12}BO$ from now on), 100 mg of vitamin B_{12} (0.075 mM) and 9.8 mg KCN (0.15 mM) were placed in a 5 mL vial. In red light, 1 mL of distilled H_2O was added. The vial was capped, and the solution was stored in the dark for 7 days. The solution was then reduced to dryness *via* rotavap under red light yielding 106 mg of $B_{12}BO$ (96.5 %). UV-visible spectra were recorded on a Varian CARY 1 Bio UV-visible spectrophotometer to monitor the conversion of B_{12} to $B_{12}BO$ using concentrations of approximately 2.5×10^{-5} M. The UV-visible spectra of this conversion are seen in Figure 5.2.

In a similar fashion, to synthesize the base-off form of methylcobalamin (to be referred to as $MeB_{12}BO$ from now on), 100 mg of methylcobalamin (0.074 mM) and 9.6 mg of KCN (0.148 mM) were used to produce 105 mg of $MeB_{12}BO$ (95.8 %). Figure 5.3 shows the UV-visible spectra of MeB_{12} and $MeB_{12}BO$.

As will be seen shortly in section 5.4, the UV-visible results are deceptive. Therefore, different amounts of KCN were added to both of the cobalamins and in the case of the synthesis of $B_{12}BO$, refluxing was also used.

5.3.2 Solid-State NMR Experiments

Solid-state ^{59}Co static NMR experiments were performed at 11.75 T on a Bruker AMX-500 NMR spectrometer and at 4.7 T on a Bruker ASX-200 NMR spectrometer using a solenoid (wideline) probe. Solid samples were crushed with a mortar and pestle and packed into 5 mm NMR tubes cut to a length of 25 - 28 mm. The spectra

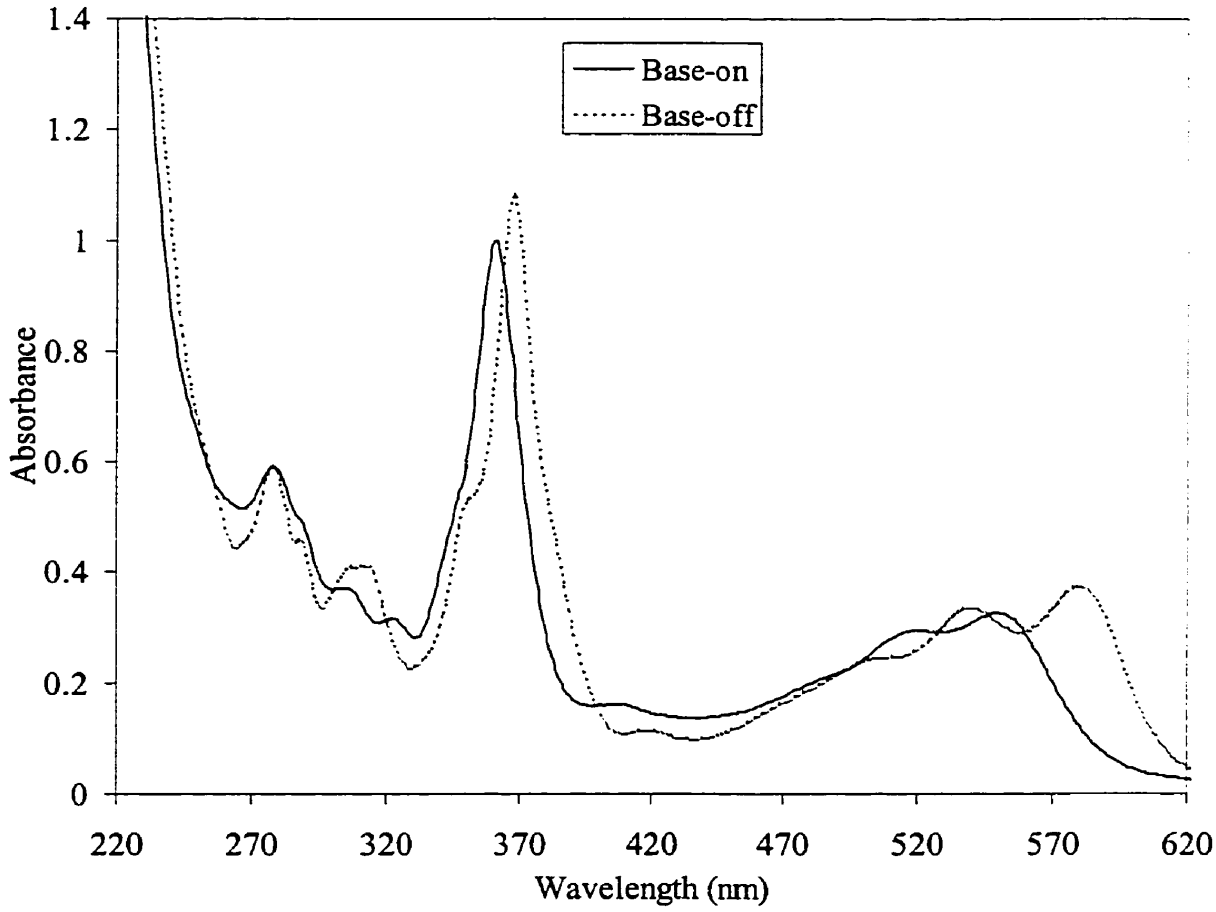

Figure 5.2: UV-visible spectra of B_{12} (solid line) and $B_{12}BO$ (dashed line).

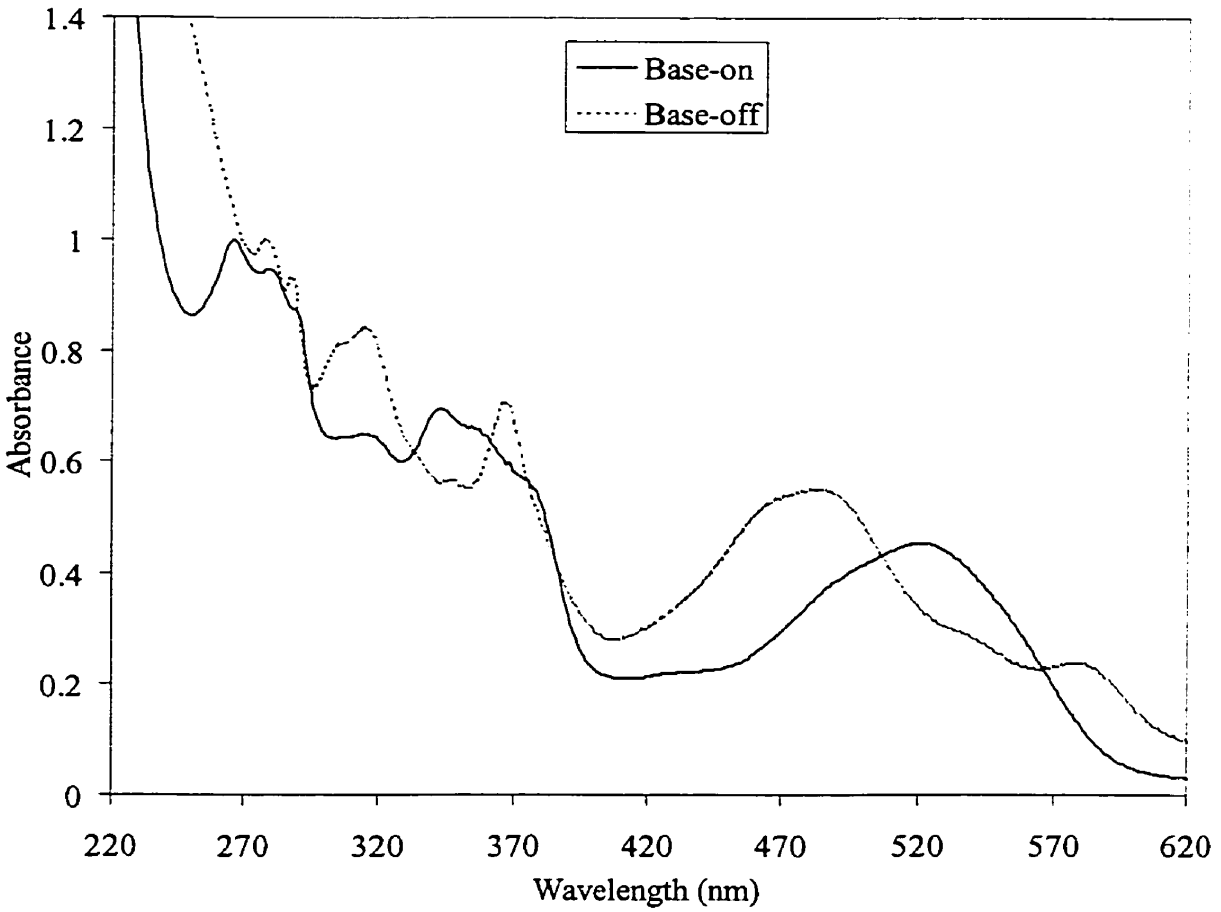

Figure 5.3: UV-visible spectra of MeB_{12} (solid line) and $MeB_{12}BO$ (dashed line).

were acquired using a spin-echo pulse sequence[122] optimized for excitation of the central transition. Cobalt-59 NMR spectra were referenced to 1.0 M $K_3Co(CN)_6$ (aq) at 0 ppm. A solid-echo pulse sequence was used to remove dead time problems. A pulse length of 1 μs was used for both pulses (the 90° pulse was 4 μs) with a delay between pulses of 7 - 10 μs. A recycle time of 50 ms was used between scans.

Solid-state ^{31}P NMR spectra were acquired at 202.4 MHz on a Bruker AMX-500 NMR spectrometer (B_0 = 11.75 T). The samples were packed in 4 mm o.d. zirconium oxide rotors. Cross polarization under the Hartmann-Hahn matching condition was used with a typical proton 90° pulse of 7.6 μs and a contact time of 3 ms. High-power proton decoupling was used during the acquisition of all spectra with a 10 s delay between scans. The phosphorus chemical shifts were referenced to 85% H_3PO_4 (aq) by setting the shift of $NH_4H_2PO_4$ to +0.81 ppm.

5.3.3 Simulation of NMR Lineshapes

Simulation of the MAS powder lineshapes were performed on a personal computer using the program WSOLIDS from Prof. R. Wasylishen and co-workers.[92] This software uses the POWDER routine[93] for simulation static spectra and the Herzfeld-Berger method[42] for MAS spectra, and there are additions for quadrupolar nuclei.[63] For the ^{59}Co NMR spectral simulations, the three principal components of the chemical shift tensor (δ_{11}, δ_{22}, and δ_{33}), the quadrupolar coupling constant (χ), asymmetry of the quadrupolar tensor (η), and the Euler angles relating the two tensors (α, β, and γ) were optimized to maximize the agreement between the experimental and calculated lineshapes of the central transition. The

^{31}P isotropic chemical shifts used in the ^{31}P NMR spectral simulations were obtained directly from the CPMAS spectra and the span (Ω) and the skew (κ) were optimized to fit both CPMAS and CP static spectra.

5.4 Results

5.4.1 Phosphorus-31 NMR Results

Phosphorus-31 NMR spectra were acquired with and without sample spinning, *i.e.*, CPMAS and CP static, respectively. The base-on complexes both only have one site but two sites are immediately observed in the MAS spectra of the base-off complexes. We have attributed this to a mixture of base-on and base-off cobalamins since one of these two sites matches the pure base-on ^{31}P NMR spectra. Using this assignment, the spectra seen in Figures 5.4 - 5.7 were simulated using the parameters in Table 5.1 with varying the amount of the two sites in the base-off spectra. The CPMAS spectra in Figures 5.5 - 5.7 all have significantly broader lines than the lines of the CPMAS spectrum in Figure 5.4 which are narrow except near the base of the peaks. The broad lines are due to low crystallinity of the samples compared to the vitamin B_{12} in Figure 5.4 where the sample is more crystalline. The broadening in Figure 5.4 is possibly due to shimming or part of the sample being less crystalline compared to the majority of the sample.

From the simulations of the base-on cobalamins, it is immediately evident that the ^{31}P chemical shift tensors are essentially identical since the spans and skews are the same within experimental error. The only difference is a slightly higher

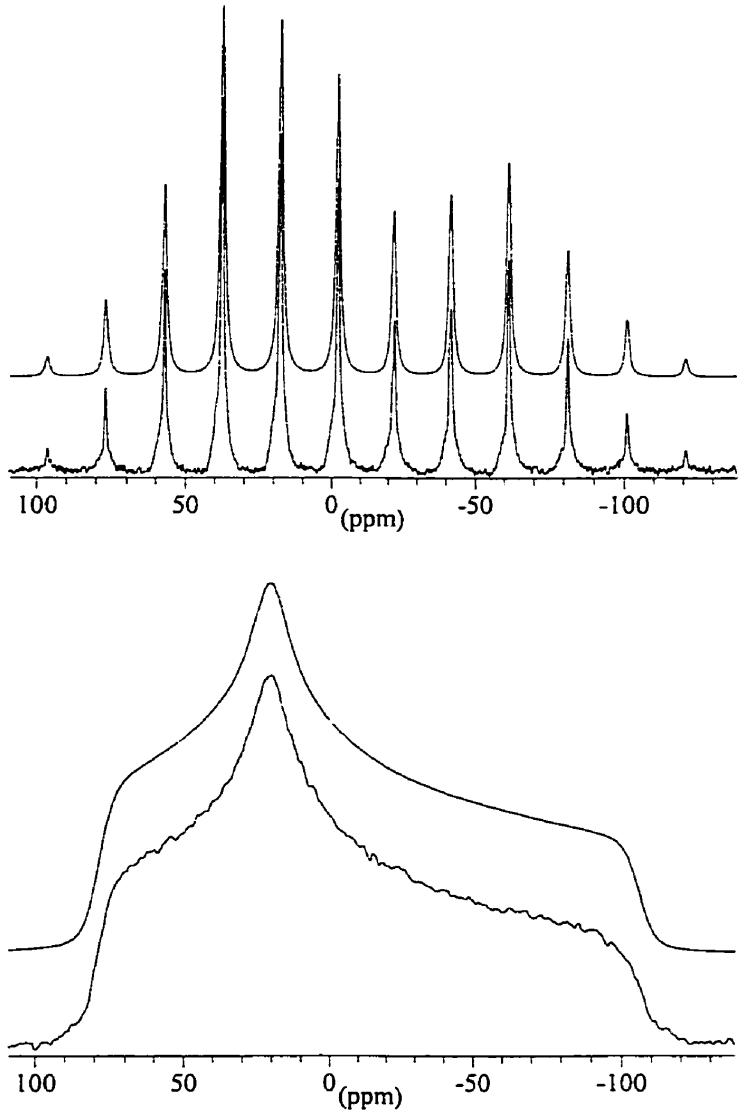

Figure 5.4: Solid state ^{31}P NMR spectra of B_{12} at 11.75 T. Upper spectra are spinning (CPMAS) at 4 kHz, lower spectra are CP static. The simulated spectra are slightly offset above the experimental spectra using the parameters in Table 5.1.

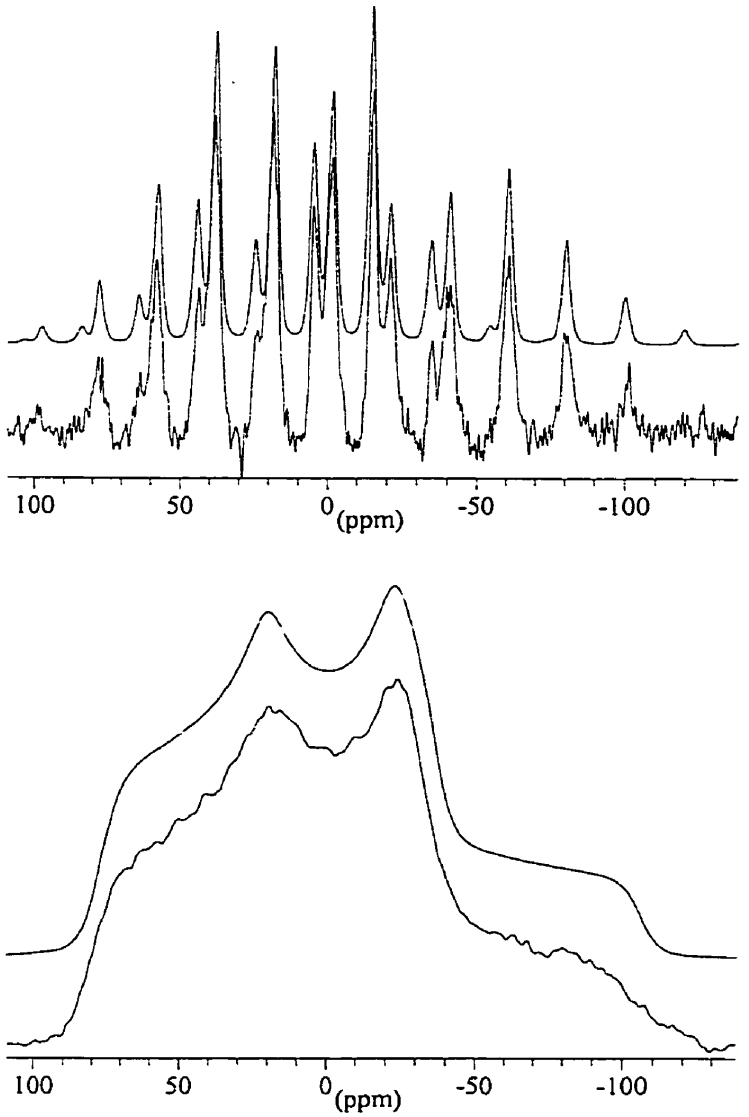

Figure 5.5: Solid state ^{31}P NMR spectra of $B_{12}BO$ (8 KCN per B_{12}) at 11.75 T. Upper spectra are spinning (CPMAS) at 4 kHz, lower spectra are CP static. The simulated spectra are slightly offset above the experimental spectra using the parameters in Table 5.1.

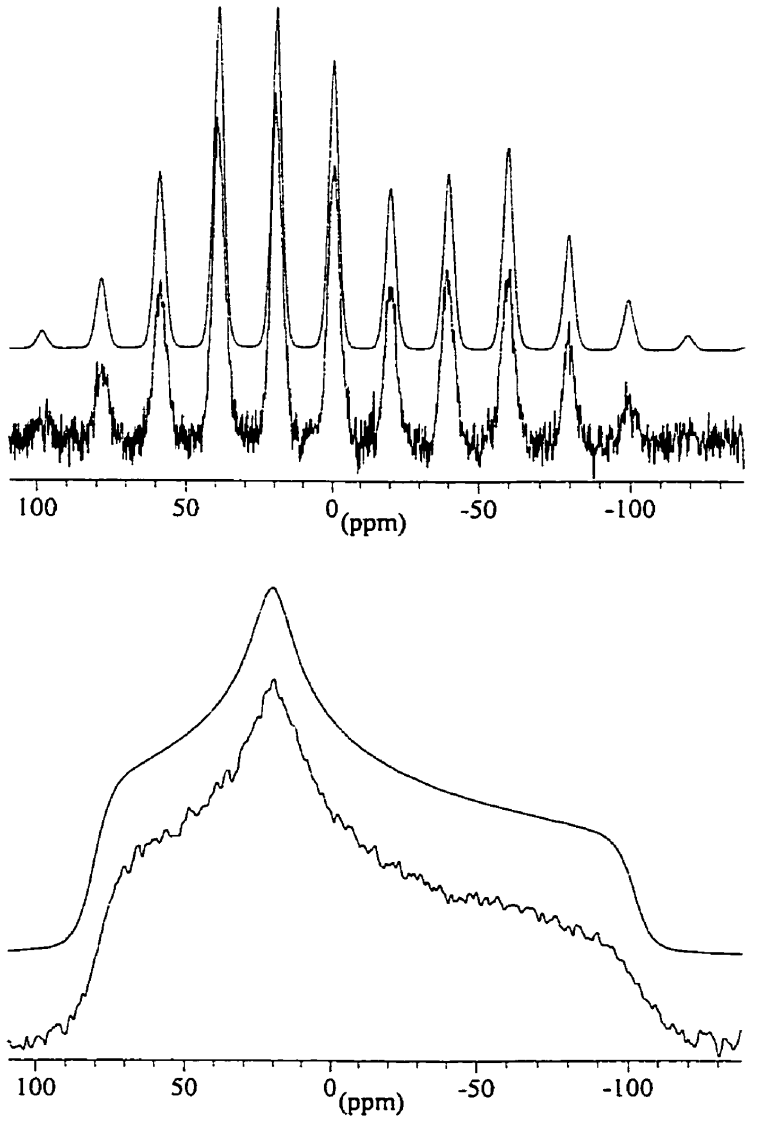

Figure 5.6: Solid state ^{31}P NMR spectra of MeB_{12} at 11.75 T. Upper spectra are spinning (CPMAS) at 4 kHz, lower spectra are CP static. The simulated spectra are slightly offset above the experimental spectra using the parameters in Table 5.1.

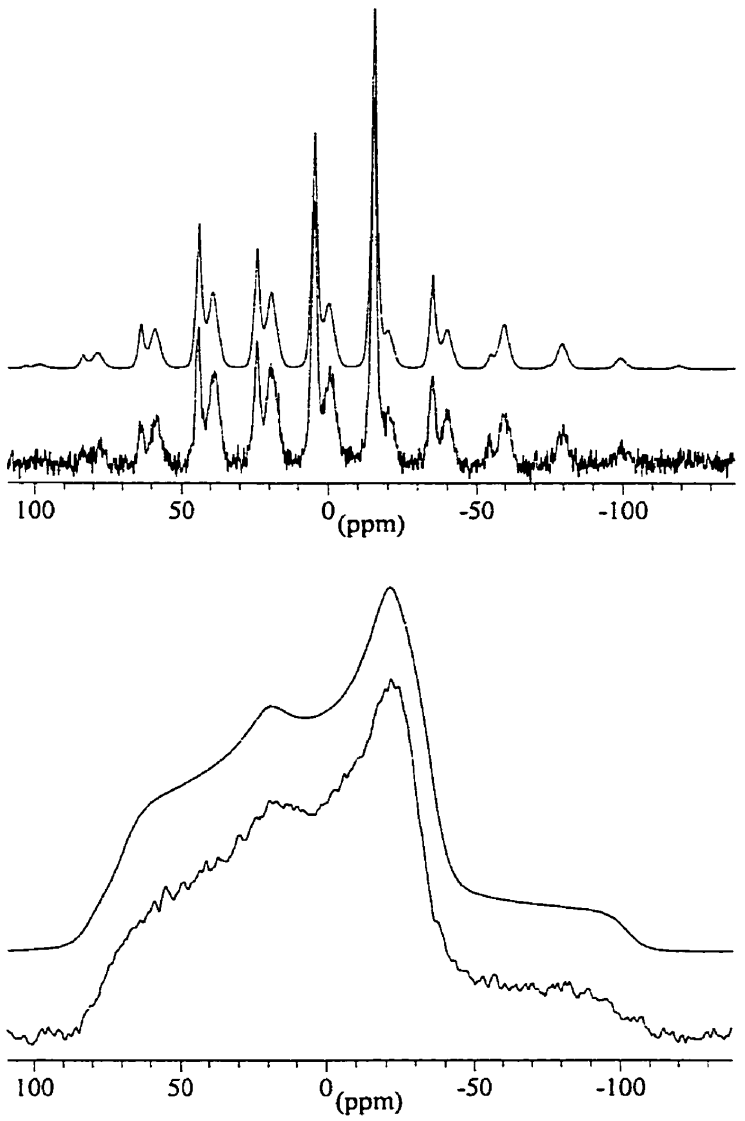

Figure 5.7: Solid state ^{31}P NMR spectra of $MeB_{12}BO$ (4 KCN per MeB_{12}) at 11.75 T. Upper spectra are spinning (CPMAS) at 4 kHz, lower spectra are CP static. The simulated spectra are slightly offset above the experimental spectra using the parameters in Table 5.1.

Table 5.1: Solid-state ^{31}P NMR results of base-on and base-off cobalamins (errors are given in parentheses).

	B_{12}	$B_{12}BO$	MeB_{12}	$MeB_{12}BO$
δ_{iso}	-2.25 (0.10) ppm	4.86 (0.10) ppm	-0.44 (0.10) ppm	4.42 (0.10) ppm
Ω	185 (2) ppm	110 (5) ppm	183 (2) ppm	105 (3) ppm
κ	0.37 (0.02)	-0.75 (0.05)	0.34 (0.02)	-0.72 (0.03)
δ_{11}	79 (1) ppm	74 (3) ppm	81 (1) ppm	70 (2) ppm
δ_{22}	21 (1) ppm	-23 (2) ppm	20 (1) ppm	-21 (1) ppm
δ_{33}	-106 (1) ppm	-36 (2) ppm	-102 (1) ppm	-35 (1) ppm

isotropic chemical shift of MeB_{12} with respect to B_{12}. Simulated spectra were performed using both the POWDER routine[93] for the static spectra and the Herzfeld-Berger method[42] for the MAS spectra using the same parameters for both spinning and static except for taking the spinning rate into account in the CPMAS spectra.

The base-off spectra were more complicated in that they contain two sites. The isotropic shift of one of the sites, as well as its spinning side band pattern, is the same as for the base-on complexes. We have assigned the second site in both spectra to be the base-off form. Approximately 35% of the spectra in Figure 5.5 and 57% of the spectra in Figure 5.7 show the cobalamin to be in the base-off conformation. The parameters used to fit the base-off portion of the spectra of both complexes are the same within experimental error and significantly different than the parameters used in fitting the base-on form. The fits in Figures 5.5 and 5.7 are a summation of base-on and base-off components.

As described in section 5.3.1, 2:1 molar equivalents of KCN with respect to

cobalamin gave UV-visible spectra that were indicative of base-off cobalamins for both the cyano and methyl forms. The spectra in Figures 5.5 and 5.7 indicate otherwise. Therefore a titration study was completed for the two complexes, the results of which are seen in Figures 5.8 (for B_{12} + KCN) and 5.9 (for MeB_{12} + KCN). As seen in Figure 5.8, B_{12} converted completely to the base-off form after the complex had been refluxed for 24 hours with 8 molar equivalents of KCN while MeB_{12} did not require such harsh conditions. Once these complexes were completely converted to the base-off forms, it was possible to obtain the ^{31}P NMR spectra seen in Figures 5.10 ($B_{12}BO$) and 5.11 ($MeB_{12}BO$).

With sample purity now, established it is possible to compare the base-off forms of the cobalamins. These two complexes have very similar chemical shift tensors. With almost identical δ_{iso} and κ, it is not surprising that the spans of the tensors only differ by approximately 10%. A comparison of the base-on and base-off forms, however, yields interesting results. The δ_{11} components of both base-on (80 $\pm$ 1 ppm) and base-off (72 $\pm$ 2 ppm) forms are quite close while the other two components of the tensor are significantly different with the δ_{22} component decreasing in chemical shift (20 $\pm$ 1 ppm in base-on to -22 $\pm$ 1 ppm in base-off) and the δ_{33} component increasing in chemical shift (-104 $\pm$ 2 ppm in base-on and -35 $\pm$ 1 ppm in base-off). These changes have a huge effect on the skew of the tensor of the base-off form such that it is negative while the skew of the base-on form is positive.

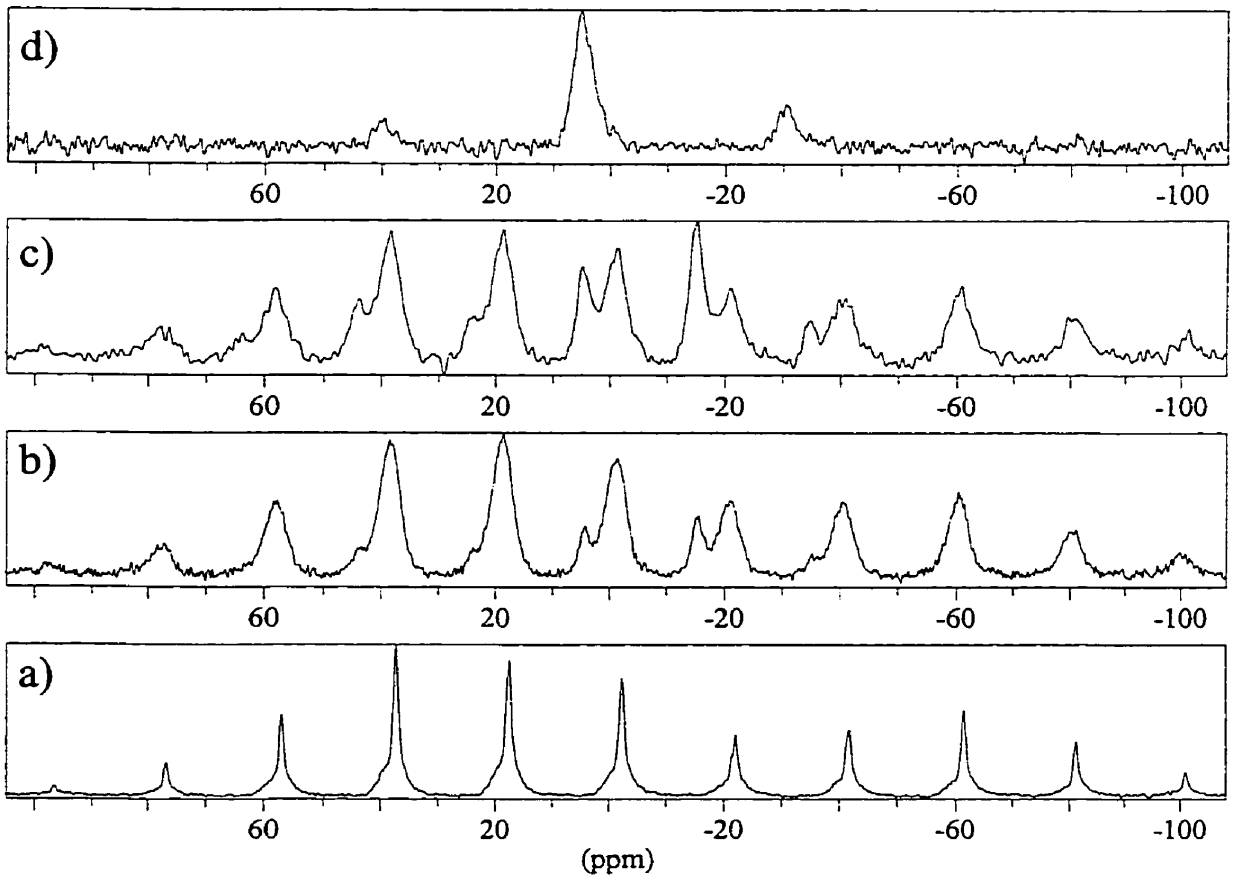

Figure 5.8: Solid state ^{31}P MAS NMR spectra (at 11.75 T) of a) B_{12} b) B_{12} + 2 KCN, c) B_{12} + 8 KCN, and d) B_{12} + 8 KCN after 24 hour reflux.

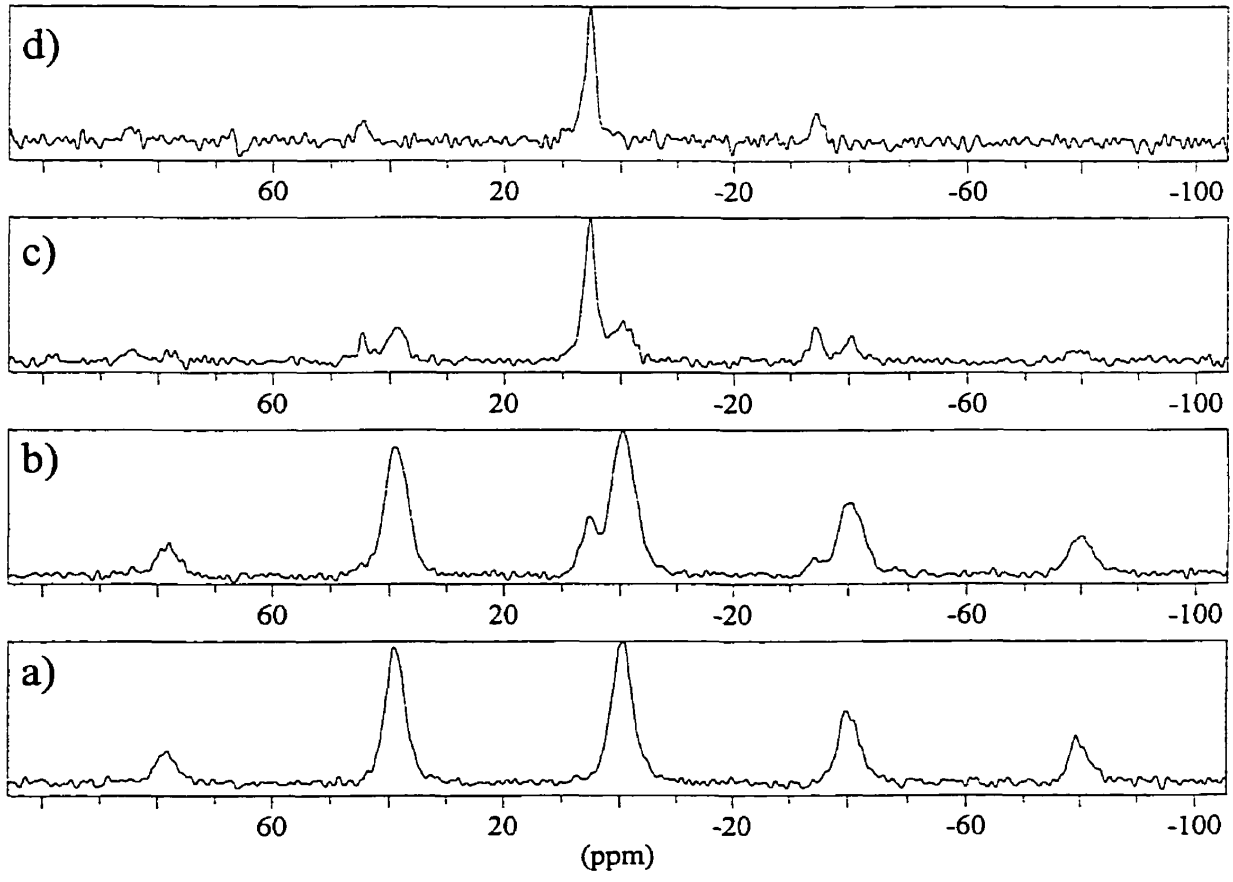

Figure 5.9: Solid state ^{31}P MAS NMR spectra (at 11.75 T) of a) MeB_{12} b) MeB_{12} + 2 KCN, c) MeB_{12} + 4 KCN, and d) MeB_{12} + 8 KCN.

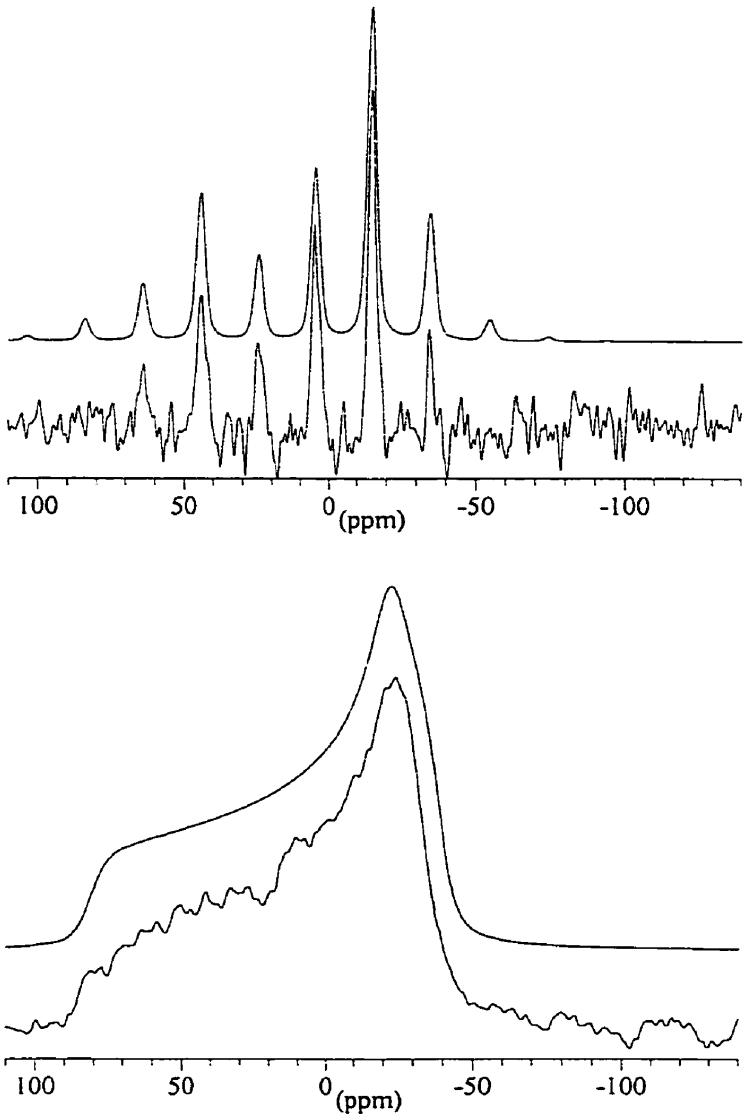

Figure 5.10: Solid state ^{31}P NMR spectra of $B_{12}BO$ at 11.75 T. Upper spectra are spinning (CPMAS) at 4 kHz, lower spectra are CP static. The simulated spectra are slightly offset above the experimental spectra using the parameters in Table 5.1.

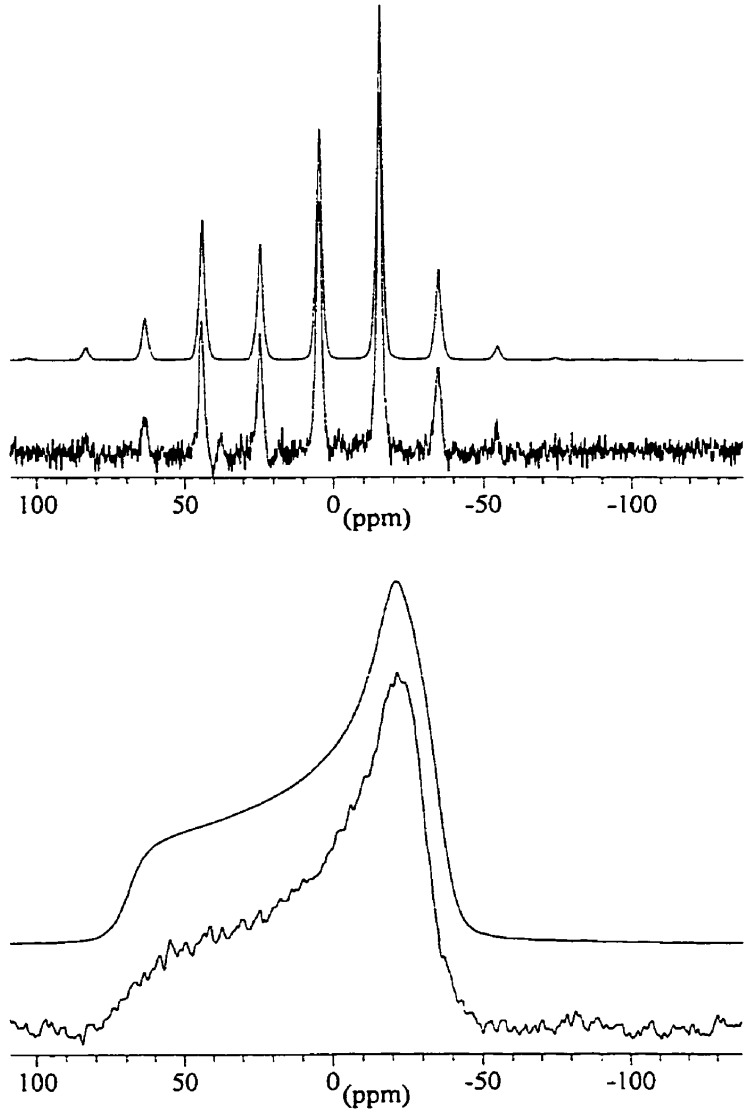

Figure 5.11: Solid state ^{31}P NMR spectra of $MeB_{12}BO$ at 11.75 T. Upper spectra are spinning (CPMAS) at 4 kHz, lower spectra are CP static. The simulated spectra are slightly offset above the experimental spectra using the parameters in Table 5.1.

5.4.2 Cobalt-59 Powder Results

The solid-state ^{59}Co NMR spectra of B_{12} and $B_{12}BO$ as well as the simulated spectra at 4.7 T and 11.75 T are seen in Figures 5.12 and 5.13. The parameters used for the simulations are given in Table 5.2. Table 5.2 also contains the parameters for the base-on complexes from the single crystal ^{59}Co NMR study described in the Chapter 3 as well as powder NMR data in the literature for MeB_{12} and dicyanocobyrinic acid heptamethylester.[24]

As described in section 5.1, there is very little data concerning ^{59}Co chemical shift and quadrupolar tensors in the literature. The results presented in Table 5.2 are the first solid-state ^{59}Co NMR results available for base-off cobalamins. The only other complex in the literature similar to B_{12} is that of dicyanocobyrinic acid[24] (also seen in Table 5.2).

It is interesting to note the similarities and differences between the base-on and base-off forms. Looking at the vitamin B_{12} base-on and base-off conformations, we note a large change in the strength of the quadrupolar tensor (a decrease of 9 MHz from base-on to base-off), but the asymmetry of this tensor stays approximately the same. The spans of the chemical shift tensor of these two complexes are close to the same (within 15% of each other) but they have opposite skew ($\kappa(B_{12})$ = 0.1 while $\kappa(B_{12}BO)$ = -0.06). Even though the direction of κ is opposite, they are both close to 0 and therefore not that different (both are close to totally non-axially symmetric chemical shift tensors). The orientations of the two tensors, however, are very different. From the B_{12} results, we know that the largest component of the quadrupolar tensor is approximately perpendicular to the corrin ring. Using

Table 5.2: Solid-state ^{59}Co NMR results (errors given in parentheses).

	B_{12}^{a}	$B_{12}BO$	MeB_{12}^{b}	$MeB_{12}BO$	Dicyanocobyrinic acid[b]
δ_{11}	5075 (45) ppm	4685 (20) ppm	6010 (100) ppm	4200 (75) ppm	4980(100) ppm
δ_{22}	4670 (43) ppm	3890 (15) ppm	3722 (100) ppm	3735 (40) ppm	4420(100) ppm
δ_{33}	3902 (42) ppm	3350 (25) ppm	3018 (100) ppm	2800 (75) ppm	3500(100) ppm
χ	27.31 (0.08) MHz	18 (1) MHz	12.1 (0.4) MHz	17 (1.5) MHz	26.7(0.8) MHz
η	0.243 (0.005)	0.3 (0.05)	0.3 (0.2)	1.0 (0.1)	0.9(0.4)
α	334.0° (13.0°)	90° (5°)	25° (40°)	40° (5°)	0°(35°)
β	41.4° (1.7°)	90° (5°)	60° (25°)	30° (5°)	95°(35°)
γ	207.3° (2.5°)	11° (3°)	0° (40°)	-20° (10°)	0°(35°)

a) From single crystal results. b) From reference [24].

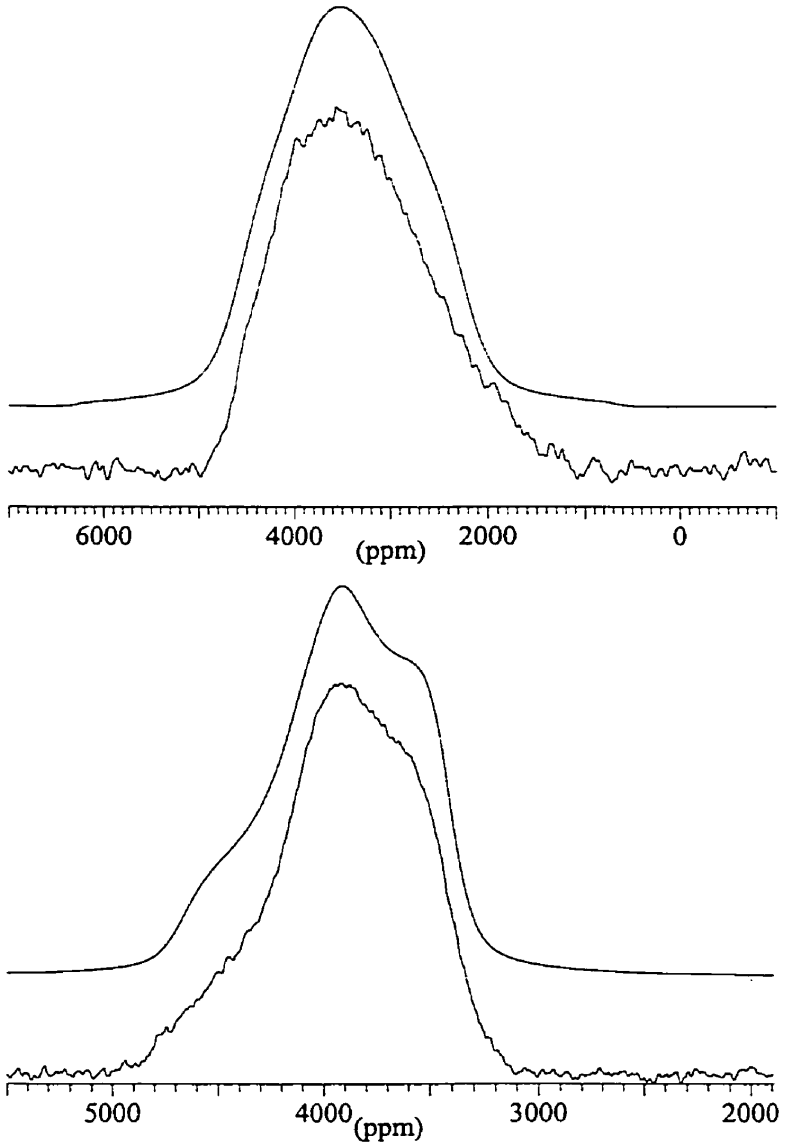

Figure 5.12: Solid state ^{59}Co NMR spectra of $B_{12}BO$ at 4.7 T (upper spectra) and 11.75 T (lower spectra). The simulated spectra are slightly offset above the experimental spectra.

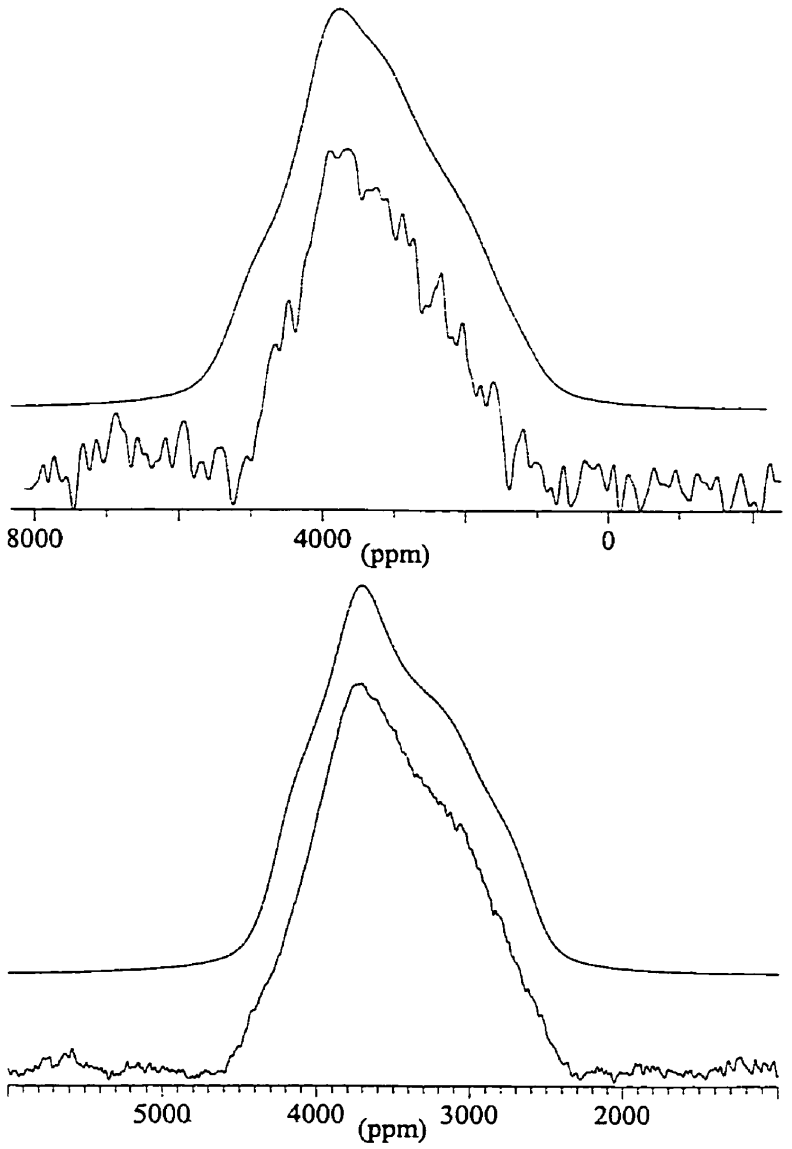

Figure 5.13: Solid state ^{59}Co NMR spectra of $MeB_{12}BO$ at 4.7 T (upper spectra) and 11.75 T (lower spectra). The simulated spectra are slightly offset above the experimental spectra.

basic symmetry arguments we would suggest that the largest component of the quadrupolar tensor of the base-off form of vitamin B_{12} is also directed perpendicular to the corrin ring. This being assumed, the least shielded component of the chemical shift tensor would likely be in the corrin ring plane since $\beta = 90^o$, which is very different from that of the base-on conformation (see Figure 3.6). Upon examination of the ^{59}Co NMR spectra of the base-on and base-off forms of methylcobalamin, very different observations are made as compared to the cyano form. The quadrupolar interaction of the base-off form is significantly larger (by 5 MHz) than the base-on form and the symmetries of the tensors are significantly different; in fact, the quadrupolar tensor of the base-off form is totally non-symmetric (*i.e.*, eq_{33} = -eq_{11} and eq_{22}=0). The span of the chemical shift tensor of the base-on complex is more than twice as large as the base-off conformation and the tensors have opposite skews (-0.18 for the base-on and 0.11 for the base-off). The relative orientations of the tensors between these two complexes are basically the same even though the β angles appear significantly different. Since $\eta = 1$ for the base-off complex, a β angle of 30° is the same as a β angle of 60° for a small η as described by the base-on complex.

There is only one trend seen across all of the dicyano corrinoid complexes (the two base-off forms as well as the dicyanocobyrinic acid) - the spans are all 1400 ± 80 ppm. The skews of all three compounds have magnitudes of about 0.1 but the signs are not all the same. The magnitudes of the quadrupolar tensors of the base-off cobalamins are very similar but are significantly smaller than for the dicyanocobyrinic acid. The quadrupolar tensors of both dicyanocobyrinic acid and

$MeB_{12}BO$ are totally non-symmetric, but the quadrupolar tensor of B_{12} has an η value of 0.3. The relative orientation of the chemical shift and quadrupolar tensors are different in all three complexes.

5.5 Discussion

Significant differences in chemical shift tensors of both the cobalt centre and in the phosphorus tail are seen when members of the B_{12} family change from base-on to base-off. In studying these nuclei, a model is hoped to be constructed that can be used in studying cobalamins bound to enzymes.

The most significant differences observed in the ^{59}Co NMR spectra are the large decreases in isotropic chemical shift. This is due largely to a switch from five nitrogen and one carbon around the cobalt centre to four nitrogens and two carbons around that centre. This phenomenon has been studied in some detail in solution ^{59}Co NMR[123] and is still in its infancy in regards to solids with only our group discussing the effects of ligand planes on cobalt chemical shifts.[59]

Assigning ligand planes responsible for specific chemical shift in cobalamins would be beneficial, if possible, to gain a better understanding of this class of compounds. However, in this study, we believe that it is not possible. The orientation of the chemical shift tensor of vitamin B_{12} shows that there is not a specific ligand plane that can be assigned to give rise to a specific chemical shift (see Figures 3.5 and 3.6). In light of these results, it would be fruitless to attempt to make ligand plane assignments since all of the complexes have ^{59}Co chemical shift and quadrupolar tensors that vary significantly.

The differences in the ^{31}P NMR spectra of the base-on cobalamins when compared to the base-off forms are substantially more informative than the ^{59}Co results. This is intriguing considering the phosphorus group is in the tail and it is not intuitive that a nucleus so far away from the centre of action would be so informative. The isotropic chemical shifts of the base-on and base-off forms are not significantly different (less than 8 ppm), not overly surprising since most biological phosphates have shifts between 5 and -15 ppm.

The spans and skews of the tensors for the two base-on forms are very close to identical, and are also similar to the ^{31}P NMR results for aquocobalamin.[121] The spans of the chemical shift tensors of these three base-on cobalamins are between 183 and 185 ppm and the skews of the tensors are 0.38 ± 0.04 indicating that the shape of the tensors is basically identical across the series of base-on cobalamins. The slight variations across the family are not surprising since the phosphate group would have different solvation in each complex. Effects of such solvation have been described recently by Frydman's group[57] on ^{59}Co, ^{13}C, ^{15}N and ^{31}P. In their study the spans of the shift tensor are seen to change with the solvation sphere while the shape of the pattern (as described by the skew) are found to be essentially identical.

When comparing the base-off forms of cobalamins, we have observed that the ^{31}P chemical shift tensors for the two complexes in this study are essentially identical. As seen in Table 5.1, the ^{31}P chemical shift tensors have spans of 107.5 ± 2.5 ppm with skews of -0.735 ± 0.015. Thus the ^{31}P chemical shift tensors for the two base-off forms are the same within experimental error.

What is most interesting to note is the ^{31}P lineshape (as demonstrated by the

skew) arising from the base-off ^{31}P chemical shift tensor is significantly different from the base-on cobalamin forms. This is seen in a positive skew for the base-on cobalamins while the base-off cobalamins have a negative skew. It is also notable that the ^{31}P chemical shift tensor for the base-off cobalamins is much closer to axial symmetry compared to the base-on forms. Upon inspection of the chemical shift tensor principal components, δ_{11} for both the base-on and base-off forms are fairly close (within 15 ppm). It is also interesting that the other two components of the base-on chemical shift tensor seem to converge (but not completely) which gives the lineshape observed for the base-off form.

Positive *vs.* negative skews are commonly seen in solid-state ^{31}P NMR studies of phosphates in biochemistry. When a phospholipid is in an inverted hexagonal phase,[124, 125] a chemical shift tensor with positive skew is observed. A positive skew is also observed for powders of phosphodiesters[118, 120] as well as aquocobalamin.[121]. The phosphate groups in the cobalamin studied here have positive skews and are also phosphodiesters. Phospholipids in bilayers, however, have ^{31}P chemical shift tensors that have negative skews[124] similar to phosphomonoesters.[120] The conversion from a bilayer phase to an inverted hexagonal phase can be induced by adding different reagents and studied *via* solid-state ^{31}P NMR.[124] In a similar fashion, we have been able to study the conversion of base-on cobalamins (positive skew) to base-off cobalamins (negative skews) using solid-state ^{31}P NMR.

One thing that is exceptional in this study is that UV-VIS spectroscopy shows only either base-on or base-off cobalamins while solid-state ^{31}P NMR can show a

mixture of the two conformations. These UV-VIS results could possibly be explained in two ways. One explanation could be based on the absorbances of the two complexes which can be observed visually as a bright red solution for the base-on form while the base-off forms are deep purple. From a UV-visible perspective, base-off cobalamins absorb more strongly than the base-on counterparts (*e.g.*, ϵ_{361} = 28.06×10^3 $Lmol^{-1}cm^{-1}$ for B_{12} while for $B_{12}BO$ $\epsilon_{369} = 30.4 \times 10^3$ $Lmol^{-1}cm^{-1}$).[126] The ^{31}P solid-state NMR spectra, however, are not affected by differences in light absorption, but only by how much of each site is in each environment. A second explanation could possibly come from solution ^{31}P NMR. Early solution ^{31}P NMR studies indicate that the base-on and base-off forms of MeB_{12} have essentially identical chemical shifts.[113] We have performed a preliminary solution ^{31}P NMR study and have obtained with interesting results. If MeB_{12} is dissolved in D_2O, it has a δ_{iso} of -0.40 ppm. If a solution of KCN is added slowly to the NMR tube, the ^{31}P chemical shift only varies slightly to higher chemical shift even if 20 equivalents of KCN are added (δ_{iso} = -0.28 ppm) comparable to the observations by Brown and co-workers.[113] However, if we dissolve the solid $MeB_{12}BO$, which had a solid-state δ_{iso} of 4.42 ppm, δ_{iso} in solution is found to be 4.55 ppm. This interesting behavior warrants further solution investigations of cobalamin base conformation by both NMR and UV-visible spectroscopy.

5.6 Conclusions

The chemical shift (for both ^{59}Co and ^{31}P) and quadrupolar tensors (for ^{59}Co) are significantly different in base-on and base-off cobalamin complexes. No spectro-

scopic trend could be determined in the ^{59}Co NMR results other than a similarity in the span of the chemical shift tensors. Trends, however, in ^{31}P chemical shift tensors have been observed. The spans and skews of base-on cobalamins are 184 $\pm$ 3 ppm and 0.355 $\pm$ 0.035 while base-off cobalamins have Ω = 107.5 $\pm$ 2.5 ppm and κ = -0.735 $\pm$ 0.015. Since the ^{31}P chemical shift tensors are significantly different in the base-on and base-off forms of B_{12} family members, the possibility exists to capitalize on these trends. The next step would be to look at the chemical shift tensors of enzyme-bound forms of cobalamins where the base is known to be either base-on or base-off and see if this trend is observed. If it is, a simple probe has been discovered to study the conformation of the nucleotide tail in cobalamin-enzyme complexes without the need for single crystals suitable for X-ray diffraction.

Chapter 6

Solid-State Deuterium NMR Study of Methyl-d_3-Cobalamins

6.1 Introduction

As discussed in the preceding chapter, the conformation (base-on *vs.* base-off) of the dimethylbenzimidazole tail of cobalamin-enzyme complexes is of great interest. Using the knowledge gained from the ^{31}P on the conformation of the tail in methylcobalamin, the dynamics of the methyl group of the base-on and base-off forms of methylcobalamin can be investigated.

The main interest in studying the dynamics of the methyl groups in methyl-d_3-cobalamins is to lay the foundation for the examination of methyl-d_3-cobalamin-enzyme complexes. The first cobalamin-enzyme complex for which the structure was definitively known was that of MeB_{12} bound to a 27-kDa fragment of methionine synthase (*Escherichia coli*) studied *via* X-ray crystallography.[21] Methionine

synthase is a methyl tranferase that allows for the conversion of homocysteine to methionine, releasing H_4folate from CH_3-H_4folate.[127] In this structure (seen in Figure 6.1)[21] the dimethylbenzimidazole tail was displaced by a histidine residue (His-759) of the protein. The nucleotide tail extended into a channel of the protein's structure, resulting in a base-off cobalamin. The histidine residue that replaces the dimethylbenzimidazole allows the enzyme to have direct control of the methyl transfer in this tranferase enzyme. This replacement around the cobalt centre will affect the cobalt-carbon bond, which presumably promotes the cobalt-carbon bond scission.

The methyl group of methylcobalamin can be replaced easily with a deuterated methyl group through chemical means. This allows for spectral selectivity in that there will be no other deuterons other than those we introduce. Solid-state ^{2}H NMR has been well established to be a useful probe of dynamics in the solid state.[128, 129, 130, 131] Relaxation measurements can provide important and unique information concerning the motion of deuterated groups in many types of materials. This chapter will describe how selectively labelled methyl-d_3-cobalamin and its base-off analogue were studied to learn about the dynamics of the methyl group in both of these complexes.

6.2 Theory

Spin-1 nuclei, such as ^{2}H, give solid-state NMR spectra with a characteristic Pake pattern. This Pake pattern is observed due to two subspectra for the two possible transitions of a spin-1 nucleus; the 1 $\leftrightarrow$ 0 transition and the 0 $\leftrightarrow$ -1 transition. The

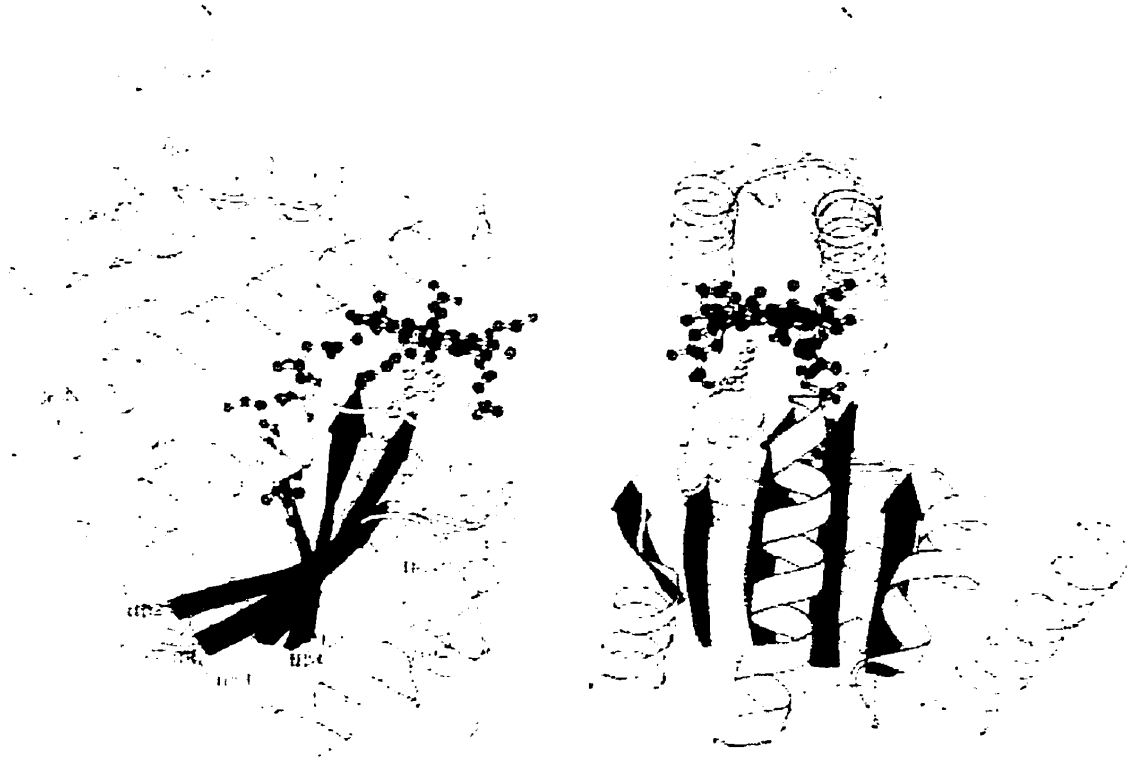

Figure 6.1: Methylcobalamin bound to methionine synthase. Reproduced from reference [21].

following equation describes these two subspectra

$$\nu(\theta,\phi) = \nu_o \pm (3\chi/4)(3cos^2\theta - 1 - \eta sin^2\theta cos2\phi) \tag{6.1}$$

where $\nu(\theta,\phi)$ is the anisotropic frequency response of the spectrum, ν_o is the Larmor frequency, χ is the quadrupolar coupling constant, η is the asymmetry of the quadrupolar tensor and the angles θ and ϕ give the orientation of the principal component of the quadrupolar coupling tensor with respect to the magnetic field. In the case of methyl groups, the principal component of the ^{2}H quadrupolar coupling tensor invariably lies along the ^{2}H-C bond. Methyl deuterons typically possess χ values of 165-180 kHz with η of zero.[132] This simplifies equation 6.1. When groups such as methyl groups undergo rapid N-fold motion (with N $\geq$ 3), the anisotropic line shape is narrowed. Taking these features into account, the following equation results for rapid motion of a methyl group

$$\nu(\psi) = \nu_o \pm (3\chi/4)(3cos^2\psi - 1)[(3cos^2\zeta - 1)/2] \tag{6.2}$$

where ζ is the angle between the N-fold rotation axis and the principal component of the ^{2}H quadrupolar coupling tensor, which, as stated above, lies along the ^{2}H-C bond and ψ is the orientation of the N-fold axis with respect to B_o.

Spin-lattice relaxation measurements of ^{2}H nuclei can be used to establish the type of motion and its rate. The spin-lattice relaxation time, T_1, is measured using the inversion-recovery pulse sequence. The standard inversion recovery pulse sequence is given as follows: 180° - τ - 90° - acquire. The 180° pulse inverts the

net magnetization from M_o to -M_o. After variable delay time, τ, a 90° pulse is applied rotating the magnetization into the plane perpendicular to the magnetic field where an FID can be recorded. At short τ, negative signals are observed. As τ increases, the signals become less negative, then positive, and continues to increase until the maximum signal is obtained when nuclei have sufficient time to return to equilibrium before the second pulse. The recovery of the magnetization is characterized by the following equation:

$$M_o - M(\tau) = 2M_o e^{-\frac{\tau}{T_1}} \tag{6.3}$$

Therefore a plot of signal intensity *vs.* τ will reveal T_1. When studying ^2H, which has a nuclear spin of 1, the 90° pulse in the inversion recovery sequence is replaced by the quadrupole echo (90° - delay - 90° - delay - acquire).[133]

From T_1 measurements, the rotational activation energy of groups, such as methyl groups, can be established.[134] If a methyl group undergoes three-fold jumps, relaxation across the powder lineshape will be anisotropic and parts of the ^2H NMR powder pattern are observed to relax faster than other parts. However, if a methyl group is undergoing rotational diffusion, all parts of the ^2H lineshape will relax at the same rate. Differences in the relaxation behaviour across the ^2H lineshape predicted for these two possibilities can be used to determine the appropriate model for methyl rotation.[135] Variable temperature spin-lattice relaxation times can also used to obtain the activation energy (E_a) of methyl rotation using

the following equations:

$$T_1^{-1} = (3\pi^2/4) < \chi^2 > [J(\omega_o) + 4J(2\omega_o)] \tag{6.4}$$

$$J(\omega_o) = \tau_c/(1 + \omega_o^2\tau_c^2) \tag{6.5}$$

$$J(2\omega_o) = \tau_c/(1 + 4\omega_o^2\tau_c^2) \tag{6.6}$$

$$\tau_c = \tau_\infty e^{-E_a/k_BT} \tag{6.7}$$

where $< \chi^2 >$ is the motionally averaged squared ^{2}H quadrupolar coupling constant, J(ω_o) and J($2\omega_o$) are spectral density functions, ω_o is the angular Larmor frequency, τ_c is the correlation time for rotation, τ_∞ is the correlation time at infinite temperature, k_B is the Boltzmann constant, and T is the temperature in Kelvin. As long as $\omega_o^2\tau_c^2 \ll 1$ (valid for all temperatures in this study), it is obvious from equations 6.4 - 6.7 that a plot of ln(T_1) *vs.* 1/T (an Arrhenius plot) will yield E_a from the slope of this plot.

Equations 6.4 - 6.7 are the traditional solid-state NMR way of describing relaxation. A slightly different approach is to use transition-state theory (TST). Figure 6.2 pictorially shows the Gibb's free energy of activation ($\Delta G^\ddagger$) for the methyl group rotation. The $\Delta G^\ddagger$ in the form of enthalpy ($\Delta H^\ddagger$) and entropy ($\Delta S^\ddagger$) of activation can be determined from an Eyring plot. To determine $\Delta H^\ddagger$ and $\Delta S^\ddagger$ from T_1, the following equation is used:

$$T_1 = \kappa \frac{k_BT}{h} e^{-\Delta H^\ddagger/RT} e^{-\Delta S^\ddagger/R} \tag{6.8}$$

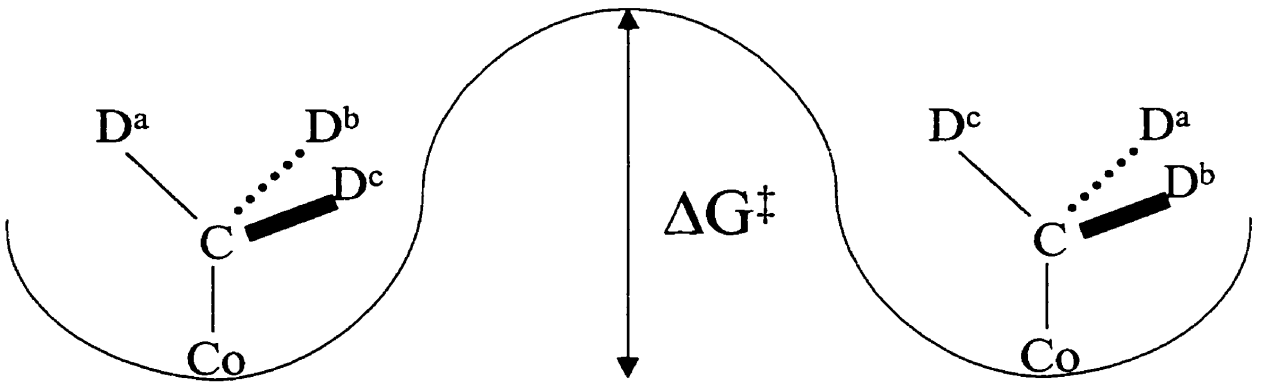

Figure 6.2: Energy *vs.* reaction coordinate showing methyl group rotation.

where κ is the transmission factor (1 s^2 in this study). Therefore an Eyring plot of $\ln(T_1T^{-1})$ *vs.* T^{-1} will reveal both $\Delta H^{\ddagger}$ and $\Delta S^{\ddagger}$.

6.3 Experimental

6.3.1 Synthesis

Methyl-d_3-cobalamin was prepared by a slight modification of a known synthesis.[90] The synthesis of methylcobalamins must be done exclusively under red light or else the cobalt-carbon bond will cleave. Vitamin B_{12} (650 mg) was dissolved with stirring in degassed water (40 mL) in a stoppered 125 mL flask while bubbling argon through it. A solution of sodium borohydride (310 mg in 4 mL degassed water) was added *via* syringe. This solution was stirred for 15 minutes and turns from red to brown to a blue/green colour (cobalt(I)). A degassed solution (6 mL water) of $FeSO_4(NH_4)_2SO_4{\cdot}6H_2O$ (105 mg) and $FeCl_3$ (505 mg) was added dropwise *via* syringe over 15 minutes to react and complex with the boron-containing materials. This solution was then left to stir for an additional 15 minutes to allow for the reaction to complete. Methyl-d_3-iodide (1g vial) was dissolved in degassed methanol (2.5 mL) and then added to the solution causing the solution to turn red again. To remove the iron salts, the solution was centrifuged, decanted, centrifuged again, then decanted again and finally filtered through a fine frit. This solution was evaporated under reduced pressure to approximately a 1 mL volume. Acetone was added to this solution until it started to show slight turbidity after which it was stored at 4°C to crystallize. The crystals were collected yielding 600 mg of

methyl-d_3-cobalamin (91%). The product was characterized by electrospray ionization mass spectrometry, showing a molecular ion at m/z = 1347 Da as compared to the unlabeled methylcobalamin at 1344 Da.

The base-off form of methyl-d_3-cobalamin was made in a similar fashion as described in chapter 5 using 8:1 molar equivalents of KCN:methyl-d_3-cobalamin. Conversion of the base-off complex was confirmed using ^{31}P NMR.

6.3.2 Solid-State NMR Experiments

Solid-state ^{2}H NMR spectra were acquired at 76.77 MHz on a Bruker AMX-500 NMR spectrometer (B_o = 11.75 T) using a solenoid probe. The samples were packed in 5 mm NMR tubes cut to a length of 24 mm. Deuterium $\pi/2$ pulse lengths of 2.2 - 2.5 μs were used. A quadrupolar echo pulse sequence was used to acquire 1D ^{2}H NMR spectra and the quadrupolar-echo inversion-recovery pulse sequence[133] was used to measure spin-lattice relaxation time (T_1) at various temperatures. Temperatures were acquired in approximately 10K increments from 300K - 180K; these temperatures were calibrated using the chemical shift separation of OD and CD_3 signals in neat methanol-d_4. Temperatures below the freezing point of methanol (175K) were obtained by extrapolation of the solution data.

6.3.3 Simulations

The inversion-recovery ^{2}H NMR spectra were simulated iteratively using the method of Wittebort.[136] In these simulations the rate of exchange was optimized to produce T_1 values and anisotropic line shapes that best fit the experimental spectra.

The effects of finite pulse widths were included, but these had little effect on the simulations. Equal populations of the sites were assumed in all cases.

6.4 Results

The 1D ^{2}H NMR solid-state NMR spectra of both methyl-d_3-cobalamin and its base-off analogue exhibit typical Pake patterns at all temperatures with a peak-to-peak splitting of 48.5 $\pm$ 0.5 kHz. A typical ^{2}H NMR spectrum is seen in Figure 6.3. This spectrum is typical of methyl deuterons undergoing three-fold motion. The static ^{2}H quadrupolar coupling constant and the angle ζ (equation 6.2) both affect the degree of motional narrowing of the spectrum from the rigid-lattice value. NMR spectra could not be obtained at sufficiently low temperatures corresponding to the rigid-lattice condition and therefore the static values of χ for each complex could not be obtained explicitly from the spectra. If a tetrahedral angle of 109.5° is assumed (and therefore ζ), a quadrupolar coupling constant of 194 $\pm$ 2kHz is obtained from the splitting. This is significantly larger than methyl groups in other biological molecules - a typical value of 167 kHz is reported for the methyl group of alanine.[132] If a χ of 167 kHz is assumed, the angle ζ is calculated to be 105.9°. Both of these approaches provide a relatively narrow range of these parameters and therefore the extremes of these covariant ranges (167 kHz $< \chi <$ 194 kHz and 105.9° $< \zeta <$ 109.5°) will be investigated.

Examples of the experimental and simulated solid-state inversion-recovery ^{2}H NMR experiments for the base-on form of methyl-d_3-cobalamin are seen in Figures 6.4 (experimental) and 6.5 (simulated). All of the spectra for both complexes

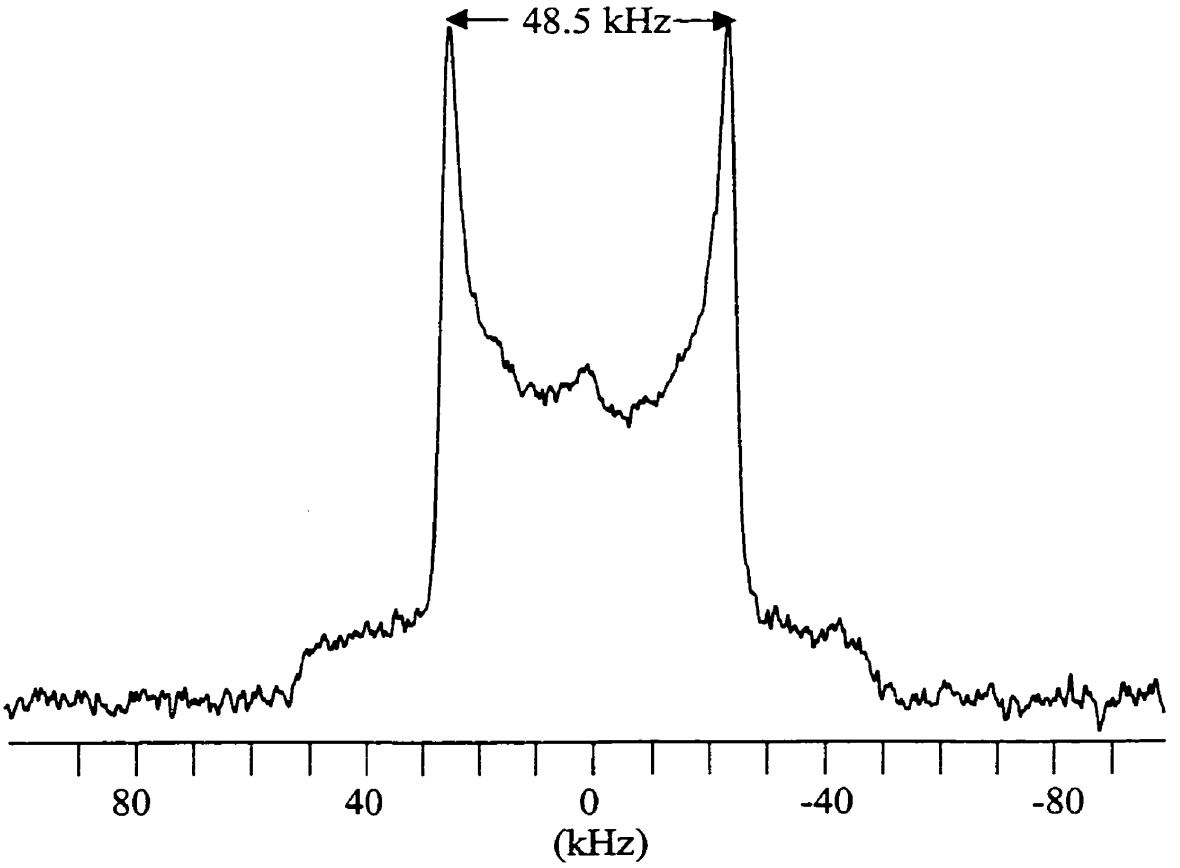

Figure 6.3: Solid-state ^{2}H NMR spectrum of methyl-d_3-cobalamin at 76.77 MHz ($B_o = 11.75$ T) at 294K. The splitting of 48.5 kHz provides evidence that the methyl group is motionally averaged *via* three-fold motion.

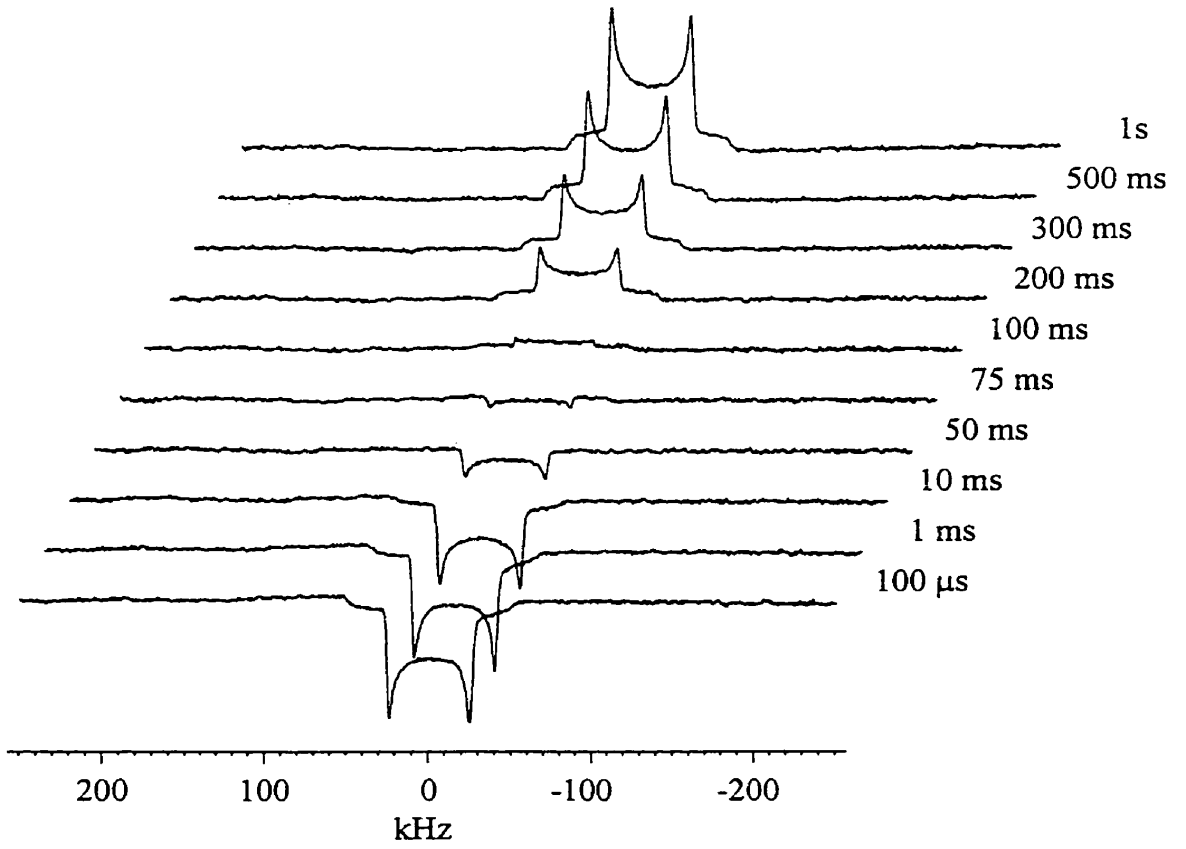

Figure 6.4: Experimental ^{2}H NMR spectra of methyl-d_3-cobalamin at 184 K. Note that the relaxation across the pattern does not all proceed at the same rate across the anisotropic ^{2}H lineshape. The outer shoulders recover faster than the sharp peaks, indicating that T_1 is anisotropic.

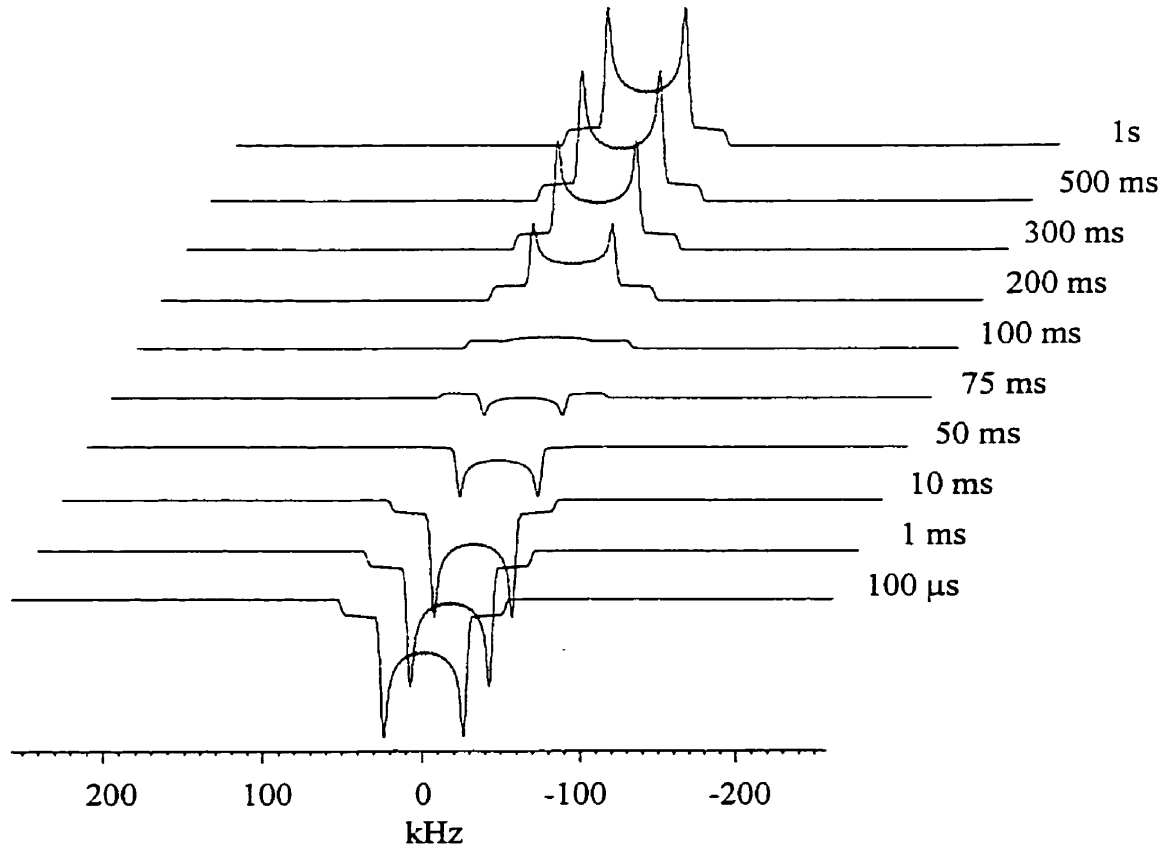

Figure 6.5: Simulated ^{2}H NMR spectra of methyl-d_3-cobalamin at 184 K. Note that the relaxation across the pattern does not all proceed at the same rate across the anisotropic ^{2}H lineshape. The outer shoulders recover faster than the sharp peaks, indicating that T_1 is anisotropic.

in this study behaved in a similar manner at all temperatures. The spin-lattice relaxation of the shoulders occurred at a much more rapid rate than relaxation of the peaks (by a factor of approximately 2). This is direct and unequivocal evidence that methyl group in both complexes undergoes three-fold motion in jumps between discrete sites rather than rotational diffusion about the methyl axis. The recovery of magnetization of the peaks in Figure 6.4 occurs with a T_1 of 145.1 $\pm$ 1.6 ms while that of the shoulders occurs at 72 $\pm$ 3 ms. The larger errors in the shoulders is a result of the more difficult assignment of the intensities for T_1 fitting in these regions of the lineshape. A similar trend of a factor of approximately 2 between the peaks and shoulders is observed at all temperatures. As a result of the lower errors in the T_1 values for the peaks, these values were used to generate best-fit simulations of the magnetization recovery lineshapes (as seen in Figure 6.5).[136] The two possible limits of χ and ζ described above were both simulated and resulted in similar rates and essentially identical spectra at each temperature. The results of the simulation for the base-on and base-off forms of methyl-d_3-cobalamin are given in Tables 6.1 and 6.2. The two limiting cases for χ and ζ have been called model A and model B; model A refers to χ = 167 kHz and $\zeta = 105.9°$; in model B χ = 194 kHz and $\zeta = 109.5°$.

The correlation times for the two complexes in this study could not be obtained directly from the relaxation data because it was not possible to obtain temperatures (due to our experimental setup) that corresponded to their T_1 minima. However, the results presented in Tables 6.1 and 6.2 from our simulations provide estimates of exchange between each of the three sites in the jump motion. The activation

Table 6.1: Temperatures, ^{2}H NMR T_1 (peaks) values, and computer simulation exchange rates obtained for methyl-d_3-cobalamin base-on.

Temperature (K)	T_1 (s)	Rate (model A) (Hz)	Rate (model B) (Hz)
287	0.900	7.50×10^{10}	1.08×10^{11}
275	0.866	6.89×10^{10}	1.04×10^{11}
263	0.745	5.90×10^{10}	8.90×10^{10}
250	0.514	4.10×10^{10}	6.20×10^{10}
240	0.431	3.43×10^{10}	5.20×10^{10}
227	0.267	2.12×10^{10}	3.20×10^{10}
218	0.220	1.75×10^{10}	2.65×10^{10}
205	0.172	1.37×10^{10}	2.05×10^{10}
193	0.159	1.27×10^{10}	1.90×10^{10}
184	0.145	1.15×10^{10}	1.73×10^{10}
174	0.109	8.70×10^{9}	1.31×10^{10}
164	0.077	6.15×10^{9}	9.25×10^{9}

NOTE: Errors in T_1 are less than 10%, on the basis of the standard deviation of the non-linear least squares fit. Model A refers to $\chi = 167$ kHz and $\zeta = 105.9°$. Model B refers to $\chi = 194$ kHz and $\zeta = 109.5°$.

Table 6.2: Temperatures, ^{2}H NMR T_1 (peaks) values, and computer simulation exchange rates obtained for methyl-d_3-cobalamin base-off.

Temperature (K)	T_1 (s)	Rate (model A) (Hz)	Rate (model B) (Hz)
302	0.812	6.43×10^{10}	9.96×10^{10}
287	0.702	5.56×10^{10}	8.63×10^{10}
274	0.649	5.14×10^{10}	7.96×10^{10}
262	0.580	4.59×10^{10}	7.11×10^{10}
249	0.484	3.83×10^{10}	5.94×10^{10}
239	0.373	2.90×10^{10}	4.56×10^{10}
222	0.316	2.50×10^{10}	3.88×10^{10}
201	0.278	2.20×10^{10}	3.41×10^{10}
186	0.253	2.00×10^{10}	3.10×10^{10}
177	0.168	1.33×10^{10}	2.06×10^{10}
167	0.140	1.11×10^{10}	1.72×10^{10}
157	0.095	7.50×10^{9}	1.16×10^{10}
147	0.068	5.40×10^{9}	8.4×10^{9}

NOTE: Errors in T_1 are less than 10%, on the basis of the standard deviation of the non-linear least squares fit. Model A refers to $\chi = 167$ kHz and $\zeta = 105.9°$. Model B refers to $\chi = 194$ kHz and $\zeta = 109.5°$.

energy for the jump motion is obtained directly from a plot of $\ln(T_1)$ *vs.* 1000/T. Figure 6.6 shows a such a plot for both MeB_{12} (red) and $MeB_{12}BO$ (purple). The slopes of the fits were determined to be -962 K^{-1} and -672 K^{-1} for the base-on and base-off complexes respectively. Therefore an activation energy of 8.0 $\pm$ 1.3 kJ mol^{-1} is obtained for MeB_{12}. The activation energy of the base-off form is less at 5.6 $\pm$ 0.6 kJ mol^{-1}.

Looking at the fits in terms of TST, the enthalpy and entropy of activation of the methyl group rotation can be obtained from the fits seen in Figure 6.7. Enthalpy is determined from the slope and entropy from the intercept. For MeB_{12}, $\Delta H^{\ddagger}$ was determined to be 6.20 $\pm$ 1.49 kJ mol^{-1} while that of $MeB_{12}BO$ was determined to be significantly less at 3.87 $\pm$ 0.71 kJ mol^{-1}. The $\Delta S^{\ddagger}$ for the base-on and base-off complexes were determined to be very similar at -224 $\pm$ 59 J K^{-1} mol^{-1} and -234 $\pm$ 23 J K^{-1} mol^{-1} respectively.

6.5 Discussion

From the experimental data acquired on both of the complexes in this study, it has been established that both complexes undergo rapid rotation in the solid state, such that all of the NMR spectra over all temperatures in this study fall in the fast-exchange limit. Being able to add this selective label to these two complexes allows for the the acquisition of solid-state ^2H NMR spectra without any background signals. This type of label can be used in many bioinorganic systems to selectively study specific sites within a complex. Other similar types of labels are unique nuclei within a molecule, *e.g.*, ^{59}Co as described in chapters 3 and 5, and the ^{31}P

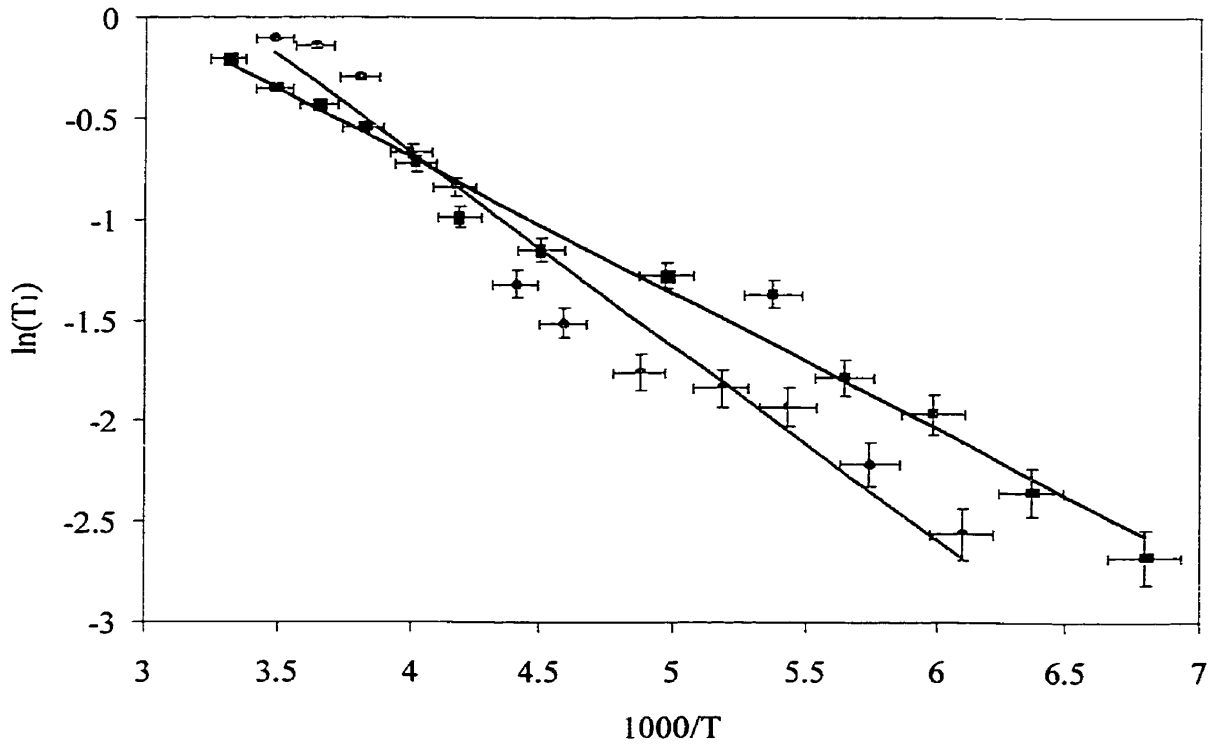

Figure 6.6: Plot of $\ln(T_1)$ *vs.* 1000/T for MeB_{12} (red) and $MeB_{12}BO$ (purple).

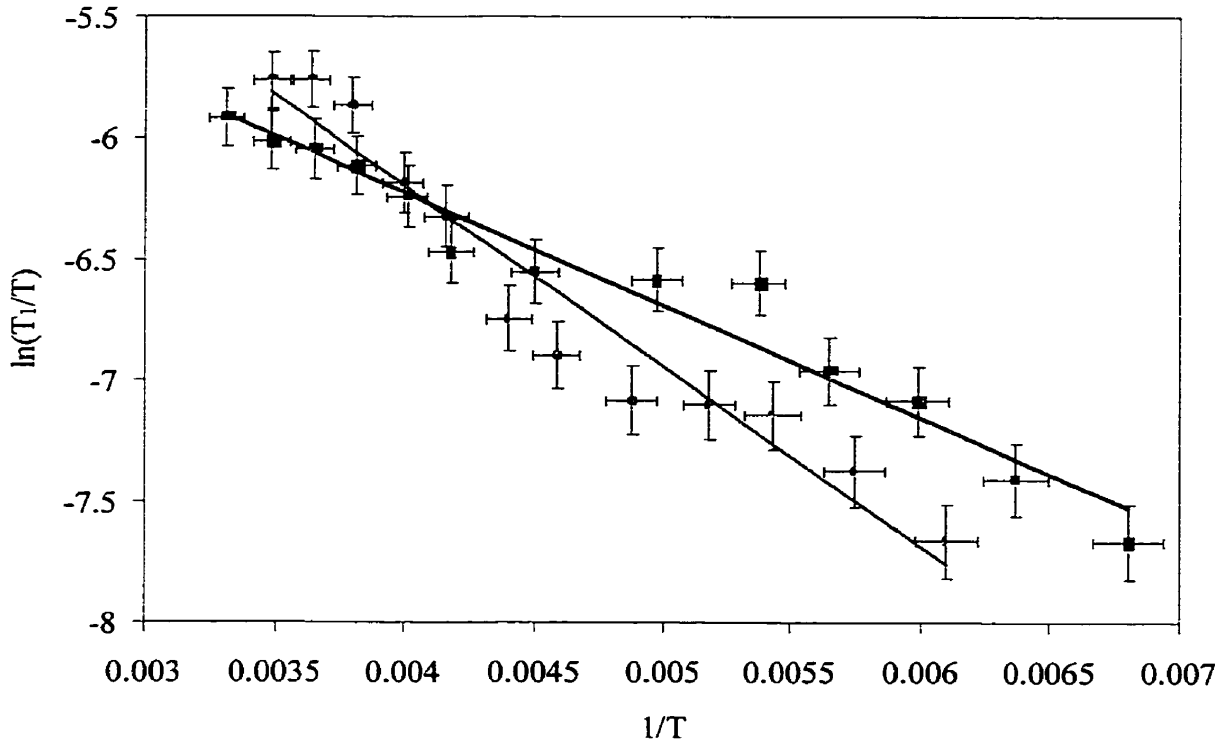

Figure 6.7: Plot of $\ln(T_1T^{-1})$ *vs.* T^{-1} for MeB_{12} (red) and $MeB_{12}BO$ (purple).

study in chapter 5. Introduction of ^{13}C nuclei was described in chapter 4 and, as described there, different information is available by introducing these types of labels. However, since there is a significant natural abundance of ^{13}C (1.1%), these types of experiments are not as selective as that described in this chapter. It is also significant that to perform solid-state NMR experiments, single-crystals are not needed allowing for the study of a much larger range of complexes. With respect to biologically relevant samples, lyophilized samples from water and/or from a buffer solution can be used allowing for easily prepared samples.

We only know of one report of a ^2H NMR study of a methyl group directly attached to a metal - $[W(\eta\text{-}C_5Me_5)(CD_3)_4][PF_6]$.[131] In this complex there are two types of methyl groups bound to the tungsten in a 3:1 ratio (1 axial and 3 equatorial). The E_a of the axial methyl group in this tungsten complex was found to be 26.8 kJ mol^{-1} while that the equatorial methyl groups was 10.9 kJ mol^{-1}. It is interesting to note that the axial group was in the slow exchange limit while the equatorial groups were in the fast exchange limit. The methyl groups in the fast exchange limit seem to be similar to the results for the methyl-d_3-cobalamins. However, the ^2H lineshape of the methyl groups in the tungsten complex were found to be significantly asymmetric ($\eta = 0.2$). From the lineshape analysis, the quadrupolar coupling constant for this complex were determined to be 178 kHz.

Quadrupolar coupling constants for ^2H methyl groups have been studied in many organic compounds, biological compounds, and salts as well as in the just mentioned tungsten complex. Invariably χ is between 165 and 180 kHz in these types of methyl groups (*e.g.*, 174 kHz in *tert*-butyliodide,[137] 167 kHz in alanine,[132] and

168 kHz in tetramethylammonium salts[138]). Since all of the spectra acquired for both complexes in this study fall into the fast-exchange limit with respect to methyl rotation, it was not possible to obtain independent values of χ and ζ from the single peak-to-peak splitting of 48.5 $\pm$ 0.5 kHz. Both values have to be obtained using equation 6.2, thus only ranges of χ (167 to 194 kHz) and ζ (105.9° to 109.5°) could be determined. For the base-on form where an X-ray crystal structure is available,[139] an estimate of the Co-C-H angle is available. In the crystal structure, the C-H bond length, however, is significantly shortly than usual (0.977 - 1.036 Å) as compared to normal values of 1.09 Å.[140] Also, the angles are larger than those expected for a carbon in such an environment as in this complex. Interestingly, the shorter C-H bond length correlates to a larger Co-C-H bond angle. Since hydrogen positions are notoriously difficult to determine *via* X-ray diffraction, extrapolation of the bond angles was performed using a bond length of 1.09 Å to determine an angle of 106.7°. Using this angle for ζ, a χ of 171.9 kHz is obtained for methyl-d_3-cobalamin, which is in the range of those for the complexes mentioned above.

The motion of the methyl groups in both the base-on and base-off forms of methyl-d_3-cobalamin are best described as jumps between three equivalent sites, rather than free rotation or rotational diffusion about the methyl axis. The anisotropy in the T_1 for both complexes is direct evidence for this conclusion. The activation energy of the jumping motion, however, is significantly different between the base-on and base-off forms. The activation energy of the base-off form is 5.6 kJ mol^{-1} which is only 70% of that of the base-on form (8.0 kJ mol^{-1}). This is an indication that the Co-C bond in the base-off form is weaker (and therefore longer) than

in the base-on form. This is consistent with results for cobaloximes, models for cobalamins, for which is has been shown that there is a strong *trans* influence on the Co-C bond length.[141, 142] In any case, both complexes in this study have activation energies that are significantly smaller than other methyl groups in organic/biological complexes or salts. Typical values fall in the range of 17 - 27 kJ mol^{-1}[132, 138] in sterically crowded environments (like alanine), and can be as low as 8.6 - 17.6 kJ mol^{-1}[143, 144] in less hindered sites like that in methionine. The low activation energies observed in the two complexes in this study are probably a reflection of two factors arising from the structures: the lability of this methyl group through the weak Co-C linkage important to its biological function, and the lack of any steric hindrance within the "puckered bowl" of the corrin ring.

Solid-state NMR is becoming more and more popular to use to investigate biological mechanism and structure. Studelska *et al.*[145] were able to follow an enzymatic reaction *via* solid-state NMR. In this study, solid-state NMR experiments of selectively isotopically labelled phosphoenolpyruvate complexed with shikimate 3-phosphate and EPSP synthase (a 46 kDa protein) were used to elucidate the structure of intermediates in the enzymatic reaction. The advantage of using solid-state NMR as compared to solution NMR is that there is no upper limit on the size of the complexes that can be studied. McDermott and co-workers have been using ^2H NMR as a selective probe in paramagnetic compounds, both coordination complexes[146, 147] and biological materials,[148, 149] to great success. On the basis of the selectivity of the ^2H solid-state NMR results presented in our work, the capacity to provide detailed information about the dynamics involved (includ-

ing both the type of model and the rates of motions) as well as the ability to use polycrystalline samples, we believe that we can use this technique to study larger biological systems. Drennan *et. al.*[21] published the first crystal structure of methylcobalamin bound to a fragment of methionine synthase. In this structure, it was observed that the cobalamin is in a base-off configuration which His-759 replaces the dimethylbenzimidazole. However, using solid-state NMR, we could look at the holoenzyme containing bound ^{2}H labelled cobalamin since we do not need to worry about being able to grow crystals of the complex. It might even be possible to follow the complete reaction of the conversion of homocysteine to methionine using stop-flow techniques to quench the reaction at specific times and analyzing these samples by the solid-state NMR techniques described in this thesis.

6.6 Conclusions

Deuterium NMR has been shown to be an excellent probe of the dynamics of the methyl group in methylcobalamin. The rotation of the methyl group in methyl-d_3-cobalamin and its base-off form were both determined to correspond to a three-fold jumping motion. An enthalpy of activation of 6.20 kJ mol^{-1} was determined for the base-on form of methylcobalamin while that of the base-off form was determined to be less than two thirds of this at 3.87 kJ mol^{-1} while the entropy of activation was found to be very similar for the two complexes varying less then 10 JK^{-1}mol^{-1}. The differences in the $\Delta H^{\ddagger}$'s give hope that solid-state ^{2}H NMR will be a useful probe to study an enzyme-bound methyl-d_3-cobalamin and could possibly give insight into the methyl transfer in enzymes that use methylcobalamin as the methyl source.

Chapter 7

Concluding Remarks

The goal of this thesis was to add to the body of knowledge pertaining to the cobalamin family of compounds using solid-state NMR as a research tool. In particular we wanted to learn about enzyme-free cobalamins to set the basis for the future study of enzyme-bound cobalamins using solid-state NMR techniques.

In Chapter 3, the single-crystal ^{59}Co NMR study of vitamin B_{12} was described. This was the first example of the application of single-crystal NMR study to the elucidation of the local environment of a metal in a biologically relevant system. From this study, we were able to determine that the cobalt chemical shift tensor is highly anisotropic, with principal components of $\delta_{11} = 5075 \pm 45$ ppm, $\delta_{22} = 4670 \pm 43$ ppm, and $\delta_{33} = 3902 \pm 42$ ppm. The quadrupolar tensor, as described by the quadrupolar coupling constant ($\chi = 27.31 \pm 0.08$ MHz) and asymmetry parameter ($\eta = 0.243 \pm 0.005$) was also determined. The orientation of the two tensors in the molecular frame was unambiguously determined. With the success of this study, it would be interesting to perform equivalent studies on both methylcobalamin and

co-enzyme B_{12} in the near future.

Chapter 4 described ^{15}N and ^{13}C CPMAS and CP static NMR experiments. Selective labelling of the cyano group of vitamin B_{12} with ^{15}N and ^{15}N,^{13}C cyanide show that there is no notable effect from the cobalt on the ^{15}N spectra. From the ^{13}C CPMAS NMR spectrum of cyano-^{15}N,^{13}C-cobalamin, a Co-C one-bond J-coupling of 165 $\pm$ 10 Hz is observed. The ^{13}C CPMAS spectrum of methyl-^{13}C-cobalamin, however, could not be simulated but has lead to a new idea. Since we can attach one ^{13}C label readily, if a second ^{13}C label could be introduced into the dimethylbenzimidazole tail biochemically, distance measurements could be determined using rotational resonance[101] or RFDR[102] and one could study base-on *vs.* base-off cobalamins using ^{13}C NMR. Also, since there is a large background in ^{13}C NMR, double CP[99] could be used to study the methyl group if it was doubly labelled with both ^{13}C and ^{2}H. One could then perform CP from ^{1}H to ^{2}H followed by CP from ^{2}H to ^{13}C to remove the majority of the background carbon signals.

Using solid-state ^{31}P NMR, we believe that we have determined a method to readily identify whether cobalamins are base-on or base-off. Chapter 5 described both ^{31}P and ^{59}Co NMR studies of base-on and base-off cobalamins. The ^{59}Co NMR chemical shift and quadrupolar tensors of the base-off forms for vitamin B_{12} and methylcobalamin are described. From these results, it was realized that further studies of base-off cobalamins need to be performed with a nitrogen bound ligand to replace the dimethylbenzimidazole instead of cyanide to gain a better understanding of the cobalt centre of base-off cobalamins. The ^{31}P chemical shift

tensors of the base-on and base-off cobalamins are significantly different (δ_{on}= -1.3 ± 1 ppm, δ_{off}= 4.6 ± 0.3 ppm, Ω_{on}= 184 ± 3 ppm, Ω_{off}= 107.5 ± 2.5 ppm, κ_{on}= 0.355 ± 0.035, κ_{off}= -0.735 ± 0.015). Knowing the differences in the base-on and base-off cobalamin solid-state ^{31}P NMR results, the next step would be to test our hypothesis on enzyme-bound cobalamins that are known to be base-off.

Deuterium NMR relaxation studies of methyl-d_3-cobalamin and its base-off analogue revealed information about the dynamics of these two complexes. Chapter 6 described this study where the activation energy for methyl group rotation of the base-on form was determined to to 8.0 ± 1.3 kJ mol^{-1} while the base-off form was determined to only be 70% of this value at 5.6 ± 0.6 kJ mol^{-1}. In both cases the methyl group is undergoing three-fold jumping motion. From these results, we believe that using deuterium as a probe to study an enzyme bound methyl-d_3-cobalamin could give insight into the methyl transfer in enzymes that use methylcobalamin as the methyl source *via* a solid-state ^{2}H NMR study where the methyl transfer is quenched at different times in the reaction.

The results presented in this thesis are encouraging and indicate that we will be able to enter the world of enzyme-bound cobalamins well prepared. Recently an enzymatic pathway was studied *via* solid-state ^{31}P NMR.[145] This enzymatic turnover is the first of its kind studied using solid-state NMR techniques, but we expect many more to follow in the near future. These results together with our efforts lead us to believe that enzyme-bound cobalamins are well within the grasp of solid-state NMR techniques and that these enzyme-bound complexes will be one of the next to be found in the literature.

Appendix A

Raw Data From The Single-Crystal Vitamin B_{12} Study

The following three tables contain the raw data used to determine the quadrupolar and chemical shift tensors for ^{59}Co in vitamin B_{12}. In the analysis of the data, the angles were shifted slightly (-6.8° for the X-rotation and -4.7° for the Z-rotation). The data from these tables were fitted using Microsoft Excel. Appendix B has a complete error analysis of the data and includes a step by step analysis of site 3.

Table A.1: Raw data for the X-rotation of the ^{59}Co single-crystal NMR study.

Rotation Angle	Sites 1/4	Sites 2/3
0°	517070 Hz	583518 Hz
15°	531728 Hz	593290 Hz
30°	562997 Hz	566906 Hz
45°	593290 Hz	532705 Hz
60°	585472 Hz	515115 Hz
75°	519024 Hz	519024 Hz
90°	477005 Hz	517070 Hz
105°	435963 Hz	491663 Hz
120°	447689 Hz	447689 Hz
135°	483845 Hz	434986 Hz
150°	517069 Hz	470164 Hz
165°	520001 Hz	520001 Hz
180°	517070 Hz	583518 Hz

Table A.2: Raw Data for the Y-rotation of the ^{59}Co single-crystal NMR study.

Rotation Angle	Site 1	Site 2	Site 3	Site 4
0°	447881 Hz	506475 Hz	506475 Hz	447881 Hz
15°	442998 Hz	482061 Hz	511357 Hz	469365 Hz
30°	445928 Hz	446904 Hz	512817 Hz	518193 Hz
45°	458623 Hz	427373 Hz	534795 Hz	545537 Hz
60°	511357 Hz	455693 Hz	578740 Hz	581670 Hz
75°	538701 Hz	509404 Hz	588506 Hz	597295 Hz
90°	584600 Hz	570928 Hz	570928 Hz	584600 Hz
105°	597295 Hz	590459 Hz	512822 Hz	539678 Hz
120°	580693 Hz	580693 Hz	456670 Hz	507451 Hz
135°	545537 Hz	534795 Hz	426396 Hz	458623 Hz
150°	509404 Hz	510381 Hz	449834 Hz	451787 Hz
165°	472294 Hz	510381 Hz	484990 Hz	445928 Hz
180°	447881 Hz	506475 Hz	506475 Hz	447881 Hz

Table A.3: Raw Data for the Z-rotation of the ^{59}Co single-crystal NMR study.

Rotation Angle	Site 1	Sites 2/3	Site 4
0°	566314 Hz	566314 Hz	596995 Hz
15°	604400 Hz	569244 Hz	544830 Hz
30°	613189 Hz	572174 Hz	506008 Hz
45°	598541 Hz	577057 Hz	484283 Hz
60°	576080 Hz	576080 Hz	474517 Hz
75°	546783 Hz	588775 Hz	494049 Hz
90°	527252 Hz	590728 Hz	512603 Hz
105°	498932 Hz	588775 Hz	536041 Hz
120°	475494 Hz	586822 Hz	555572 Hz
135°	462799 Hz	582916 Hz	582916 Hz
150°	478424 Hz	581939 Hz	596588 Hz
165°	522369 Hz	577057 Hz	607330 Hz
180°	566314 Hz	566314 Hz	596995 Hz

Appendix B

Single-Crystal Vitamin B_{12} Error Analysis

To determine the final errors in the quadrupolar coupling and chemical shift tensors in vitamin B_{12}, the error must be propagated through all steps of the analysis as done regularly in statistics. Looking at site 3 of B_{12}, the following table gives the 15 parameters as well as the errors of fit for the single-crystal ^{59}Co NMR data. To

Table B.1: Best-fit parameters for site 3 single-crystal ^{59}Co NMR experiments with errors in parentheses (all values in Hz).

	Rotation x	Rotation y	Rotation z
A	516 184 (1 025)	511 169 (908)	579 572 (912)
B	42 884 (1 409)	-32 009 (1 243)	-10 433 (1 252)
C	39 390 (1 490)	53 281 (1 323)	2 923 (1 328)
D	34 171 (1 424)	27 619 (1 243)	-718 (1 258)
E	-5 350 (1 476)	-15 647 (1 323)	798 (1 322)

follow the propagation of error through the data analysis, it is convenient to look at the quadrupolar coupling tensors first followed by the chemical shift tensor, and concluding with errors in the Euler angles.

B.1 Quadrupolar Tensor

The errors in the quadrupolar coupling tensor can be determined from the errors in the D and E terms since these terms are solely due to the quadrupolar interaction. Therefore the terms obtained from rotation x (Q_{yy} - Q_{zz} and Q_{yz}) must be solved in terms of D_x and E_x using equations 2.92 and 2.93. The following is the result of such a rearrangement.

$$Q_{yz}^2 = Constant \times (D_x - (D_x^2 + E_x^2)^{\frac{1}{2}}) \tag{B.1}$$

$$(Q_{yy} - Q_{zz})^2 = Constant \times (-D_x - (D_x^2 + E_x^2)^{\frac{1}{2}}) \tag{B.2}$$

The errors in equations B.1 and B.2 will be the same since the error in D_x = error in -D_x. Therefore, the following errors need to be determined:

$$Error(D_x^2) = 2 \times 1424 = 2848 \tag{B.3}$$

$$Error(E_x^2) = 2 \times 1476 = 2952 \tag{B.4}$$

$$Error(D_x^2 + E_x^2) = (2824^2 + 2952^2)^{\frac{1}{2}} = 4102 \tag{B.5}$$

$$Error((D_x^2 + E_x^2)^{\frac{1}{2}}) = \frac{1}{2} \times 4102 = 2051 \tag{B.6}$$

Table B.2: Summary of error analysis of raw quadrupolar coupling tensor.

Component	Error (Hz)
Q_{xx}	663
Q_{yy}	888
Q_{zz}	878
Q_{xy}	1108
Q_{yz}	1248
Q_{zx}	1100

$$Error(D_x - (D_x^2 + E_x^2)^{\frac{1}{2}}) = (1424^2 + 2051^2)^{\frac{1}{2}} = 2497 \quad \text{(B.7)}$$

Hence the errors in Q_{yz}^2 and (Q_{yy} - Q_{zz})^2 are both 2497 and the errors in Q_{yz} and (Q_{yy} - Q_{zz}) are 1248. In a similar fashion the errors in the other components of the raw quadrupolar coupling tensor can be determined. To determine the errors of the diagonal components (as they obviously are determined as a pair so far), the errors must be squared and solved as a series of equations as follows:

$$Error(Q_{yy}^2 + Q_{zz}^2) = 1248^2 = 1558532 \quad \text{(B.8)}$$

$$Error(Q_{zz}^2 + Q_{xx}^2) = 1100^2 = 1210107 \quad \text{(B.9)}$$

$$Error(Q_{xx}^2 + Q_{yy}^2) = 1108^2 = 1228203 \quad \text{(B.10)}$$

The error in Q_{yy} is given as ((B.8 - B.9 + B.10)/2)$^{\frac{1}{2}}$ = 888. A summary of the error analysis the results for the raw quadrupolar coupling tensor are given in Table B.2.

The next step in the process was to diagonalize the following raw quadrupolar

tensor.

$$Q_{raw} = \begin{pmatrix} -281357 & -79353 & 120420 \\ -79353 & -351010 & -38262 \\ 120420 & -38262 & 632367 \end{pmatrix} \tag{B.11}$$

This was done simply with the software package, *Maple*, the results of which are given by the following Eigenvectors,

$$Q_{Eigenvalues} = \begin{pmatrix} -0.567 & 0.813 & 0.132 \\ -0.823 & -0.566 & -0.048 \\ 0.036 & -0.136 & 0.990 \end{pmatrix} \tag{B.12}$$

for which the Eigenvalues are -404.0 kHz, -246.3 kHz, and 650.3 kHz. However, to propagate error through such a process is not a trivial matter. Using Prof. LeRoy's report,[54] the following process was performed. The uncertainty (U) of a given component of a diagonalized matrix is given as

$$U = \sqrt{D^T \cdot \bar{1} \cdot D} \tag{B.13}$$

where D is a column matrix with elements that depends on the errors in the components of the raw matrix as well as uncertainty introduced *via* trial values added

to the numbers of the raw matrix done one at a time. This can be written as

$$D = \begin{pmatrix} U(Q_{xx}) \times (\frac{\partial Q_{11}}{\partial Q_{xx}}) \\ U(Q_{xy}) \times (\frac{\partial Q_{11}}{\partial Q_{xy}}) \\ U(Q_{zx}) \times (\frac{\partial Q_{11}}{\partial Q_{zx}}) \\ U(Q_{yy}) \times (\frac{\partial Q_{11}}{\partial Q_{yy}}) \\ U(Q_{yz}) \times (\frac{\partial Q_{11}}{\partial Q_{yz}}) \\ U(Q_{zz}) \times (\frac{\partial Q_{11}}{\partial Q_{zz}}) \end{pmatrix} \tag{B.14}$$

for the 11 component, Q_{11}, of the diagonalized quadrupolar tensor. The size of the trial value is usually on the order of ten percent of the errors (addition of 100 was used for the quadrupolar tensor). Thus, 100 is added to the xx component of the raw quadrupolar tensor and it is then diagonalized. This gives news values for all of the component of the quadrupolar tensor. The difference in the original Q_{xx} component and the new Q_{xx} component is ∂Q_{xx}. This procedure is then repeated for the remaining five different elements to obtain the other ∂Q_{ij} values. For Q_{33}, the following D matrix is obtained.

$$D_{Q_{33}} = \begin{pmatrix} 662 \times 0.175 \\ 888 \times 0.002 \\ 878 \times -0.980 \\ 1108 \times -0.128 \\ 1249 \times -0.095 \\ 1100 \times -0.262 \end{pmatrix} = \begin{pmatrix} 11.57 \\ 2.08 \\ -860.26 \\ -14.14 \\ -119.51 \\ -287.82 \end{pmatrix} \tag{B.15}$$

Table B.3: The quadrupolar coupling tensor including errors (in parentheses) in the cube frame.

Q_{11}	Q_{22}	Q_{33}
-404.0 (2.5)	-263.2 (2.3)	650.3 (1.8)
-0.567 (0.007)	0.813 (0.005)	0.132 (0.002)
-0.883 (0.005)	-0.566 (0.007)	-0.048 (0.003)
0.036 (0.003)	-0.136 (0.002)	0.990 (0.000)

The errors in this D matrix must all be multiplied by a factor of two to determine the uncertainty for 2 standard deviations (95% confidence). If the new matrix 2×D is then put into equation B.13 to find the error in component Q_{33} the result is 1830 Hz. In a similar manner, the errors of the other two Eigenvalues as well as the nine components of the Eigenvectors were obtained. Table B.3 contains the quadrupolar coupling tensor with the errors (in parentheses) of both the Eigenvalues (in kHz) and Eigenvectors. These values correspond to the quadrupolar tensor in the cube frame of the experiment. To convert from the cube frame to the crystal frame, a rotation matrix is needed. This matrix is prepared with knowledge of the orientation of the crystal on the rotation plate *via* X-ray crystallography or from the rotation plots. In this case the rotation plot x gave the angles needed, since in rotation x, the crystal was rotated about the a-axis of the cell; hence this angle was zero. The point where the four sites give only one signal in rotation x is 24° (this is when c is along B_o). This is the angle needed to rotate between the crystal

and cube frames using the following rotation matrix.[28]

$$R = \begin{pmatrix} 1 & 0 & 0 \\ 0 & \cos 24 & -\sin 24 \\ 0 & \sin 24 & \cos 24 \end{pmatrix} = \begin{pmatrix} 1 & 0 & 0 \\ 0 & 0.914 & -0.407 \\ 0 & 0.407 & 0.914 \end{pmatrix} \tag{B.16}$$

The results from this rotation (including errors) are given in Table 3.2.

B.2 Chemical Shift Tensor

After the errors are determined for the raw quadrupolar tensor, they can be removed from the errors in the A, B, and C terms thus allowing for the elucidation of the errors in the raw chemical shift tensor *via* rearrangement of equations 2.89, 2.90, and 2.91. Using A_x, B_x, and C_x to determine the errors in $\delta_{yy} + \delta_{zz}$, $\delta_{yy} - \delta_{zz}$, and δ_{yz} the following equations are obtained (all of the constants are removed for simplicity except for ν_o which is needed to convert Hz to ppm).

$$\delta_{yy} + \delta_{zz} = (A_x - (Q_{yy}^2 + Q_{zz}^2 - Q_{yy}Q_{zz} + Q_{yz}^2 + Q_{zx}^2 + Q_{xy}^2)/\nu_o \tag{B.17}$$

$$\delta_{yy} - \delta_{zz} = (B_x - (Q_{yy}^2 - Q_{zz}^2 + Q_{xy} - Q_{yz}^2))/\nu_o \tag{B.18}$$

$$\delta_{zy} = (C_x - ((Q_{yy} + Q_{zz})Q_{yz} + Q_{zx}Q_{xy}))/\nu_o \tag{B.19}$$

For the squared terms, the error is just 2 $\times$ the error of the term. The product terms give errors that are less than one and thus will be ignored. Therefore, the

errors in $\delta_{yy} + \delta_{zz}$, δ_{yy} - δ_{zz}, and δ_{yz} can be determined as follows.

$$\begin{aligned} Error(\delta_{yy} + \delta_{zz}) &= (1025^2 + 1776^2 + 1758^2 + 2498^2 + 2200^2 + 2216^2)^{\frac{1}{2}}/\nu_o \\ &= 4826/\nu_o = 40.7\,\text{ppm} \end{aligned} \tag{B.20}$$

$$\begin{aligned} Error(\delta_{yy} - \delta_{zz}) &= (1409^2 + 1776^2 + 1758^2 + 2216^2 + 2200^2)^{\frac{1}{2}}/\nu_o \\ &= 4826/\nu_o = 35.7\,\text{ppm} \end{aligned} \tag{B.21}$$

$$Error(\delta_{yz}) = 1490/\nu_o = 12.6\,\text{ppm} \tag{B.22}$$

Likewise, the errors in A_y, B_y, C_y, A_z, B_z, and C_z can be used to determine the errors of the other components of the raw chemical shift tensor. Like the raw quadrupolar tensor, the diagonal components come in pairs (either *via* addition or subtraction) and therefore the errors must be determined through solution of a series of equations after the addition errors have been squared.

$$Error(\delta_{xx}^2 + \delta_{yy}^2) = 39.2^2 = 1537 \tag{B.23}$$

$$Error(\delta_{yy}^2 + \delta_{zz}^2) = 40.7^2 = 1653 \tag{B.24}$$

$$Error(\delta_{zz}^2 + \delta_{xx}^2) = 39.3^2 = 1544 \tag{B.25}$$

The error in δ_{xx} is given as ((B.17 - B.18 + B.19)/2)$^{\frac{1}{2}}$ = 26.7. Similarly the errors δ_{yy} and δ_{zz} are 28.8 ppm and 28.7 ppm respectively. Unlike the quadrupolar coupling tensor, the subtraction errors also could be used to find the errors of the

Table B.4: Summary of error analysis of raw chemical shift tensor.

Component	Error (ppm)
δ_{xx}	26.0
δ_{yy}	26.7
δ_{zz}	27.2
δ_{xy}	11.2
δ_{yz}	12.6
δ_{zx}	11.1

diagonal components. Upon doing such calculations the errors in δ_{xx}, δ_{yy}, and δ_{zz} are found to be 25.3 ppm, 24.7 ppm, and 25.9 ppm. An average of the addition and subtraction errors will be used for further propagations. A summary of the errors of the raw chemical shift tensor are seen in Table B.4.

The next step is the diagonalization of the raw chemical shift tensor below.

$$CS_{raw} = \begin{pmatrix} 4580 & -1 & 406 \\ -1 & 4761 & 371 \\ 406 & 371 & 4305 \end{pmatrix} \tag{B.26}$$

This was also performed with *Maple* and the Eigenvectors were found to be

$$CS_{Eigenvalues} = \begin{pmatrix} 0.467 & -0.742 & -0.481 \\ 0.675 & 0.651 & -0.348 \\ 0.571 & -0.162 & 0.805 \end{pmatrix} \tag{B.27}$$

with Eigenvalues of 5075 ppm, 4670 ppm, and 3902 ppm. The propagation of error for the chemical shift tensors was accomplished by the same means as that

Table B.5: The chemical shift tensor including errors (in parentheses) in the cube frame.

δ_{11}	δ_{22}	δ_{33}
5075 (45)	4670 (43)	3902 (42)
0.467 (0.060)	-0.742 (0.036)	-0.481 (0.039)
0.675 (0.055)	0.651 (0.052)	-0.348 (0.030)
0.571 (0.028)	-0.162 (0.065)	0.805 (0.018)

of the quadrupolar coupling tensor using numerical methods described in LeRoy's report.[54] The size of the trial value used here was 1. Using this trial value the following D matrix for the δ_{33} component can be determined.

$$D_{\delta_{33}} = \begin{pmatrix} 26.0 \times 0.232 \\ 26.7 \times -0.121 \\ 27.3 \times -0.647 \\ 11.2 \times -0.335 \\ 12.6 \times 0.560 \\ 11.1 \times 0.776 \end{pmatrix} = \begin{pmatrix} 6.03 \\ -3.23 \\ -17.66 \\ -3.75 \\ 7.06 \\ 8.61 \end{pmatrix} \quad \text{(B.28)}$$

As for the quadrupolar tensor, each of these values must be multiplied by two to give a value for two standard deviations. If the new matrix $2\times D_{\delta_{33}}$ is then put into equation B.13 to find the error in component δ_{33} the result is 42 ppm. In a similar manner, the errors of the other two Eigenvalues as well as the nine components of the Eigenvectors were obtained. These errors are summarised in Table B.5. These values correspond to the chemical shift tensor in the cube frame of the experiment. To convert to the crystal frame the rotation matrix (the same as was used for the

quadrupolar coupling tensor) is needed. The results of rotation of $CS_{Eigenvalues}$ are given in Table 3.2.

B.3 Euler Angles

To obtain the Euler angles, the following multiplication of the Eigenvector of quadrupolar (Q) and chemical shift (C) tensor must be performed.

$$\begin{aligned} Q^T C &= \begin{pmatrix} -0.567 & -0.823 & 0.036 \\ 0.813 & -0.566 & -0.136 \\ 0.132 & -0.048 & 0.990 \end{pmatrix} \begin{pmatrix} 0.467 & -0.742 & -0.481 \\ 0.675 & 0.651 & -0.348 \\ 0.571 & -0.162 & 0.805 \end{pmatrix} \\ &= \begin{pmatrix} -0.800 & -0.121 & 0.588 \\ -0.080 & -0.949 & -0.304 \\ 0.594 & -0.290 & 0.750 \end{pmatrix} \end{aligned} \tag{B.29}$$

The Euler angles (E($\alpha\beta\gamma$)) come directly from this product and are given as follows.

$$\begin{pmatrix} \cos\gamma\cos\beta\cos\alpha - \sin\gamma\sin\alpha & \cos\gamma\cos\beta\sin\alpha + \sin\gamma\cos\alpha & \sin\beta\sin\alpha \\ -\sin\gamma\cos\beta\cos\alpha - \cos\gamma\sin\alpha & -\sin\gamma\cos\beta\cos\alpha - \cos\gamma\sin\alpha & \sin\gamma\sin\beta \\ \sin\beta\cos\alpha & \sin\beta\sin\alpha & \cos\beta \end{pmatrix} \tag{B.30}$$

Since E($\alpha\beta\gamma$) = Q^TC, the Euler angles can be easily determined to be 334.0°, 41.4°, and 207.3°. To find the errors in these angles, the errors of the Q and C Eigenvectors must be propagated throughout. Since this is a simple multiplication

of two 3 X 3 matrices, the error in each component is a sum of the errors obtained from the 3 multiplications squared and then the square root of the sum. Since we know the error of each of the components of Q and C, we obtain E($\alpha\beta\gamma$) with the following errors

$$\begin{pmatrix} -0.800 & (0.057) & -0.121 & (0.048) & 0.588 & (0.033) \\ -0.080 & (0.058) & -0.949 & (0.043) & -0.304 & (0.036) \\ 0.594 & (0.029) & -0.290 & (0.064) & 0.750 & (0.019) \end{pmatrix} \tag{B.31}$$

Now to calculate the error β we can look at the 33 position of the matrix. A β of 39.7° is obtained if the error is considered to be negative and a β of 43.1° is obtained if the error is considered to be positive. The difference of these two angles divided by 2 gives and error of $\pm$ 1.7° in β. In a similar manner, the errors in α and γ can be obtained giving the following Euler angles (and errors): α = 334.0° (13.0°), β = 41.4° (1.7°), and γ = 207.3° (2.5°).

Bibliography

[1] Lippard, J. S.; Berg, J. M. *Principles of Bioinorganic Chemistry;* University Science Books: Mill Valley, CA, 1994.

[2] Combe, J. S. *Trans. Med.-Chirurg. Soc. Edinburgh* **1824,** *1*, 194.

[3] Oster, W.; McCrae, T. *The Prinicples and Practice of Medicine;* Appleton: New York, 1916.

[4] Minot, G. R.; Murphy, W. P. *J. Am. Med. Assoc.* **1926,** *87*, 470.

[5] Castle, W. B. *Am. J. Med. Sci.* **1929,** *178*, 748.

[6] Hodgkin, D. C.; Kamper, J.; Lindsey, J.; MacKay, M.; Pickworth, J.; Robertson, J. H.; Brink-Shoemaker, C.; White, J. G.; Prosen, R. J.; Trueblood, K. N. *Proc. R. Soc. London A* **1959,** *242*, 228.

[7] Hodgkin, D. C.; Pickworth, J.; Robertson, J. H.; Prosen, R. J.; Sparks, R. A.; Trueblood, K. N. *Proc. R. Soc. London A* **1959,** *242*, 306.

[8] White, J. G. *Proc. R. Soc. London A* **1962,** *266*, 440.

[9] Hodgkin, D. C.; Lindsey, J.; MacKay, M.; Trueblood, K. N. *Proc. R. Soc. London A* **1962,** *266,* 475.

[10] Hodgkin, D. C.; Lindsey, J.; Sparks, R. A.; Trueblood, K. N.; White, J. G. *Proc. R. Soc. London A* **1962,** *266,* 494.

[11] Brink-Shoemaker, C.; Cruikshank, D. W. J.; Hodgkin, D. C.; Kamper, M. J.; Pilling, D. *Proc. R. Soc. London A* **1964,** *278,* 1.

[12] Lippard, J. S. E. *Progess in Inorganic Chemistry: Bioinorganic Chemistry;* John Wiley and Sons: New York, 1990.

[13] Wright, J. R.; Hendrickson, W. A.; Ozaki, S.; James, G. T. *Physical Methods for Inorganic Biochemistry;* Plenum Press: New York, 1986.

[14] Wuthrich, K. *NMR of Proteins and Nucleic Acids;* Wiley-Interscience: New York, 1986.

[15] Cavanagh, J.; Fairbrother, W. J.; Palmer, A. G.; Skelton, N. J. *Protein NMR Spectroscopy: Principles and Practice;* Academic Press: San Diego, 1996.

[16] Johansson, C.; Drakenberg, T. *Annu. Rep. NMR Spectrosc.* **1990,** *22,* 1.

[17] Bax, A.; Szejverenyi, N. M.; Maciel, G. E. *J. Magn. Reson.* **1983,** *52,* 147.

[18] Samoson, A.; Lippmaa, E.; Pines, A. *Mol. Phys.* **1988,** *65,* 1013.

[19] Medek, A.; Harwood, J. S.; Frydman, L. *J. Am. Chem. Soc.* **1995,** *117,* 12779.

[20] Halpern, J. *Science* **1985,** *227,* 869.

[21] Drennan, C. L.; Huang, S.; Drummond, J. R.: Matthews, R. G.; Ludwig, M. L. *Science* **1994,** *266,* 1669.

[22] Mancia, F.; Evans, P. R. *Structure* **1998,** *6,* 711.

[23] Abend, A.; Nitsche, R.; Bandarian, V.; Stupperich, E.; Retey, J. *Angew. Chem. Int. Ed. Engl.* **1998,** *37,* 625.

[24] Medek, A.; Frydman, V.; Frydman, L. *Proc. Natl. Acad. Sci. U.S.A.* **1997,** *94,* 14237.

[25] Spiess, H. W. In *Dynamic NMR Spectroscopy;* Diehl, R., Fluch, E., Kosfeld, R., Eds.; Springer-Verlag: New York, 1978.

[26] Haeberlen, U. *High-Resolution NMR in Solids: Selective Averaging* In Waugh, J. S., Ed., *Advances in Magnetic Resonance, Supplement 1;* Academic Press: New York, 1976.

[27] Taylor, P. C.; Baugher, J. F.; Kriz, H. M. *Chem. Rev.* **1976,** *75,* 203.

[28] Arfken, G. *Mathematical Methods for Physicists, 3rd Ed.;* Academic Press: San Diego, 1985.

[29] Mason, J. *Solid State Nucl. Magn. Reson.* **1993,** *2,* 285.

[30] Ramsey, N. F. *Phys. Rev.* **1950,** *78,* 699.

[31] Jameson, C. J.; Mason, J. In *Multinuclear NMR;* Mason, J., Ed.; Plenum Press: New York, 1987.

[32] Malli, G.; Froese, C. *Int. J. Quantum Chem.* **1967,** *1S,* 95.

[33] Kolb, D.; Johnson, W. R.; Shorer, P. *Phys. Rev. A.* **1982,** *26,* 19.

[34] Pake, G. E. *J. Chem. Phys.* **1948,** *16,* 327.

[35] Hartmann, S. R.; Hahn, E. L. *Phys. Rev.* **1962,** *128,* 2042.

[36] Pines, A.; Gibby, M. G.; Waugh, J. S. *J. Chem. Phys.* **1972,** *56,* 1776.

[37] Bryce, D. L.; Wasylishen, R. E. *J. Am. Chem. Soc.* **2000,** *122,* 11236.

[38] Power, W. P.; Lumsden, M. D.; Wasylishen, R. E. *J. Am. Chem. Soc.* **1991,** *113,* 8257.

[39] Lumsden, M. D.; Eichele, K.; Wasylishen, R. E.; Cameron, T. S.; Britten, J. F. *J. Am. Chem. Soc.* **1994,** *116,* 11129.

[40] Volkoff, G. M. *Can. J. Phys.* **1953,** *31,* 820.

[41] Petch, H. G.; Cranna, N. G.; Volkoff, G. M. *Can. J. Phys.* **1953,** *31,* 837.

[42] Herzfeld, J.; Berger, A. E. *J. Chem. Phys.* **1980,** *73,* 6021.

[43] Maricq, M. M.; Waugh, J. S. *J. Chem. Phys.* **1979,** *70,* 3300.

[44] Schmidt-Rohr, K.; Spiess, H. W. *Multidimensional Solid-State NMR and Polymers;* Academic Press: San Diego, 1994.

[45] Wooster, A. W. *Z. Krist.* **1936,** *94,* 375.

[46] Spiess, H. W.; Haas, H.; Hartmann, H. *J. Chem. Phys.* **1969,** *50,* 3057.

[47] Spiess, H. W.; Sheline, R. K. *J. Chem. Phys.* **1970,** *53,* 3036.

[48] Mooberry, E. S.; Pupp, M.; Slater, J. L.; Sheline, R. K. *J. Chem. Phys.* **1971,** *55,* 3655.

[49] Mooberry, E. S.; Sheline, R. K. *J. Chem. Phys.* **1972,** *56,* 1852.

[50] Reynhardt, E. C. *Can. J. Phys.* **1974,** *52,* 1398.

[51] Reynhardt, E. C. *J. Phys. Chem.* **1974,** *7,* 4135.

[52] Eichele, K.; Chan, J. C. C.; Wasylishen, R. E.; Britten, J. F. *J. Phys. Chem. A.* **1997,** *101,* 5423.

[53] Vosegaard, T.; Langer, V.; Daugaard, P.; Hald, E.; Bildsøe, H.; Jakobsen, H. J. *Rev. Sci. Instrum.* **1996,** *67,* 2130.

[54] LeRoy, R. J. *Uncertainty, Sentivity, Convergence and Rounding in Performing and Reporting Least-Squares Fits;* University of Waterloo: Waterloo, 1998.

[55] von Philipsborn, W. *Pure Appl. Chem.* **1986,** *58,* 513.

[56] Kirby, C. W.; Puranda, C. M.; Power, W. P. *J. Phys. Chem.* **1996,** *100,* 14618.

[57] Medek, A.; Frydman, L. *J. Am. Chem. Soc.* **2000,** *122,* 684.

[58] Strohmeier, M.; Orendt, A. M.; Facelli, J. C.; Solum, M. S.; Pugmire, R. J.; Parry, R. W.; Grant, D. M. *J. Am. Chem. Soc.* **1997,** *119,* 7114.

[59] Kirby, C. W. *M. Sc. Thesis;* Waterloo, Ontario, 1996.

[60] Hayashi, S. *Magn. Reson. Chem.* **1996,** *34,* 791.

[61] Richert, T.; Elbayed, K.; Raya, J.; Granger, P.; Braunstein, P.; Rosé, J. *Magn. Reson. Chem.* **1996,** *34,* 689.

[62] Medek, A.; Frydman, V.; Frydman, L. *J. Phys. Chem. B.* **1997,** *101,* 8959.

[63] Power, W. P.; Wasylishen, R. E.; Mooibroek, S.; Pettitt, B. A.; Danchura, W. *J. Phys. Chem.* **1990,** *94,* 591.

[64] Chan, J. C. C.; Au-Yeung, S. C. F. *J. Mol. Struct. (THEOCHEM)* **1997,** *393,* 93.

[65] Chan, J. C. C.; Au-Yeung, S. C. F. *J. Phys. Chem. B.* **1997,** *101,* 3637.

[66] Godbout, N.; Oldfield, E. *J. Am. Chem. Soc.* **1997,** *119,* 8065.

[67] Morris, H. D.; Ellis, P. D. *J. Am. Chem. Soc.* **1989,** *111,* 6045.

[68] Wu, Y.; Lewis, D.; Frye, J. S.; Palmer, A. R.; Wind, R. A. *J. Magn. Reson.* **1992,** *100,* 425.

[69] Fernandez, C.; Delevoye, L.; Amoureux, J.-P.; Lang, D. P.; Pruski, M. *J. Am. Chem. Soc.* **1997,** *119,* 6858.

[70] Grey, C.; Veeman, W.; Vega, A. *J. Chem. Phys.* **1993,** *98,* 7711.

[71] Jarvie, R. P.; Wenslow, R. M.; Mueller, K. T. *J. Am. Chem. Soc.* **1995,** *117,* 570.

[72] Wang, S. H.; De Paul, S. M.; Bull, L. M. *J. Magn. Reson.* **1997,** *125,* 364.

[73] Harris, R. K.; Olivieri, A. C. *Progr. NMR Spectrosc.* **1992,** *24,* 435.

[74] Schurko, R. W.; Wasylishen, R. E.; Nelson, J. *J. Phys. Chem.* **1996,** *100,* 8057.

[75] Asaro, F.; Gobetto, R.; Liguori, L.; Pellizer, G. *Chem. Phys. Lett.* **1999,** *300,* 414.

[76] Brown, K. L. *Chemistry and Biochemistry of* B_{12}*;* Banerjee, R., Ed.; Wiley and Sons, Inc.: New York, 1999.

[77] Brown, K. L.; Gupta, B. D. *Inorg. Chem.* **1990,** *29,* 3854.

[78] Kaplan, S.; Pines, A.; Griffin, R. G.; Waugh, J. S. *Chem. Phys. Lett.* **1974,** *25,* 78.

[79] Sardashti, M.; Maciel, G. E. *J. Phys. Chem.* **1988,** *92,* 4620.

[80] Wu, G.; Wasylishen, R. E. *J. Phys. Chem.* **1993,** *97,* 7863.

[81] Kroeker, S.; Wasylishen, R. E. *Can. J. Chem.* **1999,** *77,* 1962.

[82] Brown, K. L.; Hakimi, J. M. *Inorg. Chem.* **1984,** *23,* 1756.

[83] Brown, K. L.; Peck-Siler, S. *Inorg. Chem.* **1988,** *27,* 3548.

[84] Duncan, T. M. *A Compilation of Chemical Shift Anistropies;* The Farragut Press, Chicago, 1991.

[85] Kim, A. J.; Butler, L. G. *Inorg. Chem.* **1993,** *32,* 178.

[86] Wu, G.; Kroeker, S.; Wasylishen, R. E. *Inorg. Chem.* **1995,** *34*, 1595.

[87] Curtis, R. D.; Ratcliffe, C. I.; Ripmeester, J. A. *Chem. Commun.* **1992,** 1800.

[88] Pulkkinen, A.; Hiltunen, Y.; Jokisaari, J. *Liq. Crystal* **1988,** *3*, 737.

[89] Kaczka, E. A. *J. Am. Chem. Soc.* **1951,** *73*, 3569.

[90] Dolphin, D. *Methods Enzymol.* **1971,** *18*, 117.

[91] Hayashi, S.; Hayamizu, K. *Bull. Chem. Soc. Jpn.* **1991,** *64*, 688.

[92] Eichele, K.; Wasylishen, R. E. *J. Magn. Reson.* **1994,** *46*, A106.

[93] Alderman, D. W.; Solum, M. S.; Grant, D. M. *J. Chem. Phys.* **1986,** *84*, 3717.

[94] Frish, M. J.; Trucks, G. W.; Schlegel, H. B.; Gill, P. M. W.; Johnson, B. G.; Robb, M. A.; Cheeseman, J. R.; Keith, T.; Petersson, G. A.; Montgomery, J. A.; Raghavachari, K.; Al-Laham, M. A.; Zakrzewski, V. G.; Ortiz, J. V.; Foresman, J. B.; Cioslowski, J.; Stefanov, B. B.; Nanayakkara, A.; Challacombe, M.; Peng, C. Y.; Ayala, P. Y.; Chen, W.; Wong, M. W.; Andres, J. L.; Replogle, E. S.; Gomperts, R.; Martin, R. L.; Fox, D. J.; Binkley, J. S.; Defrees, D. J.; Baker, J.; Stewart, J. P.; Head-Gordon, M.; C., G.; Pople, J. A. *GAUSSIAN 94, Revision D.4;* GAUSSIAN, Inc.: Pittsburgh, PA, 1995.

[95] Kräutler, B.; Konrat, R.; Stupperuch, E.; Färber, G.; Gruber, K.; Kratky, C. *Inorg. Chem.* **1994,** *33,* 4128.

[96] Jameson, C. J.; Jameson, A. K.; Oppusunggu, D.; Willie, S.; Burrell, M.; Mason, J. J. *J. Chem. Phys.* **1981,** *74,* 81.

[97] Dykes, D.; Huckerby, T. N.; Oldham, C. *Inorg. Nucl. Chem. Lett.* **1977,** *13,* 63.

[98] Kofod, P. *Inorg. Chem.* **1995,** *34,* 2768.

[99] Schaefer, J.; MacKay, R. A.; Stejskal, E. O. *J. Magn. Reson.* **1979,** *34,* 443.

[100] Hing, A. W.; Vega, S.; Schaefer, J. *J. Magn. Reson.* **1993,** *A103,* 151.

[101] Raleigh, D. P.; Levitt, M. H.; Griffin, R. G. *Chem. Phys. Lett.* **1988,** *146,* 71.

[102] Griffiths, J. M.; Lakshmi, K. V.; Bennett, A. E.; Raap, J.; Van Der Wielen, C. M.; Lugtenburg, J.; Herzfeld, J.; Griffin, R. G. *J. Am. Chem. Soc.* **1994,** *116,* 10178.

[103] Cheng, J. T.; Edward, J. C.; Ellis, P. D. *J. Phys. Chem.* **1990,** *94,* 553.

[104] Eaton, D. R.; Buist, R. J.; Sayer, B. G. *Can. J. Chem.* **1987,** *65,* 1332.

[105] Chung, S. C.; Chan, J. C. C.; Au-Yeung, S. C. F.; Xu, X.-P. *J. Phys. Chem.* **1993,** *97,* 12685.

[106] Zhou, P.; Au-Yeung, S. C. F.; Xu, X.-P. *J. Am. Chem. Soc.* **1999,** *121,* 1030.

[107] Hirschinger, J.; Granger, P.; Rosé, J. *J. Phys. Chem.* **1992,** *96,* 4815.

[108] Kempgens, P.; Hirschinger, J.; Elbayed, K.; Raya, J.; Granger, P.; Rosé, J. *J. Phys. Chem.* **1996,** *100,* 2045.

[109] Ganguly, P.; Venkatraman, T. N.; Rajamohanan, P. R.; Ganapathy, S. *J. Phys. Chem. B.* **1997,** *101,* 11099.

[110] Medek, A.; Frydman, V.; Frydman, L. *J. Phys. Chem. A.* **1999,** *103,* 4830.

[111] Gorenstein, D. G. *J. Am. Chem. Soc.* **1975,** *97,* 898.

[112] Gorenstein, D. G.; Kar, D. *Biochem. Biophys. Res. Commun.* **1975,** *65,* 1073.

[113] Brown, K. L.; Hakimi, J. M. *Inorg. Chim. Acta* **1982,** *67,* L29.

[114] Brown, K. L.; Hakimi, J. M.; Jacobsen, D. W. *J. Am. Chem. Soc.* **1984,** *106,* 7894.

[115] Brown, K. L. *Inorg. Chem.* **1986,** *25,* 3111.

[116] Brown, K. L.; Marques, H. M.; Jacobsen, D. W. *J. Biol. Chem.* **1988,** *263,* 1872.

[117] Brown, K. L.; Evans, D. R.; Zubkowski, J. D.; Valente, E. J. *Inorg. Chem.* **1996,** *35,* 415.

[118] Kohler, S. J.; Klein, M. P. *Biochemistry* **1976,** *15,* 976.

[119] Herzfeld, J.; Griffin, R. G.; Haberkorn, R. A. *Biochemistry* **1978,** *17,* 2711.

[120] Terao, R.; Matsui, S.; Akasaka, K. *J. Am. Chem. Soc* **1977,** *99.* 6136.

[121] Brown, K. L.; Wilson, W. W.; Jacobsen, D. W. *J. Inorg. Biochem.* **1998,** *71,* 199.

[122] Kunwar, A. C.; Turner, G. L.; Oldfield, E. *J. Magn. Reson.* **1986,** *69,* 124.

[123] Goodfellow, R. J. In *Multinuclear NMR;* Mason, J., Ed.; Plenum Press: New York, 1987.

[124] A., K. J.; Salemink, I.; de Planque, M. R. R.; Lindblom, G.; Koeppe, R. E.; Greathouse, D. V. *Biochemistry* **1996,** *35,* 1037.

[125] Prenner, E. J.; Lewis, R. N. A. H.; Neuman, K. C.; Gruner, S. M.; Kondejewski, L. H.; Hodges, R. S.; McElhaney, R. N. *Biochemistry* **1997,** *36,* 7906.

[126] Schneider, Z.; Stroinski, A. *Comprehensive B_{12};* New York, 1987.

[127] Blakly, R. L. *The Biochemistry of Folic Acid and Related Pteridines;* North-Holland, Amsterdam, 1969.

[128] Griffin, R. G. *Methods Enzymol.* **1981,** *72,* 108.

[129] Davis, J. H. *Biochem. Biophys. Acta.* **1983,** *737,* 117.

[130] Spiess, H. W. *Adv. Polym. Sci.* **1985,** *66,* 23.

[131] Maus, D. C.; Copie, V.; B., S.; Griffiths, J. M.; G., G. R.; Luo, S.; Schrock, R. R.; Lui, A. H.; Seidel, S. W.; Davis, W. M.; A., G. *J. Am. Chem. Soc.* **1996,** *118,* 5665.

[132] Beshah, K.; Olejniczak, E. T.; Griffin, R. G. *J. Chem. Phys.* **1987,** *86,* 4730.

[133] Davis, J. H.; Jeffrey, K. R.; Bloom, M.; Valic, M. I.; Higgs, T. P. *Chem. Phys. Lett.* **1976,** *42,* 390.

[134] Bloembergen, N.; Percell, E. M.; Pound, R. V. *Phys. Rev.* **1948,** *73,* 679.

[135] Torchia, D. A.; Szabo, A. *J. Magn. Reson.* **1948,** *49,* 107.

[136] Wittebort, R. T.; Olejniczak, E. T.; Griffin, R. G. *J. Chem. Phys.* **1987,** *86,* 4511.

[137] Mooibroek, S.; Wasylishen, R. E.; Macdonald, J. B.; Ratcliffe, C. I.; Ripmeester, J. A. *Can. J. Chem.* **1988,** *66,* 734.

[138] Ratcliffe, C. I.; Ripmeester, J. A. *Can. J. Chem.* **1988,** *64,* 1348.

[139] Rossi, M.; Glusker, J. P.; Randaccio, L.; Summers, M. F.; Toscano, P. J.; Marzilli, L. G. *J. Am. Chem. Soc.* **1985,** *107,* 1729.

[140] Huheey, J. E. *Inorganic Chemistry: Principals of Structure and Reactivity, 3rd. Ed.;* Harper and Row: New York, 1983.

[141] Bresciani-Pahor, N.; Forcolin, M.; Marzilli, L. G.; Randaccio, L.; Summers, M. F.; Toscano, P. J. *Coord. Chem. Rev.* **1985,** *63,* 1.

[142] Randaccio, L.; Bresciani-Pahor, N.; Marzilli, L. G. *Chem. Soc. Rev.* **1989,** *18,* 225.

[143] Batchelder, L. S.; Niu, C. H.; Torchia, D. A. *J. Am. Chem. Soc.* **1983,** *105,* 2228.

[144] Keniry, M. A.; Kintanar, A.; Smith, R. L.; Gutowsky, H. S. *Biochemistry* **1984,** *23,* 288.

[145] Studelska, D. R.; McDowell, L. M.; Espe, M. P.; Klug, C. A.; Schaefer, J. *Biochemistry* **1997,** *36,* 15555.

[146] Liu, K.; Ryan, D.; Nakanishi, K.; MeDermott, A. E. *J. Am. Chem. Soc.* **1995,** *117,* 6897.

[147] Lee, H.; Polenova, R.; Beer, R. H.; MeDermott, A. E. *J. Am. Chem. Soc.* **1999,** *121,* 6884.

[148] Liu, K.; Williams, J.; Lee, H.; Fitzgerald, M. M.; Jensen, G. M.; Goodin, D. B.; MeDermott, A. E. *J. Am. Chem. Soc.* **1998,** *120,* 10199.

[149] Lee, H.; Ortiz de Montellano, P. R.; MeDermott, A. E. *Biochemistry* **1999,** *38,* 10808.